System to study Colony-Colony Interactions in Embryonic Stem Cells

by

Somponnat Sampattavanich

B.S., Biomedical Engineering (2005)

Johns Hopkins University

Submitted to the Department of Electrical Engineering and Computer Sciences in Partial Fulfillment of the Requirement for the Degree of

Master of Science

at the

Massachusetts Institute of Technology

May 2007

[June 2007]

Signature of Author .....
Department of Electrical Engineering and Computer Science
May 25, 2007

Certified by .....
Joel Voldman
Associate Professor of Electrical Engineering and Computer Science
Thesis Supervisor

Accepted by .....
Arthur C. Smith
Chairman, Department Committee on Graduate Theses

System to study Colony-Colony Interactions in Embryonic Stem Cells

by

Somponnat Sampattavanich

Submitted to the
Department of Electrical Engineering and Computer Sciences

May 25, 2007

in Partial Fulfillment of the Requirement for the Degree of
Master of Science

Abstract

Many efforts have been made to characterize the necessary regulatory factors involved in self-renewal of embryonic stem cells (ESCs). Recent studies suggested that different autocrine factors exist in murine ESCs (mESCs) and can influence their self-renewal and proliferation, predominantly in deficiency conditions. These observations were investigated based on a comparison of different groups of mESCs that were plated at varying cell densities. In this study, we developed an experimental platform to study colony-colony interactions in mESCs. We have used stencil cell patterning to precisely localize mESC colonies on the culture substrate. This technique allows the formation of mESC colonies with precise shape and controllable inter-colony distances. We monitored colony proliferation, motility and fusion in response to different initial colony configurations over time using the developed image analysis algorithms and immunohistochemistry techniques. Different cultivating conditions commonly used for mESCs were tested to identify the environment where autocrine signaling is significant.

Thesis Supervisor: Joel Voldman
Title: Associate Professor of Electrical Engineering and Computer Science

ACKNOWLEDGMENT

First, I would like to thank my advisor, Prof.Joel Voldman for giving me the opportunity to join his research group and to let me indulge my passions. Joel has given me continual supports, and meaningful advice, without which I would not complete this thesis. I also would like to express my appreciation for his understanding and willingness to help when I struggle both in research and in life.

I own many thanks to all members of the Voldman group. Mike is the transport guru who has helped rescue me a number of times. Salil was the first person at MIT who taught me how to do fabbing and has been my very generous big brother. Lily and Adam both have helped me in my research in a number of ways and are my magnificent HST mentors. Brian is the main figure in the group who always makes the lab cheerful and pleasing and is very willing to help me out. Joseph has been my studymate in different classes and shared many thoughts and ideas with me in both research and life. Nick is my brilliant officemate who has helpful comments. I also would like to thank other past and present Voldman group members: Hsu-yi, Katarzyna, Alison, Katarina and Wei Mong for contributing to a wonderful research environment.

I am also very grateful to a number of faculty members and researchers at MIT. I would like to thank my academic adviser, Prof.Sangeeta Bhatia for her support and kindness in giving me advices both academically and in research. Prof.Dennis Freeman is a very kind person and has given many valuable advices for my project. I have also learnt many new ideas about image processing from Prof.William M. Wells. I would like to kindly thank Kurt Broderick, Paul Tierney and Dennis Ward for teaching me various fabrication techniques in EML and TRL. Members of Sangeeta's group have also been very kind to me. I would like to thank Salman for first introducing me to stencil patterning technique, Elliot for his generosity in sharing his manuscripts and giving me valuable advices, and Alice for teaching me about RNAi basics.

I also would like to thank my previous research mentor, Nathane Hwang for training and still being very kind to me until now, as well as my previous research advisor, Prof.Jennifer Elisseeff for giving me the opportunity four years ago to do research in embryonic stem cells where I found my passion. Two UROP students who used to work with me, Christine and Sharon, were very helpful and enthusiastic even though they both work in the lab very briefly. So I'd like to thank them as well for their helps.

Last but foremost, I would like to thank my family for sending me supports and encouragements: my parents, Supatcharin and Sunai, for their unlimited loves and cares; my brothers, Suranart and Passaron for their encouragement. Last of all, I own my girlfriend, Nattaporn, so much for her caring and supports especially while I was writing this thesis. I would like to thank her for her understanding and being patient with me.

TABLE OF CONTENTS

TABLE OF FIGURES

TABLES

CHAPTER 1: INTRODUCTION

Embryonic stem cells (ESCs) are special cell types with the ability to give rise to all cell types in the adult and to self-renew indefinitely in vitro[1, 2]. Within the past few years, researchers have demonstrated that human embryonic stem cells (hESCs) can give rise to almost all mature cell types in the human body *in vitro*, such as neural tissue, insulin secreting cells, cardiomyocytes, hematopoietic cells, endothelial cells, osteoblasts, and hepatocytes[3]. Using techniques in regenerative medicine to implant functional cells into the defective organs, many people hope that hESCs will become an unlimited cell supply and enable therapy of cell-degenerative diseases such as Juvenile Diabetes, Parkinson's or Arthritis. In order for ESCs to be ready for any clinical purpose, a number of fundamental understandings about ESCs must still be investigated. This thesis is an attempt to study the role of colony-colony interactions in ESCs, an important cell behavior of ESCs that is critical for maintenance of ESCs *in vitro*. We have observed in our preliminary study that colonies that are formed from individual mouse embryonic stem cells (mESCs) plated at high cell density fuse with their neighbor colonies at later time points (Figure 1-1). Because large colonies can cause both hESCs and mESCs to differentiate, it is interesting to examine how such colony-colony interactions may affect the cell fate decision of ESCs. Before we can answer this question, we need to determine first whether ESC colonies can actually sense the presence of their neighbors. What are the underlying mechanisms of these interactions? While it is challenging to demonstrate whether colonies can communicate with one another biologically, we have attempted to answer these questions by analyzing the physical changes of ESC colonies such as colony proliferation and colony motility. Once we confirm whether and how these interactions occur, we hope to investigate the role of colony-colony interactions in self-renewal of ESCs.

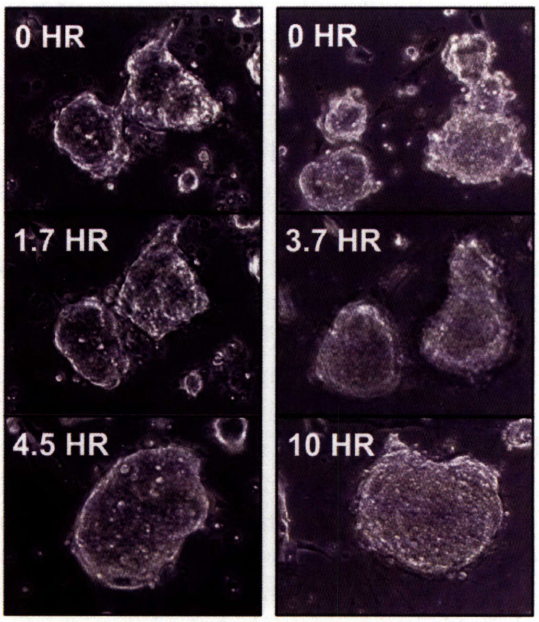

Figure 1-1 Colony fusion: mESCs that are plated at high density using conventional culturing method will first form colonies on the substrate. At later time point, these colonies will fuse to form larger colonies.

We will discuss in this chapter important background concepts necessary to investigate colony-colony interactions. We will first discuss how microenvironments can pass on signals to cue cells and how these signals can control the fate decision of ESCs, specifically for ESC self-renewal. We will then explore some of the possible ligand-receptor pairs that may underlie interactions among ESC colonies and some of the already observed autocrine effects in mESCs. Finally, we will discuss some of the newly-developed technologies that can be used to manipulate cell microenvironment and discuss how these tools may help us investigate colony-colony interactions.

1.1 Issues in embryonic stem cell research

At present, many researchers in ESC research community focus their work on determining the recipes that can be used either to maintain ESCs in the undifferentiated state or induce the cells to differentiate into different mature cell types most efficiently. Some of the techniques that have been demonstrated to help maintain ESC self-renewal or induce their differentiation include supplementation with the appropriate cytokines, co-culturing of ESCs with another supportive cell types, using genetic engineering strategies to modify their genome, or cultivating the cells with important extracellular matrices[4]. While many of these techniques have shown to successfully control the fates of ESCs *in vitro*, the underlying mechanisms of how these culture conditions interact with the cells are still not very well understood. Other groups of researchers therefore try to characterize the molecular mechanisms which underlie self-renewal and pluripotency of ESCs and to understand how signaling networks are changed as a consequence of the imposing conditions[5, 6]. It is therefore essential that we also understand the molecular mechanisms that are involved in fate decision of ESCs before any therapeutic potentials of ESCs can be realized. In addition to the previously discussed technical issues, there are at least three important prerequisites for the use of stem cells in medicine[4, 7]. First, we need to have a cell source that will be able to provide enough number of cells for the treatment and provide cells that are compatible and safe for transplantation into the patient. The derivation of ESCs via therapeutic cloning can give rise to cells that are immunohistogenic compatible to the patients but is still one of the most debatable ethical issues nowadays[8]. Adult stem cells are the promising candidates for ESCs since their derivations are much less ethically debatable. However, these multipotent adult progenitor cells are rare and difficult to identify in the body[7, 9]. Since these stem cells are very precious, the second prerequisite is to have cells that can be expanded *in vitro* without sacrificing their potency. The last prerequisite involves efficiency and safe differentiation techniques for stem cells. We may need to differentiate some of these stem cells completely *in vitro* prior to cell transplantation to prevent any tumor formation *in vivo*. It has been shown that transplantation of undifferentiated ESCs can lead to tumor formation despite the observed therapeutic achievements from the transplant[10, 11]. Thorough understanding of the molecular mechanisms that underlie both self-renewal and multipotency of stem cells is therefore one of the urgent to suffice these prerequisites for the use of ESCs in medicine. Regarding the techniques to maintain self-renewal of ESCs, recent studies have reported the drawbacks of currently used hESC cultivation media[12]. Prolonged culture of hESCs in these media were shown to promote karyotypic changes[13, 14]. It is believed that such states arise from the continual selection of genetic variants that force the cells not to apoptose or differentiate appropriately[12]. Inhomogeneous populations of ESCs are also observed throughout the developmental path of ESCs. As early as the blastocyst stage , clonal mESC lines derived from a single inner cell mass were shown to differentially

express the leukaemia inhibitory factor receptor gene, a cell-surface receptor critical for maintaining self-renewal in mESCs[15]. hESCs were also found to have heterogenous population of pluripotency cells that possess distinct cell-cycle properties, clonogenic capacity and expression of ESC transcription factors[16]. In terms of differentiation, different hESC lines are observed to have different differentiation characteristics[17]. The observed heterogeneity subjects the cells to diverse phenotypes when we try to differentiate these cells for clinical usages with the currently available methods. The worst clinical scenario is the development of teratomas from any remaining pluripotent cells, which can be detrimental for the patient. It is therefore necessary that the properties of ESCs and the important mechanisms to control their fate decision be understood thoroughly both *in vitro* and *in vivo* before we can use ESCs for any clinical purposes.

1.2 Cell fates of ESCs

Fate decision in ESCs is extremely complicated. The three possible cell fates of ESCs are self-renewal, differentiation and apoptosis (Figure 1-2). When ESCs are cultivated in the appropriate cytokine cocktails, they will divide symmetrically and give rise to daughter cells that still maintain ESC properties. It was first believed that the signals required from the media only inhibited cell differentiation[18]. In this sense, differentiation can be viewed as a default cell state of ESCs while self-renewal is like an unsteady state where the cells are maintained within a narrow local minimum at high state-energy. Even though ESCs are pluripotent, these cells can differentiate directly into only three cell types: the primitive ectoderm, the primitive endoderm and trophectoderm cells, reflecting similar developmental capability to their *in vivo* relatives, the inner cell masses[19]. In order to maintain self-renewal of ESCs, signaling to induce differentiation of ESCs along any of these three lineages must be prohibited.

Recently, apoptosis was found to be another important cell state that can occur together with cell differentiation. Thus, not only are differentiation-inhibiting factors required, but promotion of cell proliferation has also been shown to be critical for ESC self-renewal. To observe the role of apoptosis, we will first look at spontaneous apoptosis commonly found in hESCs. It is known that hESCs can only be passaged in clumps rather than in single cells. When the cells are passaged in single cells, the cells usually undergo apoptosis[20]. Supplementing survival factors like neurotrophin into the cultivating medium has been shown to improve survival of hESCs[21]. In mESCs, apoptosis occurs along with cell differentiation[22]. For instance, the tumor suppressor gene p53 usually responds to cell stresses, such as DNA damage during cell division, by forcing cells to die or become arrested in the cell-cycle. It was observed that p53 maintains DNA integrity in mESCs via a novel mechanism, by promoting cell differentiation[22]. When DNA damage occurs in mESCs, p53 binds to the promoter of Nanog, an important transcription factor for mESC self-renewal, and ultimately inhibits Nanog protein synthesis. Once the cells differentiate, apoptosis and cell-cycle arrest can then be controlled in the normal fashion by p53.

The fates of ESCs are controlled by both extrinsic signals and intrinsic programs[23]. A special microenvironment called "niche" is the physical location where extrinsic signals are present to maintain the cells in the appropriate cell fate. The intrinsic genetic programs are the gene regulators that are the ultimate switches for determining ESC fate. Usually, these two mechanisms are linked by signaling cascades that will choose the appropriate cell response for the environment in which the cells are situated. It is our attempt to identify the

appropriate niche where the regulation of differentiation and proliferation of ESCs are balanced appropriately, helping to maintain self-renewal stably in long-term.

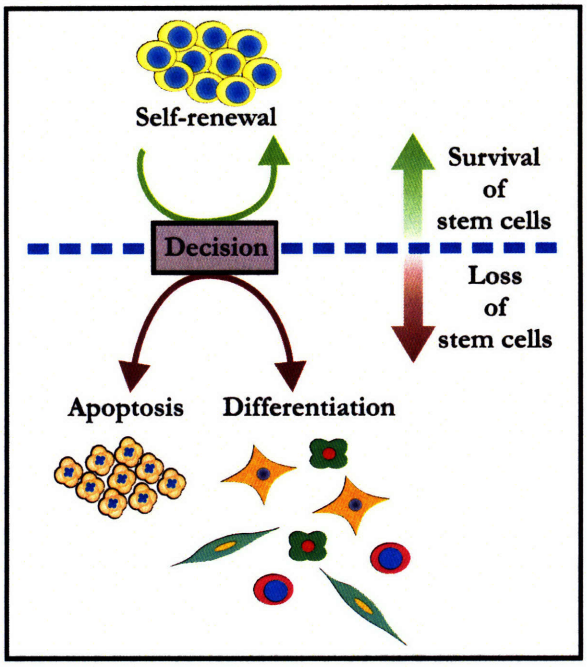

Figure 1-2 Embryo stem cell fates: Self-renewal of ESCs is an unsteady state that is maintained by anti-apoptosis signals and inhibition of cell differentiation. When these signals are inadequate, ESCs will either differentiate or commit programmed cell death depending on the microenvironment that the cells are experiencing. (Modified from [12])

1.3 Cell microenvironment

The fate decision of ESCs is governed by the microenvironment that surrounds the cells. Cells can interact with their surrounding via three main mechanisms: 1) via diffusive, soluble signals, 2) via contact with insoluble extracellular matrices (ECM) and 3) via direct cell-cell contact. The diffusive, soluble ligands usually interact with cells by binding to their corresponding receptors inside or outside the cells. We will discuss in the next section some of the ligand-receptor pairs in different signaling cascades that are important for ESC self-renewal. Diffusive signals are also observed to be critical in multiple systems such as: hematopoiesis[24, 25], differentiation of neural crest stem cells in C. elegans[26], and proliferation of female germ line stem cells in Drosophila[27]. Cells interact with the ECM via cell-surface structures called integrins that are composed of two subunits (α and β) and are unique for each different ECM. Three types of ECM are found in most tissues: 1) proteoglycans , 2) collagen fibers, and 3) multiadhesive matrix proteins[28]. It has been shown that these ECM are also critical for ESC fate decision[29]. Different types of ECM can differently maintain self-renewal of ESCs. Some of these ECMs can promote differentiation of ESCs or create three-dimensional environments that are critical for differentiation into specific cell lineages[30, 31]. For direct cell-cell interactions, cells can bind with other cells via three types of surface molecules: 1) cadherins, 2) immunoglobulin (Ig)-superfamily, and 3) selectins[28]. An important example of signaling via cell-cell contact is that of the Notch receptor and its ligand Delta, which are both transmembrane proteins[27]. We will concentrate in this thesis on microenvironmental effects mediated by diffusive signals only. For further information on

cell-adhesion molecules and ECM, the reader is directed to this previous review[28]. Comprehensive reviews of stem cell niche are discussed in these literatures[23, 32].

1.4 Molecular regulation of ESC self-renewal

In this section, we will look at important signaling cascades known to have critical roles in inhibiting differentiation and promoting proliferation of ESCs. These signaling cascades sense, amplify and pass on extracellular signals to the transcription factors that ultimately determine cell fates of ESCs. As we shall see later, the regulatory signaling cascades in mESCs and hESCs are similar but unique to each species. For a more elaborate details of the molecular mechanisms involved in self-renewal of ESCs, the readers are encouraged to visit recent review articles[5, 6, 19].

In mESCs, the two most important signaling cascades in self-renewal are currently thought to be the LIF-STAT pathway and the BMP-Smad pathway (Figure 1-3). Leukemia inhibiting factor (LIF) or D factor is a member of the IL-6 cytokine family and the first molecule identified to be important for maintaining self-renewal in mESCs[33, 34]. Supplementing this molecule in serum-containing medium can adequately maintain self-renewal of mESCs without needing feeder cells. It is now known that LIF functions via the JAK-STAT3 pathway to prevent the cells from differentiating into primitive endoderm cells[19]. LIF first binds to the LIF receptor (LIFR), which will be dimerized with another membrane-bound protein, GP130. The dimerized receptors activate janus-associated tyrosine kinase (JAK). Signal transducer and activation of transcription 3 (STAT3) molecules are then recruited to the receptors and phosphorylated by JAK[35]. The phosphorylated STAT3s dimerize, translocate into the nucleus and finally bind to their target genes, namely the Myc gene[36].

While LIF is critical for maintaining self-renewal in mESCs, LIF alone cannot prevent differentiation in serum-free condition. It is now known that LIF can also activate extracellular receptor kinase (ERK) and p38 mitogen-activated protein kinase (MAPK) signaling. The MAPK activation will provoke mESCs to differentiate along the neuronal lineage. Bone morphogenic proteins (BMPs) were found to help maintain self-renewal of mESCs when supplemented together with LIF. BMPs such as BMP4 bind to their heterodimeric receptors and send signals to the nucleus via th phosphorylated Smad1/5 proteins. In order for Smad1/5 to translocate into nucleus, they must be conjugated with the co-Smad, Smad4 protein. This Smad complex can then move into nucleus and finally interact with their target genes, the inhibitor-of differentiation (ID)[37]. While BMP signaling can promote self-renewal in mESCs together with activation of LIF-STAT pathway, addition of BMPs alone cannot maintain mESC self-renewal. Instead, mESCs will differentiate along the mesoderm and endoderm lineages in the presence of BMP[38]. Evidence also showed that the BMP signaling cascade functions together with LIF by helping to deactivate ERK signaling[39, 40].

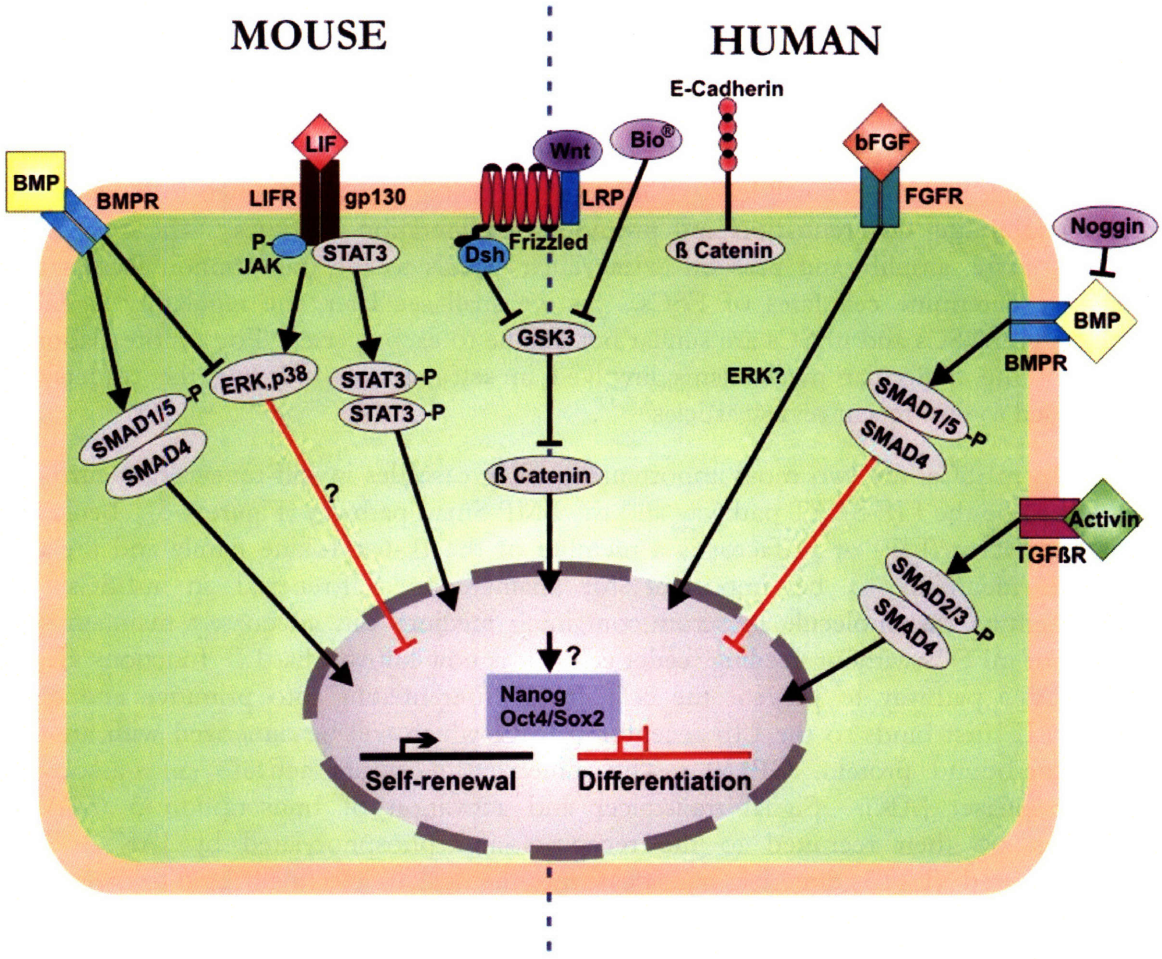

Figure 1-3 Important signaling cascades currently used to maintain self-renewal of ESCs: mESCs and hESCs have similar but unique mechanisms to maintain their own self-renewal. LIF and BMP4 are believed to be the key factors that maintain self-renewal of mESCs. Control of hESC self-renewal is more complicated. Currently, high concentration of bFGF or combination of bFGF and noggin are used to maintain hESCs. Activation of WNT pathway alone by adding a commercialized factor, Bio®, showed to be sufficient in maintaining self-renewal of hESCs. (Modified from [4, 6, 41, 42])

LIF and BMPs signaling cascades function very closely and can adequately maintain self-renewal in mESCs. However, these two signaling pathways function differently in hESCs. Activation of LIF-STAT3 signaling cascade is inadequate to maintain self-renewal of hESCs, while BMP signaling induces differentiation of hESCs along trophectoderm lineage[43-45]. An inhibitor of BMPs, such as Noggin, is therefore used to prevent hESC differentiation. For hESCs, the signaling cascades that are observed to be critical in maintaining their self-renewal are the Wnt pathway, FGF pathway, and TGFβ/Activin/Nodal pathway (Figure 1-3). Similar to LIF signaling in mESCs, FGF signaling is necessary for hESC self-renewal[46, 47]. High concentrations of bFGF alone can sustain undifferentiated hESCs[48]. While the importance of FGF signaling cascade for hESC self-renewal is indisputable, the underlying mechanism of how this signaling cascade functions is still unclear. ERK might be one of its downstream effectors, and FGF signaling may also function interactively with the BMP signaling cascade[6]. TGFβ/Activin/Nodal pathway can also promote self-renewal in hESCs, functioning via phosphorylated Smad2/3,

which inhibits Smad1/5 activity of BMP signaling[49, 50]. It was shown that feeder cells promote self-renewal of hESCs cells using the secreted Activin molecules[49]. While TGFβ/Activin/Nodal pathway is critical for hESCs, this signaling cascade was observed to be unnecessary in mESCs; inhibition of Smad2/3 activity did not affect self-renewal in mESCs[50].

The role of Wnt signaling pathway has only been discovered recently but its function is critical in both mESCs and hESCs. Activation of Wnt signaling alone can sustain self-renewal in both hESCs and mESCs[51]. Activation of the Wnt signaling pathway initiates from binding of Wnt proteins to its receptor, Frizzled (Frz) and LRP co-receptors. Dishevelled (Dsh) protein is then recruited to the membrane and becomes activated. The activated Dsh inhibits the function of glycogen synthase kinase-3β (GSK3β) protein, allowing β-catenin to be dephosphorylated and translocate into the nucleus. β-catenin then forms a protein complex with the TCF/lymphocyte enhancer factor (LEF). It is this complex protein that finally activates target genes of Wnt signaling such as c-Myc and Tcf-1[52, 53]. One may also activate Wnt signaling cascade indirectly using a GSK3β-specific inhibitor such as 6-bromoindirubin-3'-oxime (BIO)[51]. In addition, it was found that the Wnt signaling cascade can function interactively with the integrin-linked kinase (ILK) signaling. Activation of ILK signaling can inhibit GSK3β activity and also down-regulate expression of E-cadherin[54]. Some fraction of Free-form β-catenin usually binds to E-cadherin to promote linkage of E-cadherin to the actin cytoskeleton inside the cell. It was demonstrated that binding of β-catenin to E-cadherin helps prevent part of the active-form β-catenin from translocating into nucleus[55]. Since expression of ILK signaling decreases the amount of E-cadherin on the cell membrane, all β-catenin will now accumulate inside the nucleus, strengthening the effect of Wnt signaling cascade. Wnt signaling cascade can also interact with a few other signaling cascades such as FGF and Activin/Nodal signaling in hESCs and LIF in mESCs[6]. While the definite interactions among these signaling cascades are unclear, it is clear that GSK3β signaling is critical for the maintenance of self-renewal in both hESCs and mESCs.

1.5 Possible autocrine signaling in mESCs

In our attempt to determine whether colony-colony interactions can occur biologically, we first attempt to determine any possible ligand-receptor pairs that may co-exist in ESCs. If these ligand-receptor pairs are present, there is a greater possibility that ESC colonies will interact with one another via these molecules. Since the cells used in this thesis are mESCs, we will only investigate here the proteins available in mESCs. Our goal is to create a list of possible ligands secreted and receptors expressed in ESCs. Keep in mind that these protein lists only show proteins that are detected over a specific concentration threshold. Since the concentration of molecules secreted or expressed by ESCs may not reflect whether or how important these molecules are, we still need to be open-minded for the possibility of other ligands that might be secreted in a limited amount but the threshold concentration to which cells can respond are also very low.

First, we identified the possible ligands that are secreted from mESCs, based on protein analysis of cell extracts[56] as well as protein analysis of the conditioned medium[57], shown in Table 1-1. The only single molecule that was detected in both studies is the colony stimulating factor 1 (CSF-1). The activation of CSF signaling pathway was reported to control expression of RAS protein, which is important for RTK signaling in osteoclasts[58].

CSF were also observed to induce differentiation of mESCs to blood cells such as macrophage and megakaryocytes [59, 60]. Some of the proteins in this list are ligands and growth factors involve in some signaling cascades, including WNT9B, SCF, VEGF and IL-11. A few others are chemokines that can play an important role on cell motility, at least for macrophages. These chemokines mediate their effect via the 7-transmembrane G protein-coupled receptors. As mentioned earlier, the list presented here is not necessarily complete. Nagano *et al.* detected proteins that are present at greater than 10^4 molecules per cell[56]. Guo *et al.* only reported proteins that are secreted more than 25% over the baseline level detected in fresh cultivating medium (containing both serum and LIF) As an example, Guo and colleagues themselves reported earlier that mESCs secreted low amount of SDF-1 protein as well as low level of CXCR4, the receptor associated with SDF-1[61]. These molecules were however not included here. Clearly, the level of SDF-1 secreted by mESCs must be smaller than the criteria used in their later report. Nevertheless, we will focus on the proteins in this list to identify possible autocrine signaling in mESCs.

Table 1-1. Ligands secreted by mESCs: The data presented here are compiled from protein analysis [56, 57].

Protein name	Accession Number	gene symbol	Function	Mass	pI
lipase, hepatic	NM_012597	LIPC	Energy&metabolism	5627	8.40
dermcidin precursor	NM_053283	DCD	Energy&metabolism	11391	6.10
secreted protein of unknown function	NM_025424	SPUF	Energy&metabolism	18893	5.10
hydroxysteroid (17-beta) dehydrogenase 11	NM_053262	RETSDR2	Energy&metabolism	33145	8.90
VGF nerve growth factor inducible	NM_001039385	VGF	Energy&metabolism	68195	4.70
granulin	NM_008175	GRN	Energy&metabolism	68431	6.40
polynucleotide phosphorylase	NM_027869	1200003F12RIK	Energy&metabolism	86541	8.30
glucose phosphate isomerase 1	NM_008155	GPI	Energy&metabolism	62956	7.80
thymopoietin	NM_011605	TMPO	Membrane fraction transcription	76027	8.60
RIKEN cDNA 2210010C04	NM_023333	2210010C04RIK	Protein metabolism	27089	8.20
RIKEN cDNA 1810009J06	NM_023707	1810009J06RIK	Protein metabolism	27170	6.50
protease, serine, 20	NM_019974	KLK11	Protein metabolism	28327	9.00
RIKEN cDNA 1810018M05	NM_133705	LEFTB	Protein metabolism	33980	7.70
tolloid-like	NM_009390	TLL1	Protein metabolism	116740	5.80
insulin degrading enzyme	NM_031156	IDE	Protein metabolism	118438	6.10
small inducible cytokine subfamily E, member	NM_007926	SCYE1	Protein metabolism	34318	8.60
tyrosyl-tRNA synthetase	NM_134151	YARS	RNA metabolism	59410	6.60
wingless-type MMTV integration site family, member 9B precursor	NM_011719	WNT9B	Signal transduction	38855	9.20
fibronectin 1 isoform 1 preprotein	NM_010233	FN1	Signal transduction	262656	5.50
alpha-2-HS-glycoprotein	NM_001622	AHSG	Other	40098	5.40
vitronectin precursor	NM_000638	VTN	Other	55099	5.60
coagulation factor VIII	NM_007977	F8	Other	267350	6.90
colony stimulating factor 1 isoform a precursor, macrophage colony stimulating factor	NM_007778	CSF1	Interleukin	60766	5.10
macrophage migration inhibitory factor	NM_010798	MIF	Cytokine	12667	6.80
apolipoprotein E	NM_009696	APOE	Transport	35887	5.60

Table 1-1. Continued

Protein name	Accession Number	gene symbol	Function	Mass	pI
DNA segment, Chr 10, ERATO Doi 214	NM_134007	D10ERTD214E	Uncharacterized	12260	9.20
natriuretic peptide precursor type C; natriuretic peptide precursor C	NM_010933	NPPC	Uncharacterized	13483	10.2
RIKEN cDNA 2900070E19	NM_028419	2900070E19RIK	Uncharacterized	16396	6.10
cystatin 10 (chondrocytes)	NM_021405	CST10	Uncharacterized	16668	7.60
arginine-rich, mutated in early stage tumors	NM_029103	ARMET	Uncharacterized	20817	8.30
transmembrane protein 4	NM_019953	TMEM4	Uncharacterized	21096	5.00
RIKEN cDNA 1010001M04	NM_029272	NDUFS7	Uncharacterized	24952	9.90
thyrotropin releasing hormone	NM_009426	TRH	Uncharacterized	29334	5.60
peroxiredoxin 4	NM_016764	PRDX4	Uncharacterized	31261	6.70
RIKEN cDNA 2810037C14	NM_026034	2810037C14RIK	Uncharacterized	33632	8.20
RIKEN cDNA 5730592L21	NM_029720	5730592L21RIK	Uncharacterized	40361	4.50
S100 calcium binding protein A6 (calcyclin)	NM_011313	S100A6	Bind Calcium	10101	5.30
histidine rich calcium binding protein	NM_010473	HRC	Uncharacterized	84428	4.60
acid phosphatase 6, lysophosphatidic	NM_019800	ACP6	Uncharacterized	43745	6.60
glia maturation factor, beta; DNA segment, Chr 14, ERATO Doi 630, expressed	NM_022023	GMFB	Uncharacterized	16883	5.10
S100 calcium binding protein A11 (calizzarin)	NM_016740	S100A11	Uncharacterized	11247	5.30
hepatoma-derived growth factor	NM_008231	HDGF	Uncharacterized	26376	4.80
interleukin-10	NM_010548	IL-10	Interleukin	18754	
interleukin-11	NM_008350	IL-11	Interleukin	21391	
interluekin-1α	NM_010554	IL-1α	Interleukin	30892	
Oncostatin M	NM_001013365	OSM	Growth factors	29983	
Stem cell factor	NM_013598.1	SCF, kitl	Growth factors	30514	
Vascular endothelial cell growth factor		VEGF	Growth factors		
Granulocyte chemotactic protein-2		GCP-2	Chemokines		
Interferon-inducible protein-10	M33266	IP-10	Chemokines		
chemokine (C-X-C motif) ligand 1	NM_008176	KC/GROα	Chemokines	8314	
Monocyte chemoattractant protein-1, chemokine (C-C motif) ligand 2	NM_011333	MCP-1/CCL3	Chemokines	16195	
Monocyte chemoattractant protein-3, chemokine (C-C motif) ligand 7	NM_013654	MCP-3/CCL7	Chemokines	10868	
chemokine (C-C motif) ligand 22	NM_009137.1	MDC/CCL22	Chemokines	10171	
Macrophage inflammatory protein-1β, chemokine (C-C motif) ligand 4	NM_013652.2	MIP-1β/CCL4	Chemokines	10037	
Macrophage inflammatory protein-2	P10889 NM_009140	MIP-2/CXCL2	Chemokines	10490	
Matrix metalloproteinase-9		MMP-9	Other		
Tissue inhibitor of metalloproteinase type -1		TIMP-1	Other		

Having identified the possible ligands secreted by mESCs, we then searched for membrane proteins expressed in mESCs. In particular, we are interested in receptor proteins that might be able to interact with the ligands identified previously. We found one research report that identified proteins localized on the plasma membrane of undifferentiated D3 mESCs, using a combination of cell-surface labeling with biotin, subcellular fractionation of plasma membranes, and mass spectrometry–based protein identification technology [62]. It was found in this study that about 19% of the cell surface proteins are receptor proteins. The list of receptor proteins detected in this study was updated to the appropriate mouse genes and presented here in Table 1-2.

Table 1-2. Protein receptors from important signaling cascades on the surface membrane of mESCs [62]

Signaling Pathway	Protein Name	Accession Number	Gene Symbol
EGF family	avian erythroblastosis viral (v-erb-B2) oncogene homologue 2	NM_017003	Erbb2
Ephrin	Eph receptor A1	NM_023580	Epha1
	Eph receptor A2	NM_010139	Epha2
	Eph receptor A4	NM_007936	Epha4
	Eph receptor B4	NM_010144	Ephb4
FGF	Fibroblast growth factor receptor 2	NM_010207	FGFR2
Hedgehog	Patched	NM_008957	Ptch
Interferon (IFN)	Interferon (alpha and beta) receptor 1	NM_010508	IFNR1
IGF	Insulin-like growth factor 1 receptor precursor	NM-000875	IGF1R
	Insulin-like growth factor 2 receptor	NM_010515	IGF2R
IL1	Interleukin 1 receptor accessory protein, membrane form	NM_008364	IL1Rap
IL6	Interleukin 6 signal transducer	NM_010560	IL6ST, GP130
	Leukemia inhibitory factor receptor	NM_010700	LIFR
	Ciliary neurotrophic factor receptor	NM_016673	CNTFR
Insulin	Insulin receptor	NM_010568	INSR
Notch	Notch gene homolog 3	NM_008716	Notch3
PDGF	Platelet derived growth factor receptor, alpha polypeptide	NM_011058	PDGFRa
Stem cell factor (SCF)	c-kit	NM_021099	Kit
TGF-β/BMP family	Bone morphogenic protein receptor, type 1A	NM_030849	BMPR1a
	Engoglin	NM_007932	Eng
Toll-like receptor (TLR)	Toll-like receptor 2	NM_011905	TLR2
VEGF	FMS-like tyrosine kinase 4	NM_008029	Flt4/VEGFR3
	Neuropilin 2	NM_003872	NRP2
Wnt	Frizzled homolog 2	NM_020510	Fzd2
	Frizzled homolog 10	NM_175284	Fzd10
G-protein coupled eceptor	Cadherin EGF LAG seven-pass G-type receptor 1	NM_009886	CELSR1
	Cadherin EGF LAG seven-pass G-type receptor 3	NM_001407	CELSR3
	CD97 antigen	NM_011925	CD97
	G protein-coupled receptor 56	NM_018882	Gpr56
	Latrophilin 1	NM_014921	LPHN1
	Latrophilin 2	NM_012302	LPHN2
	Parathyroid hormone receptor 1	NM_011199	PTHR1
Receptor tyrosine kinase	Protein tyrosine kinase 7 isoform A precursor	NM_002821	PTK7
	Receptor tyrosine kinase-like orphan receptor 2	NM_013846	Ror2

Table 1-2. continued

Signaling Pathway	Protein Name	Accession Number	Gene Symbol
Phosphatase receptor	Protein tyrosine phosphatase, receptor type, F	NM_011213	Ptprf
	Protein tyrosine phosphatase, receptor type, G	NM_008981	Ptprg
	Protein tyrosine phosphatase, receptor type, J	NM_008982	Ptprj
	Protein tyrosine phosphatase, receptor type, K	NM_008983	Ptprk
Other pathways	Podocalyxin-like	NM_013723	Podxl
	unc5 homolog (C. elegans) 2	NM_029770	Unc5h2
	Autocrine motility factor receptor	NM_011787	Amfr

Finally, we can map the list of ligands and the list of receptors together to identify possible ligand-receptor pairs involved in autocrine signaling among ESCs. Results of the analysis are presented in Table 1-3. Five ligands and nine receptors were identified to complete autocrine loops of four signaling cascades. The roles of these four autocrine loops are very broad and can be different in different cell types. Keep in mind also that cells usually have negative feedback loops to control and stabilize the overall cell state. For example, SHP1 phosphatase or SOCS proteins are used in JAK-STAT signaling pathway to inhibit the effect of the cytokine that may induce its target genes for too long a period. In order to confirm that these aucrine loops do in fact exist and function in mESCs, studies must be conducted to confirm expression of these proteins, investigate specificity of binding between these ligands and their associated receptors and finally identify their effects in our specific cell types. In general, these preliminary observations reveal that colony-colony interactions can in fact exist in mESCs, possibly due to signaling via these ligand-receptor pairs. To further substantiate the importance of colony-colony interactions in mESCs, we will present in the next section the autocrine signaling and its roles observed in mESCs.

Table 1-3. Receptor-ligand pairs expressed in mESCs: Functions and the associated signaling pathways for each molecule comes from ontology classification suggested in the mouse genome database[63].

Detected Ligand	Molecular Weight (Da)	Detected Receptor	Signaling Pathway	Observed function	Reference
SCF/Kitl	30514	SCFR/Kit	RTK	▪ cell differentiation ▪ chemotaxis ▪ Phosphorylation ▪ germ cell development ▪ protein amino acid autophosphorylation	64
IL-11	29983	IL6ST/GP130	Gp130/JAK/STAT	▪ Regulation of cell growth ▪ Tyrosine phosphorylation of STAT ▪ Immune response ▪ Response to heat	65 65, 66 65
OSM	21391	LIFR CNTFR			
VEGF (unknown form)	17-25K	Flt4/VEGFR3 NRP2 PDGFRa	VEGF-PDGF family	▪ Anti-apoptosis ▪ Angiogenesis ▪ Cell differentiation ▪ Cell migration	67, 68 67, 68 69
WNT9B	40401	Fzd2 Fzd10	Wnt	▪ Cell-cell signaling ▪ Organ morphogenesis	(Postulation) (Postulation)

1.6 Roles of autoregulatory signals observed in mESCs

Recent studies have shown that mESCs that are cultivated *in vitro* exhibit autoregulatory signals to regulate their fate decision. The first evidence demonstrated by Ogawa *et al.* showed that differences in cell plating density also affected colony forming efficiency of mESCs[70]. When mESCs were cultivated in serum-free medium supplemented with LIF, it was found that the colonies can only be formed when the cells are plated at high density. Such phenomena were however compromised when the cells were cultivated in medium containing 10% serum and LIF. The investigators also found that supplemented peptide factors such as ACTH allows colonies to form in serum-free medium at low cell plating density. The investigators hypothesized that mESCs may produce ACTH-like peptide factors that can affect colony forming efficiency in an autocrine fashion.

Similar phenomenon was observed by Yamame *et al.* when the group found that mESCs can survive and self-renew in serum-free medium supplemented with PD98059 and LIF only in high-density cell culture[71]. In this study mESCs expressing anti-apoptosis proteins were derived and were found to be maintained stably in serum-free medium supplemented with LIF. When the investigators supplemented PD98059, an inhibitor of ERK pathway, to the medium, PD98059 prevented differentiation of the wild-type mESCs in high cell-density culture. At low cell density, the wild-type cells underwent apoptosis, possibly due to inadequate intrinsic survival-promoting factors. It is therefore possible that an anti-apoptotic factor is present in the high-density culture, affecting survival of mESCs in an autocrine fashion similarly to the previous observation.

The role of autoregulatory processes was recently confirmed from the varying levels of self-renewal-associated proteins at different positions in the colonies[72]. Oct4 and nanog are important self-renewal markers present in undifferentiated ESCs. The expression level of phosphorylated STAT3 protein (pSTAT3) was used here to quantify signaling via JAK-STAT3 pathway. The investigators first observed that Oct4, pSTAT3 and nanog expression levels within the undifferentiated colonies were radially organized, independently of the exogenous LIF. It was found that such radial organization was due to a secreted, Jak-dependent, and non-LIF autocrine factor. Using inhibitors of Jak/gp130 signaling, the investigators showed that this autocrine factor promoted STAT3 activation and could temporarily buffer cells against exogenous LIF deprivation. This hypothesis was also confirmed in their most recent report. It was found that endogenously produced ligands can influence the timing of differentiation but is insufficient to maintain mESCs[73]. The LIF-pSTAT3 dose-response experiment from this study suggests that autocrine activity is still present and functional within the first 6 hours after the concentration of LIF is altered, but decreases gradually as time progresses.

The above observations have demonstrated how autoregulatory signals can affect the cell fate decision of mESCs, but we still do not know exactly how such autoregulatory signaling operates. Identification of the underlying autocrine factors will require testing with all candidate molecules, such as the ones presented in Table 1-3. Using conventional culturing of mESCs also gives us a complicated system to work with. The unpredictable interactions generated from random positioning of mESC colonies inhibit us from quantifying accurately the contribution of autocrine signaling in colony-colony interactions. A novel experimental approach that can help us control precisely the amount and direction of autocrine signaling between mESC colonies will therefore be useful. We will next discuss

some of the microtechnology techniques developed in the past decade to help manipulate cell microenvironments.

1.7 Manipulation of cell microenvironments with microtechnologies

Microtechnologies are engineering tools that are designed to help manipulate substances with micrometer-scale sizes. These technologies originated from advancement in CMOS fabrication where the process of making an electronic device can be broken down to basic fabrication steps such as deposition, photolithography and etching. Most microtechnological devices have therefore adopted some of these CMOS fabrication techniques along their evolution processes. Within the past decade, microtechnologies have extended into almost all disciplines, and one of the important reasons was that they have showed to exhibit phenomena that can hardly be achieved when using previously available methodologies. One of the disciplines that have rapidly picked up these tools is cell biology where microtechnologies help equip researchers with various tools to manipulate cells and their surroundings. Many of the recent efforts have used microtechnologies to create microenvironments that are unique to different cell types and to help interrogate how the cells may respond in such conditions. These types of microtechnologies have given us some insights on how to establish colony-colony interactions in embryonic stem cells later on.

We will discuss in the next section the prior microtechnologies designed to manipulate diffusive signals. These technologies are important for the investigation of paracrine/autocrine signaling between cells. In order for each cell to be cued and become committed to a certain cell fate, they must receive an appropriate amount of signal at an appropriate time. To satisfy these criteria, microtechnologies to modulate diffusive signals usually try to manipulate two parameters in the system: 1) strength of the signals, and 2) signal timing. While we may control the intensity of signals extrinsic to the cells, we cannot do so for cell-secreted signals. For such scenarios, we control signal intensity by varying space between the source and the target cells or change the cell number. To reflect the practical aspects of the technologies, we will categorize the prior work into two groups: 1) technologies that regulate signals by controlling cell position only and 2) technologies that can modify the signals dynamically in both space and time.

1.7.1 Modulating diffusive signals spatially with cell patterning

Cell patterning techniques are the commonly used microtechnologies to manipulate cell position and cell shape. In the study of paracrine or autocrine signaling, we are interested to investigate the role of diffusive signals secreted by the source cells on the target cells which are the neighboring cells in the case of paracrine signaling or on the secreting cells themselves in the case of autocrine signaling. Most of the time, the secreted molecules from the cells are limited and cannot be extracted from the medium in a large enough quantity. In this scenario, cell patterning can provide a controllable platform where we can lay down the cells of our interest on the substrate that we want. Two approaches can be used to pattern cells. We can pattern cells by first patterning ECM that the cells will adhere to and then add the cells later, or we can coat ECM everywhere and manipulate cells to the position where we want (Figure 1-4).

The first cell-patterning approach relies on surface modification. The substrate surface must contain both an area where cells can adhere (adhesive region) and the area where cell adhesion is prohibited (non-adhesive region) (Figure 1-4A). We can modify the

substrate to contain both adhesive and non-adhesive molecules by adsorbing ECM onto the substrate directly or indirectly via the intermediate molecules. First, for direct ECM adsorption, the efficiency of the process relies heavily on the chemical compatibility of the substrate and the ECM, specifically whether their wettability and charges are complementary[74]. As an example, we will look at two commonly used substrates for cell culture, polystyrene and glass. Most proteins can adsorb readily to polystyrene while glass can be silanized with an aliphatic silane to promote its hydrophilicity[74]. The main drawback of direct adsorption is that cell patterns generated from this method can degrade over time usually when the cells are cultivated later in serum-containing medium. Degradation of the patterns are caused by multiple reasons including degradation of the adhesive or non-adhesive molecules, adsorption of adhesive proteins in medium to non-adhesive regions, or active remodeling of ECM by the cells[75]. An alternative approach that can help limit ECM degradation is to use indirect ECM adsorption. To implement this technique, self-assembled monolayers (SAMs) of functionalized alkane thiols are used to promote or inhibit protein adsorption on the substrate. Thiols can bind strongly to gold-coated substrates. Functional groups such as $-CH_3$ or the polar groups -COOH, -OH, or $-(OCH_2CH_2)_6OH$ are used to fine-tune substrate wettability to inhibit or promote ECM adsorption[76].

For both direct and indirect ECM adsorption, a technique called microstamping is one of the widely used methods to transfer ECM or non-adhesive molecules from the stamp containing the desired pattern to the substrate[77]. The ECM can also be delivered onto the substrate with the desired structural shape using stencil patterning[78], microfluidic patterning[79] and photolithography[80]. The adhesive molecules that are commonly used are collagen, fibronectin, laminin, and gelatin. We can inhibit cell adhesion using: 1) carbohydrates such as agarose[81], mannitol[82], and hyaluronic acid[83], 2) proteins such as albumin[78] and 3) synthetic polymers such as pluronic[84], poly-(ethylene glycol)[85], and polyacrylamide[86]. In addition to the ECM adsorption methods, adhesive molecules can be linked permanently to the substrate via covalent linkage. A short peptide sequence such as the RGD which can promote cell adhesion may be functionalized to alkane thiols that can be stamped and irreverably bound to a bold-coated substrate[87]. One can therefore engineer a substrate containing selective, permanent regions for cell adhesion.

The second cell-patterning approach is to physically manipulate cells to the desired location (Figure 1-4B). Most of the time, we will need to coat the substrate first with ECM to promote cell adhesion. For adherent cells that are less sensitive to substrate such as fibroblasts, we may not need to coat the substrate at all if the substrate can already adsorb ECM secreted from the cells. Different approaches can be used to manipulate cells to achieve the desired patterned. One approach simply uses physical barriers to prevent cells from adhering to certain regions of the substrate. These techniques includes stencil patterning[78, 88] and microwells[89]. Both techniques are similar except that stencil patterning does not limit cells to grow only within the opening region. After the stencil is removed, the cells can grow out of the patterned area if desired by also coating ECM in the area underneath the stencil. The issue that we might experience for both methods is bubble formation inside the microwells and the opening region of the stencil. To remove bubbles in the microwells, we can submerge the device underneath carbon dioxide gas phase while adding in liquid. Since carbon dioxide can dissolve quickly into water, bubbles created from carbon dioxide will disappear rapidly[89]. The second approach to manipulate cells is to use physical forces. We can apply the force directly to each cell and move the cell around, or fabricate an active substrate surface that can generate forces to trap or push the cells out of

the substrate plane. Some of the previously developed techniques in this category include optical tweezers[90, 91] and dielectrophoresis traps[92, 93].

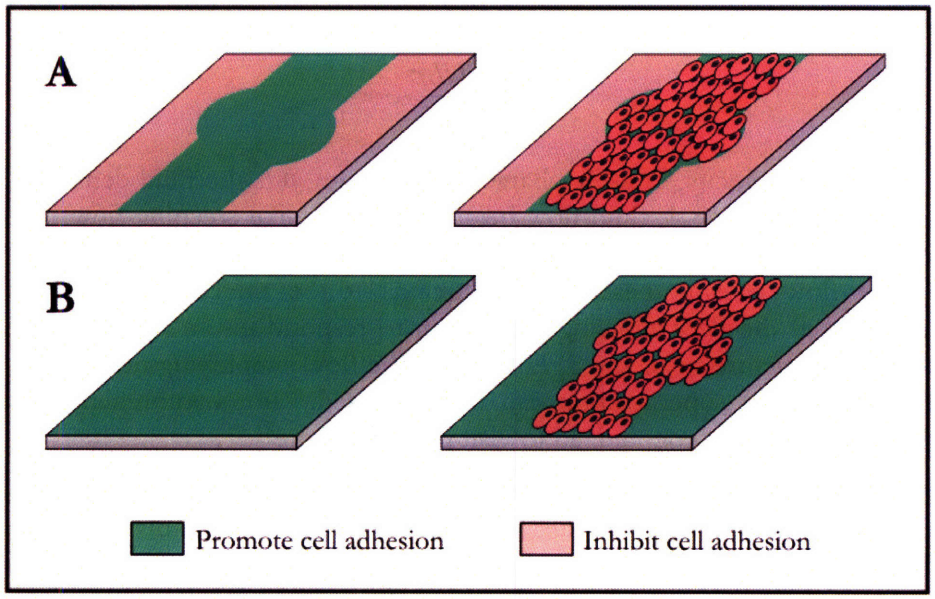

Figure 1-4 Cell patterning methods: A) Pattern ECM first and then have cells choose where to adhere and. B) Pattern ECM everywhere but later manipulate cells to give the designed shape.

1.7.2 Controlling diffusive signals spatiotemporally with microfluidics

Many biological processes such as embryo development and organogenesis are controlled by multiple cuing signals that are both space and time dependent. To mimic such complicated and highly dynamic systems, we require technologies that allow us to manipulate the signals with complete degree of freedom. Microfluidic technology is one such technology that has been used extensively in the past few years to satisfy this need. Three advantages are achieved with microfluidic technology. First, it can generate concentration profiles of diffusive molecules in any spatially varying shape[94, 95]. Such flexibility is critical and important for movement of highly motile cells like neutrophils. Using microfluidics, it was shown that neutrophils are highly sensitive to the shape of the chemokine gradients[96]. These observations are very unlikely observed using conventional methods that can generate only diffusion-based chemical gradients. Second, gradients of multiple diffusive molecules can be generated simultaneously without losing the controls over gradient shapes on each diffusive molecule[95]. An example of a biological process that requires such complicated cuing signals is the development of Drosophila embryos[97]. Third, temporal adjustment of concentration profiles can be conducted in real-time with microfluidics. This option is very useful when we want to study how sensitive the cells are to an abrupt change of cueing signals. This type of study was performed to investigate the propagation of epidermal growth factor in a single cell[98].

Microfluidic technologies earned most of their benefits from the nature of the fluid flow occurring in microfluidic devices where the size of the fluid channel is small. This type of flow is called creeping flow or Stokes flow. Creeping flow occurs when the length scales and the velocity of the fluid are small, and/or the viscosity of the fluid is extremely high. In

the macroscopic world (the length scale is large), creeping flow occur mostly when the viscosity of our fluid is large, such as that of lubricating oils or polymer melts. A parameter that is used often to approximate the overall effects of the flow is the Reynolds number, defined as

$$\mathrm{Re} \equiv \frac{UL\rho}{\mu}, \tag{1.1}$$

where U is the fluid velocity, L is the characteristic length, ρ is the fluid density and μ is the fluid viscosity. When Re<<1, fluid flow begins to behave like creeping flow. The features of creeping flow that are useful for manipulation of diffusive signals include 1) laminar nature of the flow causing nearby fluid streams to be mixed only via diffusion, 2) pseudosteadiness of the flow allowing the system to respond instantaneously to changes in fluid velocity and pressure field, and 3) linearity of the flow simplifying fluid analysis because analytical tools such as superposition can now be used. For comprehensive reviews of creeping flow, the reader is encouraged to visit prior literature[99, 100].

As we have discussed previously in §1.5 and §1.6, there are many possible molecules that may underlie interactions among ESC colonies, and each individual molecule will potentially play unique roles on the cell fate of ESCs. We have discussed extensively above how microtechnologies can be designed to engineer microenvironments, specifically the ones that are caused by diffusive, soluble signals. Instead of analyzing colony-colony interactions from the bottom up by identifying all molecules and mechanisms necessary, we hope to use microtechnology to interrogate our system at the system level and eventually rule out some of the candidates molecules that are not relevant to the physical characteristics of the system.

1.8 Device overview

The ultimate goal of this thesis is to examine whether and how colony-colony interactions may affect cell fate decision of ESCs during *in vitro* cultivation. Based on the possible autocrine factors we identified above, these molecules were observed to play important roles in cell proliferations and movement of ESCs as well as other cell types such as hematopoitic progenitor cells[57, 61]. We will therefore determine first whether colony growth and colony motility are influenced by colony-colony interactions. We will attempt to simulate colony-colony interactions by varying diffusive transport between two colonies. Our fundamental assumption is that varying such transport between two colonies will vary the concentration of any autocrine ligand produced by one colony that is sensed by the other colony. If colony-colony interactions do occur, we hope that varying signaling in time and space will result in variations in observed behavior. We will compare the behavior of colonies that are cultivated in the microenvironment with and without these putative colony-colony interactions. mESC colonies will be patterned on the substrate using stencil patterning technique. We chose stencil patterning because the colonies will be able to grow and expand normally on the substrate after the stencil is removed, unlike the other patterning techniques that tend to limit cell growth within the adhesive region. Stencil patterning was used previously in a similar investigation, to study the motility of endothelial cells[78]. The investigators first patterned endothelial cells on the substrate where the stencil defined the shapes of the cells. After the stencil was removed, cells that used to be enclosed by the stencil can now crawl out of the patterned region, allowing the study of cell migration.

In our study, we will also observe any changes in colony behavior as the intensity of colony-colony interactions vary. We can control the interaction intensity by two means, space or time. We will assume that the production of diffusive signals from the colonies is constant. As we increase the inter-colony spacing, the intensity of the signals will decrease for a fixed incubation time (Figure 1-5A). On the other hand, if we keep the distance between the two colonies fixed and vary only the time for diffusion, the diffusive signals will begin to accumulate around the colonies (Figure 1-5B). Another important way to control the global intensity of the diffusive signals is to use cultivating medium that contains the same diffusive signals. Depending on the intensity of the signals in the medium, we may strengthen or disrupt the effect of any colony-colony interactions completely. As we will discuss in more details in §2.2, we will perform our experiment in different cultivating media to find the conditions where the roles of colony-colony interactions are most dominant.

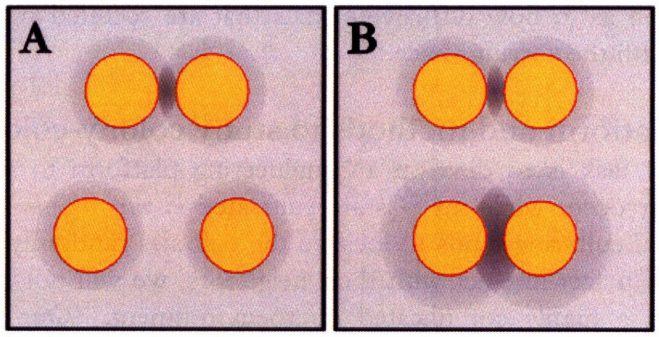

Figure 1-5 Controlling intensity of colony-colony interactions: by varying space (A) or time (B).

1.9 Thesis overview

We will discuss in Chapter 2 the experimental designs of the study and also present an analytical model of colony-colony interactions in mESCs that will give us some insight into how diffusive signaling may evolve with space and time. One of the intrinsic natures of biological systems is their stochastic behavior. In order to observe and be able to generalize the behavior of mESC colonies, we need to perform the study on a large enough population size. We have developed methods to collect and analyze the effect of colony-colony interactions at multi-timepoints from mESC colonies that were patterned at multiple locations. Chapter 3 and 4 will cover the materials and methods used for the study and explain the techniques we developed to collect and analyze colony data. We will present in chapter 5 the observed colony behaviors that are either exposed or not exposed to potential colony-colony interactions in different cultivating media with varying inter-colony spacing and incubation time. Summary and the future directions of our study will be presented in chapter 6. For the readers who might find our software implementation useful, we have compiled all MATLAB functions we used in the appendix section of this thesis.

CHAPTER 2: EXPERIMENTAL DESIGN & MODELING

Having learned about microtechnological tools that can be used to manipulate cell microenvironment, we will discuss in this chapter the engineering tools as well as our experimental designs we developed to study colony-colony interactions in mESCs. First, we will discuss the cell-patterning technique, the evolution and reasoning of the designs we chose to fabricate mESC colonies on the substrate. We will then explain our experimental designs to determine whether mESC colonies can interact with each other. Our last goal is to observe the effect of changing colony-colony spacing on mESC self-renewal. At the end of the chapter, we will go over the mass-transport analysis of colony-colony interactions to obtain some intuition as to how diffusive signals that are secreted from the colonies may develop over time with the varying space.

2.1 Develop a platform and methods to study colony-colony interactions

Our primary task is to develop an engineering platform to mimic colony-colony interactions that may occur while mESCs are cultivated *in vitro*. This platform is necessary because conventional culturing tends to localize the colonies randomly on the substrate. If mESC colonies can in fact interact with their neighbors, we will not be able to detect the interactions in such a highly complicated microenvironment. Our goal is therefore to fabricate mESC colonies with the most basic colony-colony interactions. We will use stencil cell patterning to evenly position multiple groups of ESC colonies on the substrate; each group will contains two to three colonies to create the most basic interactions. The platform will contain colony groups with varying inter-colony spacing, designed to investigate the effects of colony-colony interactions at varying length scales.

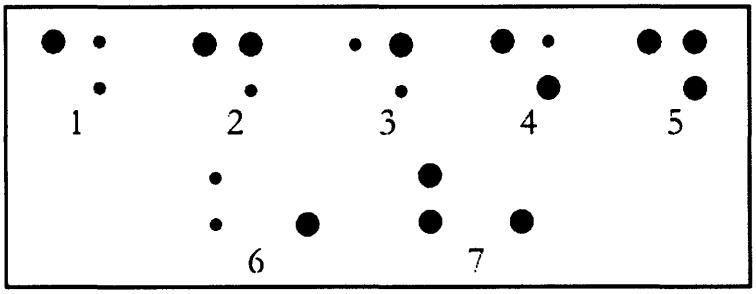

Figure 2-1 Three-colony design: The role of colony-colony interactions are observed by comparing the colony behaviors of two colony designs with only one uncommon colony parameter.

Our first colony design was the three-colony setup with varying inter-colony spacing and two choices of colony sizes, 50 microns or 100 microns in diameters (Figure 2-1). The reasoning behind this design was to investigate the effect of colony-colony interactions by comparing colony behaviors of two similar colony designs with only one varying parameter at a time. For example, we can compare pattern #2 and pattern #3 to examine the effect of colony size on the colony-colony interactions. Comparison between pattern #5 and pattern #7 is used to study the role of inter-colony spacing. While the design seems to provide

sufficient combinations to observe the role of colony-colony interactions with varying inter-colony spacing and colony sizes, our preliminary study shows that the three-colony designs are too complicated for us to postulate easily the mechanism of interactions. Some of the three-colony results are presented in Chapter 5.

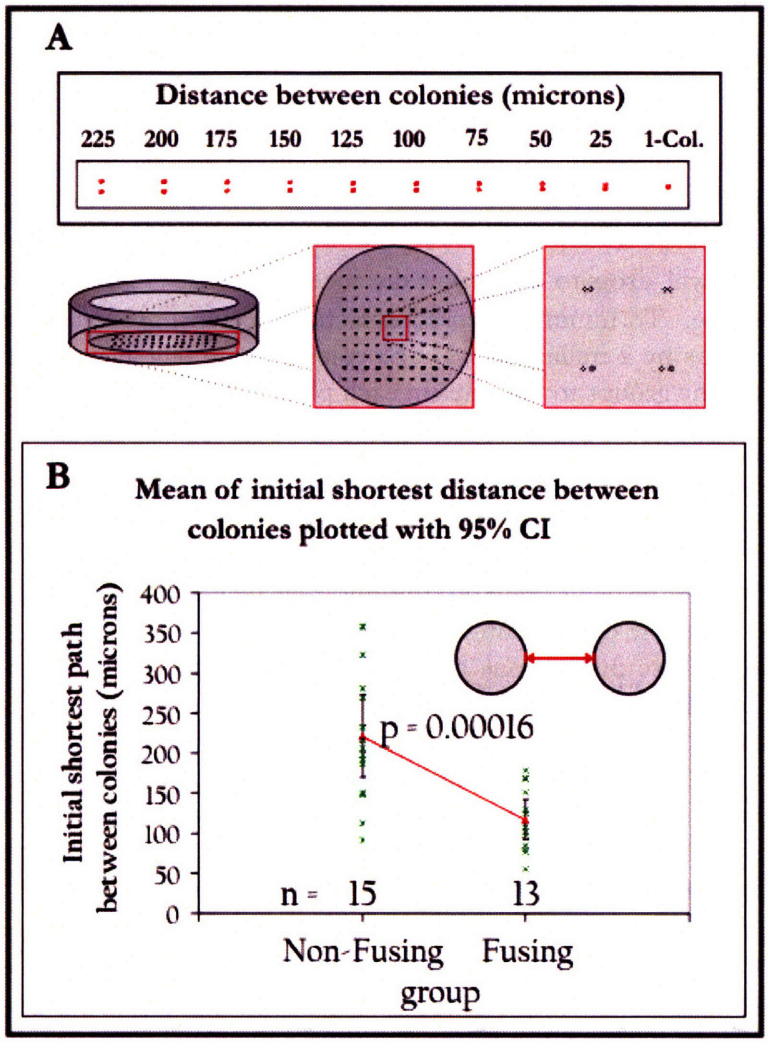

Figure 2-2 Stencil design: A) Geometry of the stencil spacing that is based on our preliminary study that was done in serum-containing medium and monitored for three days (B). The colonies that are listed not fusing here remain separated at the end of the experiment.

Based on the observation from three-colony design, we modified our final colony design to have the most basic colony-colony interactions, composed of only two colonies per each colony group (Figure 2-2). The platform also has colony groups with varying inter-colony spacing and only one size of colonies, 100 microns in diameter. The varying inter-colony spacing was designed to observe the graded effect of diffusion as the distance between colonies increases. We chose the range of inter-colony spacing based on our preliminary result performed in serum-containing condition. CCE mESCs were patterned in groups of three colonies using the first-generation platform as discussed previously. For the colony sites that have small colonies (50 microns in diameter) in the design, many groups did not have small colonies patterned, instead forming colony groups with two large colonies

(100 microns) instead. These two-colon groups were cultivated along with the three-colony groups in serum-containing medium for three days. After the experiment, we observed that some of these two-colony groups ended up combined with their neighboring colony. Others were left unfused. When we analyzed the initial inter-colony spacing between the two colonies, we found that the initial spacing between colonies that ended up fusing was significantly smaller that the spacing of the unfused two-colony groups (Figure 2-2B). The threshold length scale for colony fusion was observed to be approximately 140 microns. We therefore try to span the inter-colony spacing to cover both ends equally, ranging from 25 microns to 225 microns. Single-colony patterns with the same colony size and shape are also included in the platform as the control group to mimic a lack of colony-colony interaction. Leukemia inhibiting factor (LIF) is one of autocrine factors that are important for self-renewal of mESCs[101, 102]. LIF has a diffusivity of about $1\text{x}10^{-7}$ cm^2/s[103]. In one day, LIF concentration will drop to 10% at a distance of $2.3\sqrt{Dt} = 2.1$ mm from any fixed-concentration source. To minimize cross-interaction between groups, we separate any two nearby colony groups by 2 millimeters. Each colony group will also be repeated ten times, giving the total colony groups to 100 sites in each platform.

Another important experimental design is how to determine whether the two colonies within each colony group are in fact interacting. To view this problem from the analogy of human communication, one will be able to decide instantaneously whether two people are communicating if the language of that conversation is also known to the observer. In the more difficult scenario, the observer may not understand the language or, in the context of colony-colony interactions, may not be able to monitor the diffusive signals. Therefore, these interactions can only be predicted, based on the behavior of the two individuals or colonies. We have discussed previously that autocrine signaling can affect both proliferation and self-renewal of ESCs. We also have observed the motility of ESC colonies that tend to fuse with each other at high cell density. Since changes in self-renewal markers will require more than three days to become apparent, we cannot determine the effect of colony-colony interactions instantaneously with self-renewal changes. Colony expansion and movement can be monitored in real-time and therefore are the two outputs that we chose to use to investigate colony-colony interactions. Based on the previous observations on the macroscopic effect of autocrine signaling (§1.6), we hypothesized that colony-colony interactions will influence colony proliferation also at the single-colony level or cause biased colony movement towards or against the neighboring colony.

In order to investigate changes in proliferation and movement of multiple ESC colonies over time, we decided to monitor and infer the changes using microscopic image analysis of the colonies which will allow us to monitor colony shape and movement in real-time if required. The overall proliferation of each colony can be evaluated from its contour changes. By calculating the area and determining the centroid of the contour, we can approximate how colony growth and motility is changed due to the imposing colony-colony interactions. We also attempt to develop a method to monitor changes in local motion and growth within each colony that cannot be distinguished merely by colony contours alone. Speckle imaging is a technique to help investigate embryo segmentation used in developmental biology. The idea is to stain multiple locations within an embryo and to monitor the movement of these stained spots during the embryo development. We will discuss our preliminary results using speckle imaging in §5.3.1. Figure 2-3 illustrates the

hypothesis of how speckle imaging may be used to identify growth at different local spots in an ESC colony.

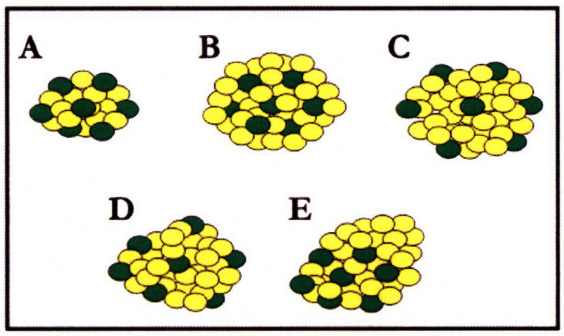

Figure 2-3 Models of local proliferation based on speckle imaging: Speckle imaging of the colony allows monitoring of local proliferation of an individual colony. The illustration shows different possibilities of the colony growth predicted by speckle imaging: A) the original colony, B) colony with growth only at the colony boundary, C) colony with uniform growth, D) colony with faster growth on the right side and E) colony with local, rapid growth towards the top-right corner.

2.2 Determine whether mESC colonies can interact with each other

The patterning techniques and the colony designs we developed previously allows us to create a microenvironment where only uncomplicated colony-colony interactions will be present. This colony platform will therefore help us visualize and predict the underlying causes of colony-colony interactions in mESCs. While bulk experiments demonstrated that self-renewal and colony survival are both influenced by autoregulatory signals created from the mESCs themselves (§1.6), our aim is to determine whether such autoregulatory signaling may contribute to colony-colony interactions at the single-colony level. To answer this question, we will design an experiment to compare the behaviors of mESC colonies that have been cultivated in the microenvironment with or without colony-colony interactions. This experiment can be physically set up by patterning mESC colonies in groups of two colonies and one colony, respectively. We will also vary inter-colony spacing to observe the colony behaviors at varying intensity of colony-colony interactions if colony-colony interactions actually exist. As we will discuss in more detail in the last section of this chapter, we can also potentially manipulate the strength of diffusive signals for a fixed length scale by controlling the duration before the medium is replenished. By varying the concentration both spatially and temporally we hope to determine whether colony-colony interactions also play a role on the growth and motility of mESCs.

As discussed in §1.8, we must also keep in mind that the extrinsic diffusive signals from the medium may also interfere with the intrinsic, cell-secreted signals (Figure 2-4). To resolve this issue, we will perform the experiments as described previously in different media mixtures. The types of media that we would like to observe and compare the effects of colony-colony interactions are: 1) serum-containing medium with LIF, 2) serum-containing medium without LIF, and 3) serum-free medium supplemented with LIF and BMP4. Serum already contains multiple soluble signals. By comparing the colony behavior cultivated in the medium mixtures with and without serum, we hypothesize that the effects of colony-colony interactions will be differently observed due to multiple growth factors in serum that may change the baseline intensity of the signaling ligands. We compared the colony behaviors in

the cultivating conditions with and without LIF to determine whether LIF may be the signaling molecule that underlies colony-colony interactions. If LIF in fact underlies colony-colony interactions, we may observe different colony behaviors from the two experiments.

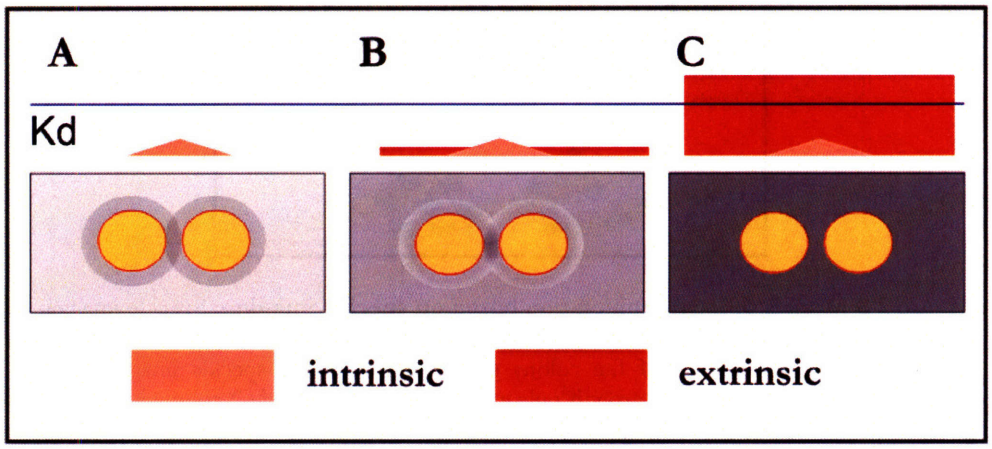

Figure 2-4 Interference of colony-colony interactions from the media: The cultivating medium may contain extrinsic diffusive signal that can interfere with the concentration gradient established by intrinsic signals. As the concentration of the extrinsic signal increases (from A to C), the effects of spatially-varying intrinsic signals may become less dominant.

2.3 Identify the roles of colony-colony interactions on self-renewal

Having identified whether ESC colonies can interact with one another, our final task is to determine preliminarily how any potential colony-colony interactions might affect the cell fate decisions of ESCs. Figure 1-2 illustrates at least three cellular-fate processes that are important for ESCs. Each process requires a separate set of assays to quantify the cell population that ends up in that particular state. In this thesis, we will attempt to monitor only self-renewal of ESC colonies and to determine whether cells within each colony will respond to any potential colony-colony interactions unanimously or individually. This information could therefore provide a first clue of whether heterogeneity within ESC populations is linked to colony-colony interactions.

2.4 Mass-transport analysis of colony-colony interactions

To help understand how diffusive signals evolve for varying inter-colony spacing and incubation time, we will develop an analytical expression and numerically solve for the concentration gradient of the signaling ligands using pseudo-steady state arguments. To begin the analysis, we will make the following assumptions.

1. Each ESC colony will be assumed to secrete a constant and uniform flux of ligands from its surface (N_o, moles m^{-2} s^{-1}). For simplicity of analysis, we will use spherical coordinates and assume that each colony has a hemispheric shape with radius a.

2. The autocrine ligands can bind to their receptors on the colony surface, described by:

$$R + L \underset{k_{off}}{\overset{k_{on}}{\rightleftharpoons}} R \cdot L, \tag{2.1}$$

where R is the receptor and L is the autocrine ligand. Assuming no internalization of receptor from endocytosis, we can describe the rate of change of receptors at the colony surface due to binding from:

$$\frac{dC_R}{dt} = -k_{on} C_R \, C_L\big|_{r=a} + k_{off} C_{R\cdot L} \tag{2.2}$$

where C_L is the concentration of ligand (moles/m^3), C_R is the concentration of free receptors (moles/m^2), $C_{R\cdot L}$ is the concentration of occupied surface receptors (moles/m^2), k_{on} is the binding rate constant (moles^{-1}m^{3}s^{-1}) and k_{off} is the dissociation rate constant (s^{-1}). The kinetics of ligand binding to its receptor can be described using the dissociation constant, K_d, which is defined as k_{off}/k_{on} (moles/m^3). Assuming also that the total number of receptors in the system is constant, the sum of bound and unbound receptors is therefore constant throughout the experiment and equal to $C_{R,total} = C_R + C_{R\cdot L}$. At equilibrium, we may estimate the receptor occupancy from:

$$\frac{C_{R\cdot L}}{C_{R,total}} = \frac{1}{1+\dfrac{K_d}{C_L}} \equiv ROR(\text{receptor occupancy ratio}). \tag{2.3}$$

3. The wall of the tissue culture dish cannot bind autocrine factors. We will also assume no flux through walls. We will assume that the size of the culture dish is infinitely large compare to the diffusive length scale during the time period we are interested.

4. We will use the following transport parameters for our further investigation. These data are the reported parameter values from interleukin-2 (IL-2) autocrine system[104].

Table 2-1 Model parameter values

Parameter	Values	
D	1x10^{-11}	m^2/s
$C_{R,total}$	10000	No/cell
a	10 x10^{-6}	m
K_d	0.7x10^{-11}	M
K_{on}	1.9x10^9	M^{-1}min^{-1}
K_{off}	1.4x10^{-2}	min^{-1}
N_0	300	No./min

The governing equation of the system is:

$$\frac{\partial C_L}{\partial t} = D\nabla^2 C_L . \tag{2.4}$$

The boundary conditions are:

$$\begin{aligned} &D\nabla C_L = -N_o + k_{on} C_R \cdot C_L\big|_{r=a} - k_{off} C_{R\cdot L}, \text{ on colony surface} \\ &C_L(\infty, t) = 0 \end{aligned} \tag{2.5}$$

We will now use these equations to solve for the concentration of ligand at steady state. We can rewrite equation (2.4) at steady state using spherical coordinates as:

$$0 = D\frac{1}{r^2}\frac{d}{dr}\left(r^2\frac{dC_L}{dr}\right). \tag{2.6}$$

Presenting the concentration of receptor-ligand using the total receptor concentration, we can rewrite the boundary conditions as:

$$\begin{aligned} &D\frac{dC_L}{dr} = -N_o + k_{on}C_R \cdot C_L\big|_{r=a} - k_{off}\left(C_{R,total} - C_R\right), \text{ on colony surface} \\ &C_L(\infty) = 0 \end{aligned} \tag{2.7}$$

The first boundary condition is coupled to the reaction on the colony surface via receptor concentration. In order to simplify the system, we will assume first that the diffusive time scale of the system is much smaller than the reaction time scale. This assumption allows us to solve for ligand concentration profile using fixed receptor concentration for the time scale that we are interested. The solution for equations (2.6) and equation (2.7) is:

$$C_L = -\frac{A_o}{r}. \tag{2.8}$$

We can solve for the constant A_o using the first boundary condition. Doing some algebra, we obtain:

$$\begin{aligned} \frac{DA_o}{a^2} &= -N_0 - \frac{k_{on}C_R A_0}{a} - k_{off}(C_{R,total} - C_R) \\ A_0 &= \frac{-N_0 - k_{off}(C_{R,total} - C_R)}{\left(\frac{D}{a^2} + \frac{k_{on}C_R}{a}\right)} \end{aligned}$$

$$\text{and } C_L(r) = \frac{N_0 + k_{off}(C_{R,total} - C_R)}{\left(\frac{D}{a^2} + \frac{k_{on}C_R}{a}\right)}\frac{1}{r}. \tag{2.9}$$

Having determined concentration profile for the time point where we assume fixed concentration of the receptors, we can now plug equation (2.9) back into equation (2.2) to determine how the concentration of receptors will vary with time.

$$\begin{aligned} \frac{dC_R}{dt} &= -k_{on}C_R\frac{N_0 + k_{off}(C_{R,total} - C_R)}{\left(\frac{D}{a^2} + \frac{k_{on}C_R}{a}\right)}\frac{1}{a} + k_{off}\left(C_{R,total} - C_R\right) \\ \frac{dC_R}{dt} &= \frac{\left(-k_{on}aN_0 - k_{off}D\right)C_R + Dk_{off}C_{R,total}}{ak_{on}C_R + D} \end{aligned}$$

which can be generalized to:

$$\frac{dC_R}{dt} = \frac{\beta C_R + \chi}{\delta C_R + \varepsilon}, \text{ where}$$
$$\beta = \left(-k_{on} a N_0 - k_{off} D\right), \chi = D k_{off} C_{R,total} \quad (2.10)$$
$$\delta = a k_{on}, \text{ and } \varepsilon = D.$$

To solve for C_R, we use the following integral formula:

$$\int \frac{dx+e}{bx+c} \partial x = \frac{bdx + (be - cd)\log(c+bx)}{b^2} \quad (2.11)$$

The solution of equation (2.10) is an implicit time-dependent equation for C_R:

$$\beta^2 t + \Phi = \beta\delta C_R + (\beta\varepsilon - \chi\delta)\log(\chi + \beta C_R) \quad (2.12)$$

We can solve for C_R in the above equation numerically using the parameters we defined earlier. By substituting the result we found for C_R is equation (2.9), we can approximate ligand concentration as a function of both space and time. Since the receptor concentration is spatially-independent, the function of ligand concentration will still be varying in space with 1/r. The time variation of ligand concentration will be governed by the receptor concentration function. Figure 2-5A illustrates the solution of C_R from equation (2.12), presented in the form of receptor occupancy ratio ($C_{R\cdot L}/C_{R,total}$). When the dissociation constant is greater, we observed lower occupancy of the receptors on the colony which agree with our intuition. Figure 2-5B shows the resulted plot of ligand concentration reevaluated with time-varying concentration of receptors. The concentration profile of the ligand shift upwards rapidly at the beginning of the process and starts to change more slowly as the binding of ligand and receptors approach steady state.

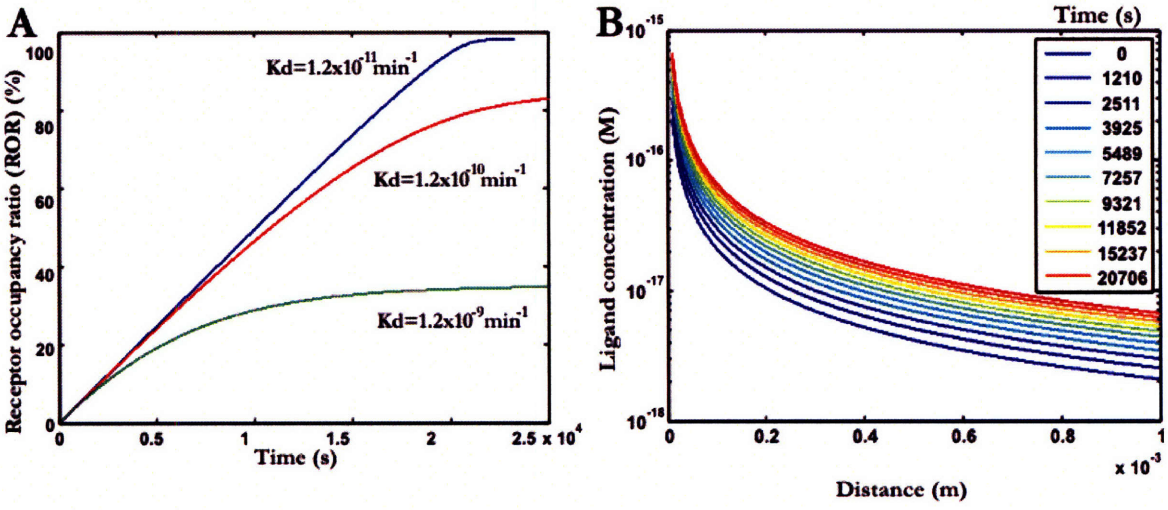

Figure 2-5 Autocrine modeling: A) Plot of receptor occupancy ratio with varying time for different dissociation constants. B) Resulting ligand concentration based on quasi-steady state assumption, and re-estimated using the time-varying receptor concentration solved above.

How far can soluble signal propagate away from the colony?

To answer this question, we will compare the propagation of the signal when there is no reuptake of ligands to the colony. The solution of this problem is simply

$$C_L(r) = \frac{N_0 a^2}{Dr}. \tag{2.13}$$

To compare the effective distance, we will determine the distance where concentration of the ligand is equal to K_d (i.e., the concentration at which half of the receptors are occupied). The solutions we obtain from both cases are:

1. For secreting colony without surface reaction:

$$r_{critical} = \frac{N_0 a^2}{DK_d} = \frac{a^2/D}{K_d a/N} a = \frac{\tau_{\text{diff}}}{\tau_{\text{secretion}}} a \tag{2.14}$$

2. For secreting colony with surface reaction, we can manipulate equation (2.9) to get:

$$r_{critical} = \frac{\left(N_0 + \frac{k_{off} C_{R,total}}{2}\right)}{\left(D + \frac{a k_{on} C_{R,total}}{2}\right)} \frac{a^2}{K_d}. \tag{2.15}$$

Figure 2-6 demonstrates the effects of different transport parameters on the critical length when we include ligand binding and when no ligand binding is allowed. The equation for critical length above is valid only at the distance greater than the colony radius. Figure 2-6A shows that the effects of autocrine signaling becomes stronger as secretion of ligands from the cells increases. In term of the strength of binding, the effect of autocrine is more evident as the binding rate constant increases (Figure 2-6B). When the dissociation rate constant is large, the autocrine effect diminishes, becoming like the case we allow no binding (Figure 2-6C). The critical length also depends strongly on the number of receptors available on its surface. When the number of receptors increases, the critical length quickly approach the colony radius (Figure 2-6D). In addition to controlling time and distance between colonies, it is clear from the analysis here that the strength of colony-colony interactions also depends significantly on how strong the ligand can binds to its receptors, the number of receptors available on the colonies as well as the amount of ligand secreted. Since we are not certain about the types of molecules that are underlying colony-colony interactions, we must be careful in choosing the distance between colonies and allow enough options of inter-colony spacing for the autocrine effects to be observed. In terms of prevention of cross-interaction between colony groups, we may used the parameters in Table 2-1 Model parameter values with the cell radius instead equal to the radius of mESC colony to help justify our choice of 2 millimeters between colony groups. We found that the critical lengths of the reported IL-2 system is in the order of 10^{-5} m. Even when the colony is set to produce ligand by 100 times the reported data, the critical length is still in the order of 10^{-4} m which is still an order of magnitude below the choice of distance between colony groups we chose (Figure 2-6D). This analysis thus justifies our selected distance between colony groups.

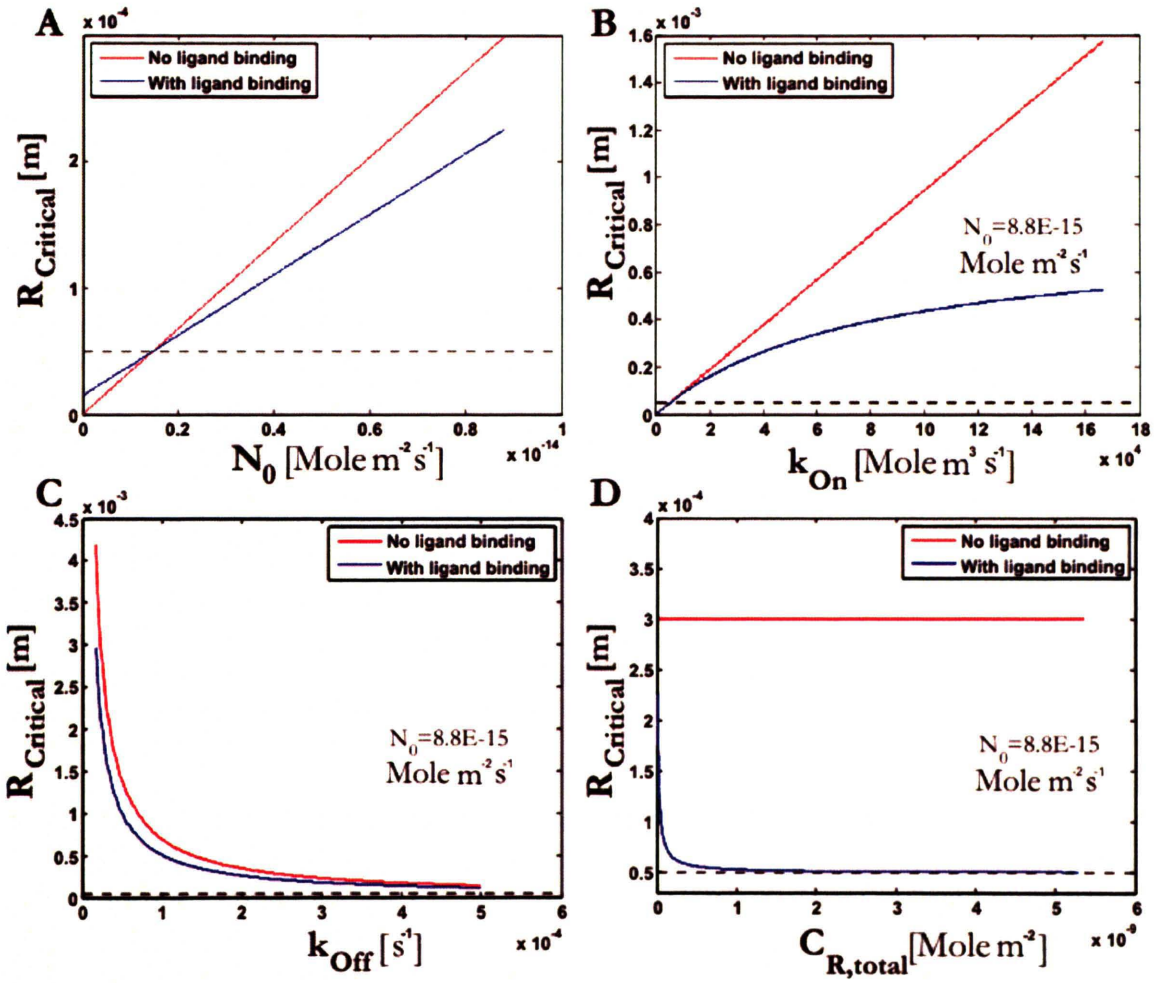

Figure 2-6 Effects of different transport parameters on critical length: Critical length for varying A) Flux, B) k_{on}, C) k_{off}, D) $C_{R,total}$. Unless stated, the parameters used for calculation are the same as those in Table 2-1. The radius (a) used is the approximated radius of our patterned mESC colony which is approximately 50 microns and shown in all plots as dotted lines.

How strong can the soluble signals be?

While designing the platform for the study of colony-colony interactions, we might also want to know the maximum strength of the diffusive signals that can be generated by the cells. If this concentration is already much smaller than the concentration that the cells can respond to, we will therefore need to redesign the system to elevate the background concentration in the medium to be within the range that the cells are responsive. The maximum intensity of the signaling ligand is limited by the case where the colony simply secretes a constant flux into the medium and does not bind any ligand. We can simply evaluate for this concentration using equation (2.13). Therefore, the maximum concentration is:

$$C_{\max} = \frac{N_0 a}{D}. \tag{2.16}$$

If we now allow ligand binding at the colony surface, we can substitute colony radius, a in equation (2.9) to get:

$$C_{\max} = \frac{N_0 + k_{off} C_{R,total} ROR}{\frac{D}{a} + k_{on} C_{R,total} (1 - ROR)}, \tag{2.17}$$

where ROR is the receptor occupancy ratio at a specific time point. We can calculate for ROR as demonstrated in Figure 2-5A. For the IL-2 system with the cell radius of 10 microns, the maximum concentration without ligand binding is 6.6 μM which is still 5 to 6 orders of magnitude larger than K_d. When binding is allowed, the maximum concentration is 6.2 μM at the cell membrane using final ROR of 45%. However, as we have seen in Figure 2-5B, the concentration of IL-2 drops abruptly when we move away from the cell membrane. The analysis here demonstrates that IL-2 system can potentially exhibit autocrine effects if the appropriate length scale is chosen.

CHAPTER 3: MATERIALS AND METHODS

3.1 Cultivating murine embryonic stem cells

ESC-CCE cell line was cultivated in feeder-free condition with cultivating medium consisting: Dulbecco's modified Eagle's medium (DMEM) (Cat#11960044, Invitrogen, Carlsbad, CA) supplemented with ES-qualified fetal bovine serum (Cat#16141079, Invitrogen, Carlsbad, CA), 4 mM L-glutamine (25030081, Invitrogen, Carlsbad, CA), 100 μM ß-mercaptoethanol (Cat#M7522, Sigma,St. Louis, MO), 1 mM non-essential amino acids (Gibco), 50 U/mL penicillin, 50 μg mL streptomycin (15140122, Invitrogen, Carlsbad, CA), and 500 pM leukemia inhibitory factor (LIF, ESGRO, Chemicon, Temecula, CA). We will call this medium serum-containing medium throughout this thesis.

For the study of colony-colony interactions, we also observe colony behaviors in other cultivating media. First, we removed LIF from the serum-containing medium to observe the role of LIF on colony-colony interactions. We will refer to this medium as serum-containing medium without LIF. Another type of medium used is a defined serum-free medium. We used a commercially available, pre-mixed medium (ESGRO Complete clonal grade medium, Chemicon). In brief, this medium contains DMEM/F12 basal medium, N2 supplement, B27 supplement, Murine LIF, and BMP4[37]. We will refer to this medium as serum-free medium.

3.2 Patterning embryonic stem cell colonies with stencils

Elastomeric stencils were first used for cell micropatterning by Folch *et al*[88]. and were applied for cell spreading study of endothelial cells in Ostuni *et al*[78]. Stencil cell patterning allows normal colony expansion, and the cells can be patterned in almost any desirable shape. In this study, we used stencil patterning to localize mESC colonies on the culturing substrate (tissue culture dish with Nunclon delta surface).

3.2.1 Stencil fabrication

We modified the fabrication of stencils based on previously published work[78, 88]. A master wafer with posts of the desired shapes must first be fabricated using photolithography. Silicon wafers with polished backsides were used, and the wafer was first cleaned with piranha (mixture of 98% sulfuric acid and 30% hydrogen peroxide in a volume ratio of 3:1) for 15 minutes to promote adhesion with photoresist later on. After rinsing and spin-drying the wafer, we then dehydrated the silicon wafer at 130°C for 30 minutes. SU-8 2050 photoresist (Microchem) was poured carefully onto the wafer. The required volume of SU-8 is 1-2 ml. per each inch of the wafer diameter. The wafer spin speed was held at 500 rpm/s for 10-15 second to spread the resist to cover the wafer uniformly. We then ramped the spin speed to 1650 rpm at 300 rpm/s, and spun for 30 s to yield feature heights of 100 μm. We then prebaked the wafer on a hot plate at 65 °C for 4 minutes, immediately shifted to 95 °C for 20 minutes, and finally ramped the temperature down to 65 °C. After prebaking, we expose the wafer to a UV doze of 10 mW/cm^2/sec for 24 seconds (total exposure energy of 240 mJ/cm^2). The finished master wafer is shown in Figure 3-1A. We then processed the post exposure bake (PEB) by first warming the wafer at 65 °C for 3 minutes, heating at 95 °C for 9 minutes and finally ramping it down to 65 °C. After PEB process, the wafer was developed by submerging in 1-methoxy-2-propanol Acetate for 15 minutes or until all

unexposed resist was removed. The wafer was rinsed with isopropanol and immediately air-dried using pressurized nitrogen or air. To prevent adhesion of master wafer and the molded silicone, we silanized the master wafer by exposing the wafer to vaporized (tridecafluoro-1,2,2-tetrahydrooctyl)-1-trichlorosilane in a vacuum desiccator for at least 6 hours.

After silanizing the master wafer, stencils can be fabricated by applying uniform pressure to fabricate a thin membrane of silicone with micrometer-sized holes in it. Polydimethylsiloxane (PDMS) was prepared by mixing the base monomer and the curing agent with a mixing ration of 10:1 by weight. After mixing the two components well together and degassing it, we carefully poured PDMS to the center of the wafer, tilted and rotated the wafer to spread PDMS to cover the whole wafer. A transparency film was then placed on top of PDMS to prevent sticking of the cured PDMS to the metal plate. To prevent bubble formation between the transparency film and the PDMS, we folded the transparency and slowly placed it on PDMS from one edge of the wafer. We then clamped the wafer between a stack of metal plates, rubber sheath and glass plate on a hot plate as shown in Figure 3-1B. After heating the pressurized wafer with PDMS for 2 hours at 65 °C, a cured PDMS membrane was obtained. Since the PDMS membrane is very thin and deformable, we made an annular ring of PDMS and glued it on top of the membrane for ease in handling. To attach the annular ring on the PDMS membrane, we simply painted uncured PDMS on the ring, placed it on the membrane and reincubated the membrane with the annular ring at 65 °C for two hours. After cutting around the annular ring and carefully removing it from the master wafer, we obtained the stencil as shown in Figure 3-1C.

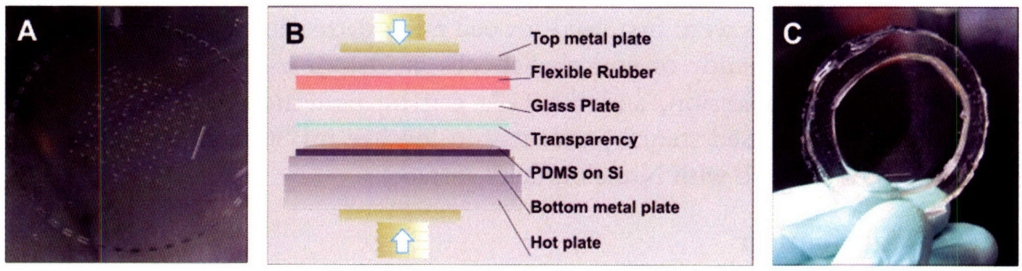

Figure 3-1 Stencil Fabrication: A) Microfabricated master wafer using photolithography. B) Stack of materials required to uniformly pressurize and cure PDMS on the wafer. C) Finished stencil that is already bound to a PDMS annular ring.

3.2.2 Patterning procedures

To use stencils for cell patterning, we need to make sure first that any leftover curing agent in the PDMS is removed and the stencil is sterile. We adapted the cleaning process from the published protocols [78, 105]. In brief, we rinsed the stencils in the series of solvents: acetone, isopropanol, 80% ethanol and water, each for 12 hours. We then air-dried the stencil immediately and autoclaved it for sterility. The stencil is now ready for cell patterning. The stencil was first placed on the desired culturing substrate. To pattern the cells precisely on the substrate, it is critical that we have conformal contact of the stencil and the substrate. We ensured complete conformal contact by adding a few drops of ethanol on the substrate and carefully place the stencil down. We then put the attached components in a vacuum desiccator which vaporized and removed ethanol from the stencil, leaving stencil fully attached to the substrate. Depending on the cell types, it may be necessary to coat

proteins on the substrate before loading the cell suspension to the stencil. For mESCs, it is conventional to culture the cells on a gelatinized substrate. We first coated the gelatin inside the hole by loading gelatin (0.1% in water, Cat#ES-006-B, Chemicon) in the stencil and waited for 30 minute to have the gelatin adsorbed to the polystyrene substrate. The region underneath the PDMS membrane can be coated with gelatin later after the cells already adhered to the substrate and the stencil was removed. This method of gelatin coating can give uniform gelatin coating as shown in Figure 3-2.

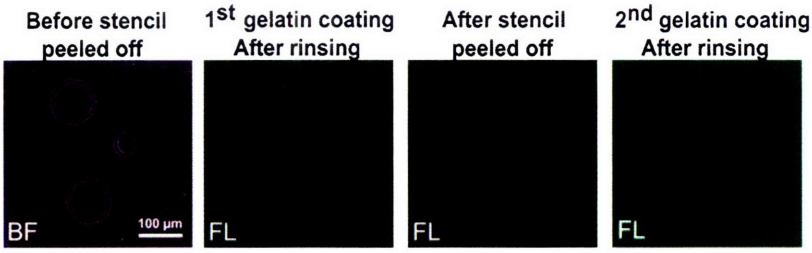

Figure 3-2 Two-step coating of gelatin when using stencils: Gelatin is first coated in the stencil holes. After the cells attached to the substrate, second gelatin coating is done after the stencil is removed. Shown here, fluorophore-conjugated gelatin is used here to demonstrate the uniformity of gelatin using this two-step coating method.

Depending on the size of the holes in the membrane, bubbles may be formed on top of each hole. To prevent bubble formation, we first degassed the stencil that had already been loaded with gelatin for approximately 20 minutes. After degassing, the bubbles will become larger, can be easily seen and removed by flushing with extra gelatin near the stencil surface using a disposable syringe. After the substrate is already coated, we then followed the cell loading steps shown in Figure 3-3. We first removed the gelatin in the stencil while leaving a thin layer of gelatin to prevent formation of bubbles in the holes. To ensure uniform cell density across the substrate, mixing of cell suspension in stencil is recommended. The number of cells loaded depends on the size of the stencil. In our study, we used the stencil with inner diameter of 2.5 cm and loaded the stencil with half a million cells in 3 ml of cultivating medium. Between step 1 and 2, we waited 12 hours to let the cells attach to the substrate. After removing the stencil off the substrate, we can do a second coating of gelatin by putting gelatin (0.1% in PBS) in the culture dish and incubate at 37 °C for 5 minutes.

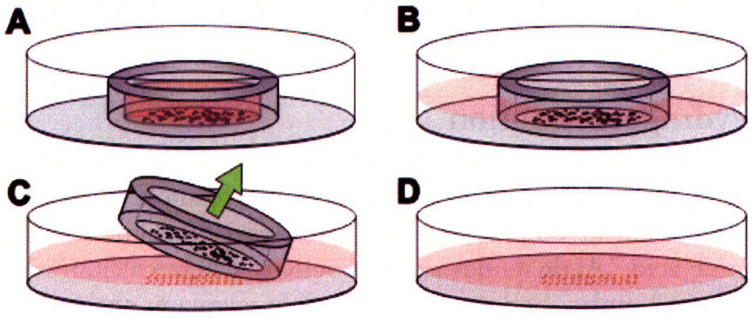

Figure 3-3 Stencil patterning procedure: A) Cell suspension is loaded into stencil. B) Cultivating medium inside the stencil is removed after cells already attach to substrate. Cultivating medium is filled in the outer region of the culture dish to prevent cell damage while removing stencil. C) Stencil is carefully removed. D) Rinse with cultivating medium to take away unattached cells.

3.3 Fabrication of substrate-coordinate registering features

Registering image stacks at multiple points in space and time is a laborious task to perform manually. In order to perform automatic image registration, noticeable and permanent control points must be available in all images. The registration algorithm we used is explained descriptively in §4.1. Here, we will explain how artificial, permanent control features can be added to the substrate plane using a thin sheet of PDMS embedded with fluorescent beads. We first suspend 5-μm-diameter fluorescent beads (Cat#F8841, Invitrogen) in ethanol and aliquot the suspension liquid on a flat surface (50,000 beads/cm^2). We may also use a gridded dish to create blank borders that are useful for the determination of substrate's rotation angle. We need to distribute all the beads randomly on the surface, but the features would function best if they are equally dispersed. After waiting until ethanol evaporate, the beads will be aligned in the same surface plane, allowing simple focusing during data collection process. We then pour a thin layer of PDMS liquid to cover the bead-coated substrate. After degassing the PDMS to remove all bubbles and incubating at 65°C for 2 hours, we can then peel off the cured PDMS layer that is now embedded with fluorescent beads. This PDMS sheet can be attached to the bottom surface of a tissue culture dish or a glass slide to help define substrate-space coordinates. This easily made florescent-bead film replaces the necessity of physically modifying the substrate surface to contain structural features and can be used repeatedly.

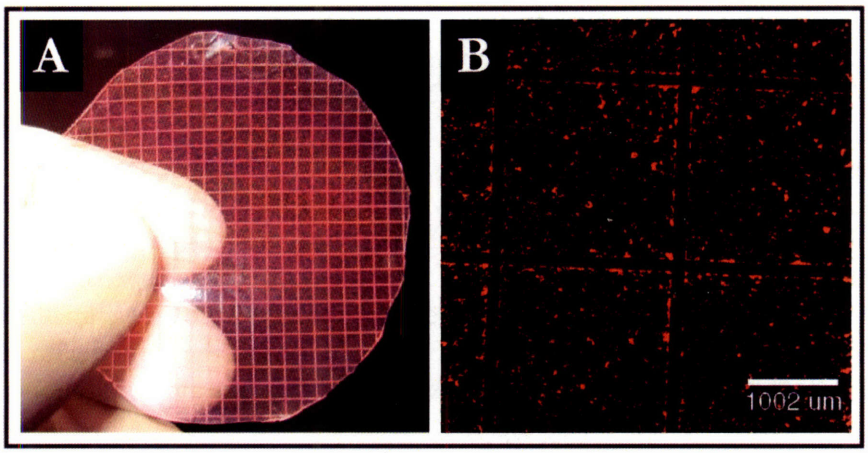

Figure 3-4 Registering features on PDMS membrane: A) PDMS membrane embedded with fluorescent beads. B) Zoomed-in image of the membrane. Here, we used gridded dish to fabricate the membrane. The square structures created from the gridded dish can be used to determine rotation angle of the substrate.

3.4 Alginate hydrogel formation

To prevent convection that may occur as we cultivate the cells in the open-topped tissue culture dish, alginate hydrogel was sometimes formed on top of the patterned colonies. Alginate is a linear co-polymer built from two monomeric units: D-mannuronic acid and L-guluronic acid. Alginate has calcium activity where calcium ions are trapped and bound inside diamond holes between two aligning alginate chains, creating hardening gelation. In our experiment, alginate polymer mixture was first prepared by mixing sodium alginate (2%, ISP, San Diego, CA) in the sodium chloride solution (0.15 M, Sigma Aldrich) buffered with HEPES (20 mM, Sigma Aldrich). The alginate mixture was autoclaved and filtered for sterilization. To form alginate hydrogel, the polymer mixture was mixed with

gelling solution composed of calcium chloride (102 mM, Sigma Aldrich) and HEPES (20 mM, Sigma Aldrich).

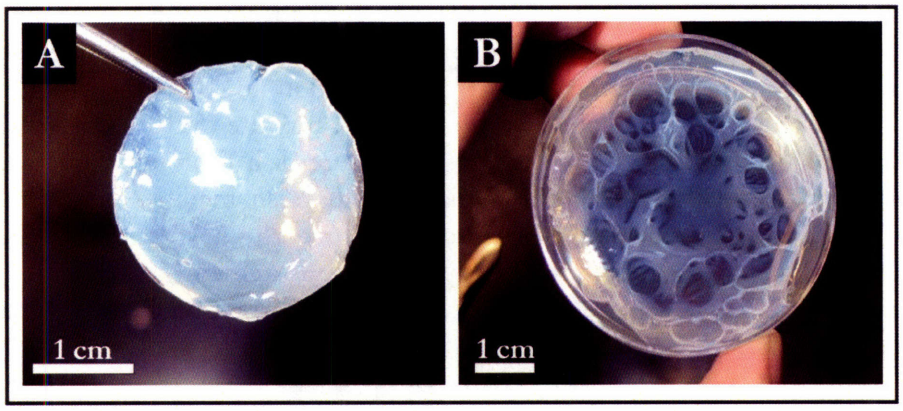

Figure 3-5 Alginate hydrogel formation: for A) round cover slip and B) tissue culture dish.

3.5 Speckle staining

To produce mESC colonies that are fluorescently labeled at random spots on the colonies, we first need to prepare two groups of mESCs, labeled and unlabeled cells. The labeling dye we use is the Vibrant DiI (Cat#V-22885, Molecular Probes) which is a lipophilic, membrane-labeling dye. The cells were stained as suggested in the product manual. In brief, we use 5 μL of the dye for every 1 mL of cell suspension (1 million cells/mL) or every 1 mL of cultivating medium for adhering ESCs. After incubating the cells with the dye for 20 minutes at 37°C, we wash the cells three times by performing centrifugation and replacing with fresh-medium for cell suspension, or simply incubating the cells with fresh medium for 5 minutes and rinsing them. After we labeled one group of ESCs, we can now form mESC colonies with speckles. We mixed the labeled and unlabeled cells together with the appropriate mixing ratio. The cells can then be patterned on the substrate similar to the method discussed previously in §3.2.

3.6 Cell proliferation assays

To quantify the level of cell proliferation, we can use bromodeoxyuridine (BrdU) incorporation assay to determine the level of DNA synthesis in the interested cell culture for a fixed period of time. To label the cells with BrdU, we incubated the ESC culture in BrdU-mixed cultivating medium (diluted 1:100 in fresh medium, Cat#00-0103, Zymed) for a fixed amount of time (ranging from 15 minutes to 1 hours). The cell culture was washed several times in PBS and fixed with 4% paraformaldehyde for 30 minutes at room temperature. We then denatured the DNA of the cells by incubating the cells in 2N HCl for 30 minutes. After rinsing for five times, we follow regular fluorescent immunostaining for BrdU. In brief, we first blocked non-specific binding by incubating the cells in 2% BSA at room temperature for 30 minutes. The cells were then labeled with mouse anti-BrdU alexa that is conjugated with Alexar Fluor 488 (diluted 1:20 in 2% BSA, PBS) (Cat#A21303, Molecular Probes). We then mount the stained cells with mounting solution (Fluoromount, Southern Biotech).

We may also measure cell proliferation in bulk sample using WST-1 assay (Cat#2210, Chemicon). The assay is done by cleavage of the tetrazolium salt WST-1 to formazan by cellular mitochondrial dehydrogenases. The formazan dye produced by viable cells can be measured by quantifying the absorbance of the dye solution at 440 nm. The assay was conducted as suggested in the product protocol. In brief, we prepared the reagents by adding 1 parts of the WST-1/ECS solution to 10 parts of the cultivating medium. The cells were then incubated with the assay mixture ($5x10^5$ cells/10 μL of WST-1/ECS solution) for 3 hours. After shaking the culture dish thoroughly, we aliquoted the medium from the cell culture dish and replaced with fresh medium in the case hen we intended to continue cell culturing. We then measured the absorbance of the collected medium at 440 nm (A_{440}) and referenced with the measurement at 690 nm (A_{690}). The output reading (A_{440}- A_{690}) can be used to compare proliferation of the cells in different cultivating conditions.

3.7 Self-renewal marker assays

To measure self-renewal with alkaline phosphatase, we measure its expression using an enzymatic activity assay (Cat#SCR004, Chemicon). The assay was performed as suggested in the product protocol. In brief, we fixed the colony with paraformaldehyde (4% in PBS) for only 2 minutes to preserve the enzymatic activity. We then rinse the cells with rinsing buffer (1X TBST buffer, Chemicon). We then mixed the assay reagents as suggested in the protocol and added the solution to cover the cells. After incubating in dark at room temperature for 15 minutes, the cells were rinsed again with rising medium. We then mount the culture dish with mounting solution (Fluoromount, Southern Biotech).

We may also measure self-renewal from the expression of Oct-3/4 protein. First, we fixed ESCs with paraformaldehyde (4% in PBS) for 20 minutes. After washing the samples twice with rinsing buffer, we then permeabilize the cells with Triton X-100 (0.1% in PBS) for 10 minutes at room temperature. The cells were washed (5-10 minutes each) with rinsing buffer twice and then applied with the block solution (0.1% BSA, 10% normal goat serum and 0.3% Triton X-100 in PBS) for 30-60 minutes at room temperature. Right before the incubation was about to finish, we prepared primary antibody solution (rabbit anti Oct-3/4, Cat#sc-9081, Santa Cruz Biotech.) by diluting 1:50 in PBS/0.1%BSA. It is important that the blocking solution is not rinsed off the sample. We simply removed the blocking solution by dripping and incubated the samples with the primary antibody right away at room temperature for 1 hour. After the incubation, the cells were then washed (5-10 minutes each) with rinsing buffer for three times. We prepared our secondary antibody (Alexa Fluor 488-conjugated donkey anti-rabbit IgG, Cat#A21206, Molecular Probes) by diluting 1:200 in PBS. The cells are then incubated with the secondary antibody solution for 30-60 minutes at room temperature and finally washed three times (5-10 minutes each) in the rinsing buffer. At this point, the cells can be mounted with anti-fade mounting solution or simply covered with PBS for visualization. Oct-3/4 is a transcription factor. Staining of this protein should therefore be localized to only the nucleus. In addition, ESC colonies can sometimes release gas into the mounting solution, which will block the view of colonies. It is suggested that the samples are kept in PBS for at least two to three hours before mounting.

CHAPTER 4: DATA COLLECTION & ANALYSIS

Data collection and analysis is one of the key challenges in this project. While we can pattern a number of mESC colonies easily and precisely using stencil patterning, the analysis of these colonies requires non-trivial computations that are worth a separate section to discuss these issues. Various image processing techniques used to enhance and ensure accuracy of the analysis will be discussed in this chapter. Some of these image processing algorithms are needed during the data collection process. Other algorithms are used later to quantify the changes of different phenotype parameters of the colonies including self-renewal, proliferation and motility. An automated microscope that allows programming of its settings will be needed and assumed to have for our discussion here. While we are discussing the general ideas of each image analytical techniques, the implementation of each technique is available in the appendix section of this thesis.

4.1 Overall scheme for data collection and analysis

There are three main processes that we will need to perform to analyze colony morphological changes, namely 1) image collection, 2) image registration, 3) image analysis. The first step involves image collections at varying space and time (Figure 4-1A). The first approach to collect data is to cultivate colonies right on the microscope stage and use time-lapse microscopy to monitor colonies at multiple locations, and time points. This approach requires that we have a stage incubation system that was not available for our study. The second approach is to culture the cell in a separate incubator and only take images of the colonies at specific time points. This approach also helps reduce perturbation to the fluid while culturing but it is now required that we have a technique to realign the culture dish to its initial orientation in order for the new images to be referenced correctly to the previously-taken images. Aligning the culture dish with a sub-millimeter precision is a very difficult task to achieve practically. This problem leads us to the second operation of the process, image registration, which can be used to align unmatched images after the data collection.

To register images of colonies at different time points, we may use the control-point approach or use similarity measures. First, we can identify identical locations (control points) in our time-series images either manually or automatically (Figure 4-1B). These control points will then determine the mathematical transformation function which explains the deviation of the two images. By reversing this transformation, we can align the collected images at different time points. The second approach to register image is to evaluate the similarity of the two images using similarity measures (Table 4-1). An ideal similarity method must be able to resolves images that are different by scaling, translation as well as rotation. Having aligned all images, we are now ready to determine colony morphological changes of the colonies.

The last operation to study the behavior of colonies is to analyze the registered images (Figure 4-1C). The goal is to determine morphological parameters such as colony area and colony movement displacement (Table 4-2) from the images and to use these parameters to estimate changes in colony behaviors between different study groups in our colony-colony interaction study. Some of the parameters can be determined from only one image frame. Other requires images at multiple points in time. Before these parameters can

be extracted, the first operation that we need to conduct is to segment these images. Image segmentation is used to identify regions of the object of our interest in an image. In our case, we will differentiate ESC colonies from the image background. Since ESC colonies have relatively high intensity in comparison with the image background, we will rely on a thresholding-based segmentation method to analyze colony images.

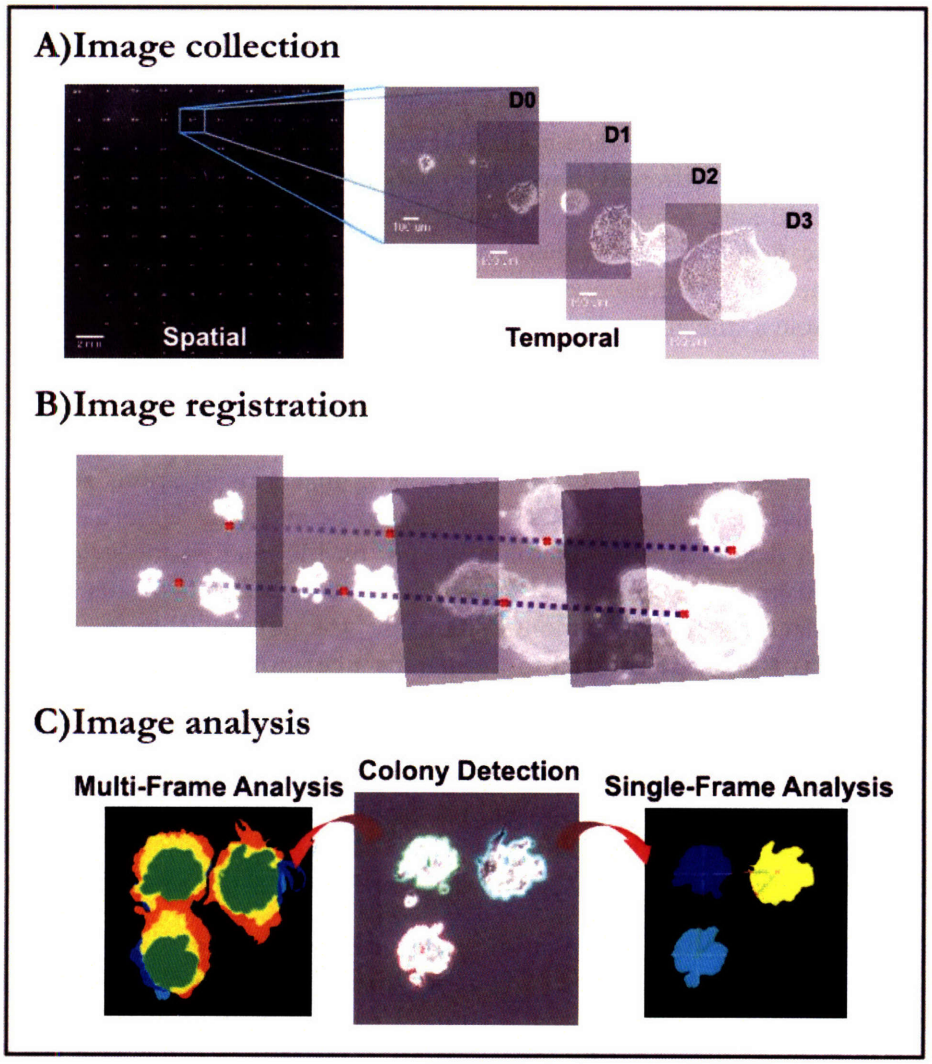

Figure 4-1 Overall schemes for data collection and analysis: A) Collecting images at different points in space and time. B) Register images based on control points or by comparing image similarity. C) Identify colonies in the images and calculate for morphological parameters.

Before we discuss different processes for data collection and analysis, it is important that we understand the two coordinate planes in our system: 1) the plane of the microscope stage (x,y) and 2) the plane of the culture substrate (u,v), shown in Figure 4-2. When we collect images of the colonies at different points in space and time, it is best to relocate the location of colony groups with respect to the substrate coordinates, rather than the stage coordinates. The plane of the substrate (u,v) can rotate, translate or tilt with respect to the stage. Therefore, the position of colony groups may change of time to time using stage coordinates. Since colonies are actually attached to the substrate, its position will be change

similarly to the substrate coordinates. We will however assume in our study that the angular distortion of the two coordinate planes is constant during each data collection process. The stage coordinates will be allowed to change only by translation because the origin of the stage-coordinate may vary between different data collection periods. While it appears in Figure 4-2 that one pair of the two basis vectors of both coordinate planes, namely **Y** and **V**, are aligned, it is difficult to ensure this configuration during the actual experiment. Since we do not necessarily culture the cells on the microscope stage, we will assume that there is a rotational misalignment of the two coordinate systems.

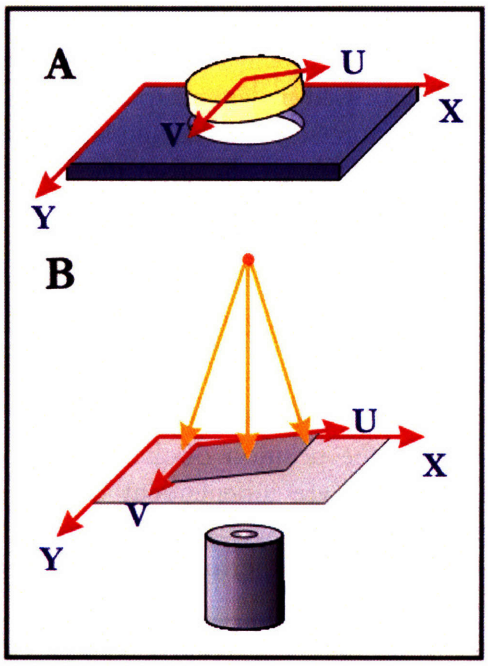

Figure 4-2 Two important coordinate spaces: A) Stage and culture substrate with different coordinate spaces. B) Tilted substrate plane in reference to the stage plane. The image recorded will be the projection of the tilted substrate of which the coordinates will be distorted.

4.2 Image collection

To collect colony images, we may write software to take images at pre-defined stage positions. This method will require that we have a colony platform that is rigorously patterned with almost no errors in colony positioning. Since this requirement is difficult to achieve practically, we may instead need to assign the colony locations manually at the beginning of each data collection process. This process is certainly very laborious especially when there are a lot of colony sites. In our study, we decided to instead take image of the whole substrate plane using scan-and-stitch algorithm (Scan slide module, Metamorph). Since the substrate plane may be misaligned from the stage plane as previously discussed, it is important that we calibrate the module at the beginning of each data collection process. To determine the colony contour, we only need to scan the whole substrate image with 5×-magnification objective lens. The whole scanning for an area of 2cm-by-2cm can be finished in approximately 20 minutes. To collect images that require higher resolution such as resulted images from staining, we first scan and stitch images of the whole substrate at low magnification (5×), define the locations of the colonies in the low-magnification image and

finally take images at the defined positions at higher magnification. This whole process can be performed using "Scan Slide" application module in Metamorph software.

4.3 Image registration

Image registration is an important process for morphological analysis of multidimensional image data. To compare morphological changes of ESC colonies, it is necessary that all colony images are first aligned properly. We will discuss in this section the theory of image registration as well as the implementation we used.

4.3.1 Image registration theory

Multidimensional images are usually composed of two types of microscopic distortions: 1) non-linear warping caused by lens-warp distortion and the focal-plane tilt and 2) the linear distortion due to rotation, scaling, skewing and translation[106] (Figure 4-3). Our task is to determine the mapping between the distorted image and the reference image, which can be written as the following transform functions:

$$x = f(u,v) \tag{4.1}$$

and

$$y = g(u,v), \tag{4.2}$$

where (x,y) are the coordinate space of the reference image and (u,v) are the coordinate-space of the target image. The lens-warp distortion is an intrinsic property of the objective that will not vary with the position of the stage or the substrate. Since both sources of the non-linear distortion are independent of space, we will apply the same correction of non-linear distortion to all images that are corrected at the same time point. Correction for linear distortion will then be performed afterwards.

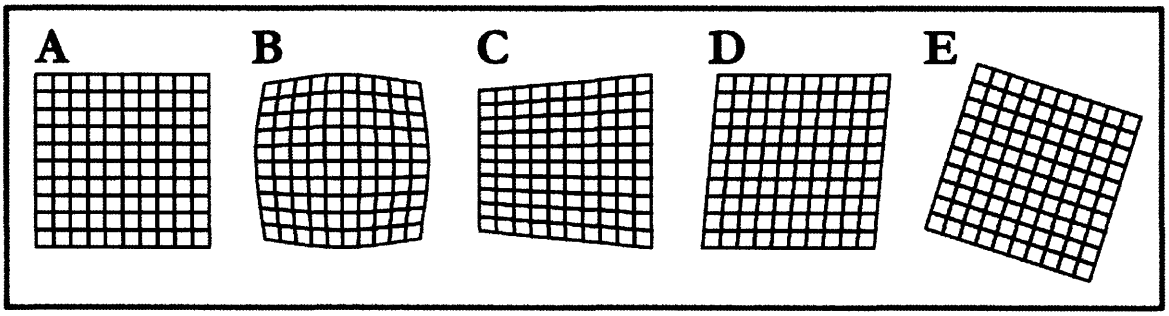

Figure 4-3 Geometric distortion of coordinate space: A) Original grid B) Warped space C) Tilted space D) Skewed space and E) Rotated space. B) and C) are non-linear transformations that can be corrected with polynomial warp model while D) and E) are linear transformations and can be corrected with affine transformation.

4.3.1.1 Non-linear warp and tilt

To correct non-linear distortion from lens warp and substrate tilting, we can approximate the transform functions in equation (4.1) and equation (4.2) by N^{th} order 2-D polynomials, or the so-called polynomial warp model[107]. We can write transform functions of non-linear warping as:

$$x = \sum_{i=1}^{N}\sum_{j=1}^{N} k_{ij}^{(1)} u^i v^j \tag{4.3}$$

and

$$y = \sum_{i=1}^{N}\sum_{j=1}^{N} k_{ij}^{(2)} u^i v^j , \tag{4.4}$$

where $k_{ij}^{(1)}$ and $k_{ij}^{(2)}$ are the mapping coefficients to be determined. The higher order terms compensate for the curvature of the warp while the cross terms $(u^i v^j \mid i, j > 0)$ are for the tilt of the images. To determine the mapping coefficients, we will need at least M pairs of control points from both the undistorted and the distorted images where M is equal to the number of mapping coefficients of each transform function. We only need a few polynomial terms to implement this method while a lot of control points can be used to achieve accurate mapping coefficients. Following a previous report[106], we can calculate the mapping coefficients by first defining:

$$\mathbf{A} = \begin{bmatrix} 1 & u_1 & u_1^2 & u_1^3 & v_1 & u_1 v_1 & v_1^2 & u_1 v_1^2 \\ 1 & u_2 & u_2^2 & u_2^3 & v_2 & u_2 v_2 & v_2^2 & u_2 v_2^2 \\ \vdots & \vdots & \vdots & \vdots & \vdots & \vdots & \vdots & \vdots \\ 1 & u_n & u_n^2 & u_n^3 & v_n & u_n v_n & v_n^2 & u_n v_n^2 \end{bmatrix}, \tag{4.5}$$

$$\mathbf{B} = \begin{bmatrix} 1 & v_1 & v_1^2 & v_1^3 & u_1 & u_1 v_1 & u_1^2 & u_1^2 v_1 \\ 1 & v_2 & v_2^2 & v_2^3 & u_2 & u_2 v_2 & u_2^2 & u_2^2 v_2 \\ \vdots & \vdots & \vdots & \vdots & \vdots & \vdots & \vdots & \vdots \\ 1 & v_n & v_n^2 & v_n^3 & u_n & u_n v_n & u_n^2 & u_n^2 v_n \end{bmatrix}, \tag{4.6}$$

$$\mathbf{k^{(1)}} = \begin{bmatrix} k_1^{(1)} & k_2^{(1)} & k_3^{(1)} & k_4^{(1)} & k_5^{(1)} & k_6^{(1)} & k_7^{(1)} & k_8^{(1)} \end{bmatrix}^T, \tag{4.7}$$

$$\mathbf{k^{(2)}} = \begin{bmatrix} k_1^{(2)} & k_2^{(2)} & k_3^{(2)} & k_4^{(2)} & k_5^{(2)} & k_6^{(2)} & k_7^{(2)} & k_8^{(2)} \end{bmatrix}^T, \tag{4.8}$$

$$\mathbf{x} = \begin{bmatrix} x_1 & x_2 & \cdots & x_n \end{bmatrix}^T, \tag{4.9}$$

and

$$\mathbf{y} = \begin{bmatrix} y_1 & y_2 & \cdots & y_n \end{bmatrix}^T. \tag{4.10}$$

We can then calculate mapping coefficients from:

$$\mathbf{k^{(1)}} = \mathbf{A}^+ \mathbf{x} \tag{4.11}$$

and

$$\mathbf{k^{(2)}} = \mathbf{B}^+ \mathbf{y}, \tag{4.12}$$

where $\mathbf{A}^+$ and $\mathbf{B}^+$ are the Moore-Penrose pseudoinverse. If $(\mathbf{A}^T\mathbf{A})^{-1}$ exists, then

$$\mathbf{A}^+ = (\mathbf{A}^T\mathbf{A})^{-1}\mathbf{A}^T \tag{4.13}$$

and $\mathbf{B}^+$ can also be calculated similarly. Note that some objective lenses such as the Zeiss Plan objectives may have already corrected lens warp distortion. Therefore, the source of non-linear distortion will be only from the substrate tilt which can be modeled simply with projective transform if desired.

4.3.1.2 Linear affine

Linear distortion due to scaling, rotation and translation can be corrected all at once using an affine transform. We can write equation (4.1) and equation (4.2) for an affine transform as:

$$x = u_T + a_1 \cdot u + a_2 \cdot v \tag{4.14}$$

and

$$y = v_T + a_3 \cdot u + a_4 \cdot v. \tag{4.15}$$

While translation is not a linear operation, we can rewrite these two equations as a linear matrix transformation using homogeneous coordinates as follows:

$$\begin{bmatrix} x \\ y \\ 1 \end{bmatrix} = \begin{bmatrix} a_1 & a_2 & u_T \\ a_3 & a_4 & v_T \\ 0 & 0 & 1 \end{bmatrix} \begin{bmatrix} u \\ v \\ 1 \end{bmatrix}. \tag{4.16}$$

At least three pairs of the control points will be needed to determine all the unknown six parameters here: a_1, a_2, a_3, a_4, u_T and v_T. To determine these coefficients, we can simply solve them by inverting the coordinate matrix on the right side of the equation or use the pseudoinverse when more than three pairs of control points are used.

1) For three pairs of control points

$$\begin{bmatrix} a_1 & a_2 & u_T \\ a_3 & a_4 & v_T \\ 0 & 0 & 1 \end{bmatrix} = \begin{bmatrix} x_1 & x_2 & x_3 \\ y_1 & y_2 & y_3 \\ 1 & 1 & 1 \end{bmatrix} \begin{bmatrix} u_1 & u_2 & u_3 \\ v_1 & v_2 & v_3 \\ 1 & 1 & 1 \end{bmatrix}^{-1} \tag{4.17}$$

2) For more than 3 pairs, the parameters of affine transform can be solved in a least square sense as follows [108]:

$$\begin{bmatrix} a_1 & a_2 & u_T \\ a_3 & a_4 & v_T \\ 0 & 0 & 1 \end{bmatrix} = \begin{bmatrix} \sum x_n u_n & \sum x_n v_n & \sum x_n \\ \sum y_n u_n & \sum y_n v_n & \sum y_n \\ \sum u_n & \sum v_n & N \end{bmatrix} \bullet \begin{bmatrix} \sum u_n^2 & \sum u_n v_n & \sum u_n \\ \sum u_n v_n & \sum v_n^2 & \sum v_n \\ \sum u_n & \sum v_n & N \end{bmatrix}^{-1} \tag{4.18}$$

4.3.2 Registering images using control-point mapping

To correct both the non-linear and linear distortion, we need to calculate the mapping coefficients from the set of suitable control-point pairs. In our study, we select control points manually using the "cpselect" tool box in MATLAB. The registering transformation can then be computed from the methods in previous section. In our study, we used a MATLAB function "cp2tform" to determine the mapping coefficients from the control points. This transform is the applied to the target image. Neighbor regions between the sampled points can be transformed using interpolation methods. The MATLAB function "imtransform" was used to apply transformation to our collected images.

Image registration with control points will be efficient when such registering features are present in all images. In this case, it is possible to use computer software to help identify possible control points and determine the best control-point pairs for registration. Automatic control-point identification can be performed using different feature selection methods[109]. In our study, the available control points in the collected images are the features and defects of the substrate which may easily disappear in poorly-focused images. It is therefore best to introduce external control points to the substrate to ensure that enough registering features are available. §3.3 discusses how this type of registration features can be fabricated. For further details on interpolation methods and fast algorithms for geometric transforms, we refer the reader to these sources[107, 108, 110, 111].

4.3.3 Registering images by manual image alignment

When we collected the scan-and-stitched images of the whole substrate, it is simpler to correct the combined image all at once. The problem that we encounter was that registration of the image of whole substrate plane is sometimes large to be processed in MATLAB without sacrificing image resolution. In our study, we used Metamorph software together with Photoshop to transform these images manually by matching identical features that are common to all images. This approach is efficient in correcting the rotational misalignment may not be able to align all colony groups accurately. Our solution is to first correct the rotational misalignment of the whole image plane and dissect the corrected image into small ones for each colony group. Since the dissected images are now only misplaced by translation, we can use a module such as "stack alignment" in Metamorph to register images at each colony position. We found that this method is a little bit easier to perform manually than identifying control points in the images. Often, the control points were very hard to identify in all images. In general, manual image registration is still too laborious and is the most critical process that we are attempting to improve. The next section discusses one possibility of how we can develop automatic image collection and registration via identification of substrate coordinates.

4.4 Using substrate coordinates for automatic image collection

We will discuss in this section how substrate-space coordinates can be determined in real-time and used to perform automatic image collection and registration. Since we allow the substrate to be movable during the experiment, stage coordinates of the colony position will be varying with the orientation of the substrate relative to the stage. We intend to instead store all objects' positions using the substrate-space coordinates so that the objects' coordinates will be invariant to any geometric transformations of the substrate itself. In brief, we will first determine the substrate-space coordinates from the stationary features that we added to the substrate plane (§3.3). Having unique features for all colony positions, we can use these landmarks to decode coordinates of the object. Below are the three important components to implement this method.

4.4.1.1 Maps

A map is the image of the whole substrate plane with stationary registration features that can be used to establish a coordinate space, here, the substrate space. The substrate map can be obtained by taking the picture of the whole substrate plane at low magnification as explained previously in §4.3.3. When a map contains unique features for every possible region across the entire map, we can assign a coordinate specific to the region of interest based on the features contained in this region. It is not necessary however that a map

contains a unique registration feature for each coordinate in the map. In fact, having complex features for all possible coordinates may require too-expensive computation and memory (Figure 4-4A). We can reduce this computation by grouping simple features such as circles or squares to code the coordinate of the region as long as these grouped features are unique within this map. Figure 4-4B shows an example of a map that uses only circles to encode coordinates of each region of interest. Two nearby regions usually contain an overlapping area with same features that contribute to the portion of code sequences common to both regions. Figure 4-4 also demonstrates very well the contrast between a map that intrinsically holds no coordinate information, only containing different features and a map that stores coordinate information. Using a map that stores coordinate information such as Figure 4-4B, we may not need to store template information and can directly extract coordinate information from the map using decoding algorithms. On the other hand, a map that relies on features to store coordinates such as Figure 4-4A will require extensive use of memories to store all possible templates to represent coordinates at different locations.

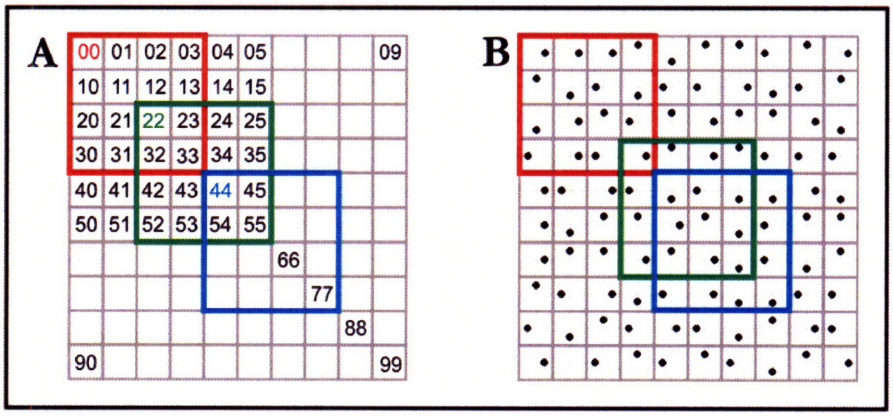

Figure 4-4 Maps with different features: Red, green and blue squares are different regions of interest in the 10-by-10 map. A) Map with complex features. The numeric structures at the top-left corner of each field-of-view windows are unique for all coordinates. This map requires a complicated pattern recognition algorithm to analyze the numerical features. B) Map with simple features. The locations of all dots within an interested region form a code sequence that can be used to code the coordinate of the region[112].

4.4.1.2 Templates

Template is a region in the map that we are interested to know its coordinates. Templates must contain enough features that can represent coordinate information. We have discussed previously that a map may or may not contain coordinate information, depending on how its features are positioned on the map. For a map that has no systematic method to store all features, comparison between the template and the map using different similarity measures will be required to determine the coordinates of the template. For the map that contains systematically positioned features, the coordinate of the template can be determined directly from the template without matching to the map.

4.4.1.3 Similarity measures

We will use similarity to compare and identify location of on the map that best matches to our template. Many similarity measures are available for different types of maps and templates. It is difficult to determine which method is the best similarity measure since each works efficiently for different applications. Table 4-1 summarizes commonly used

similarity measures and discusses advantages and drawbacks of each measure. The map and the template are represented by 2D matrices: $m(u,v)$ and $t(u,v)$, respectively. Note that the summations present in all measures are calculated across all substrate coordinates within the sliding window which has the size equal to the size of our template. For the operational costs presented, we assume that the map size is M-by-M and the template size is N-by-N. Comparison among all similarity measures should be performed to identify the most efficient method for each specific application.

To determine substrate coordinates in real-time, we need to first generate the substrate map before the culture dish is used to cultivate the cells. Geometric distortion of the map must also be corrected to achieve accurate mapping later on. After the map is obtained, the cells can then be plated into the culture dish and moved to an incubator. After the cells already adhered to the substrate, we can take the culture substrate back onto the microscope again for data collection. At this point, the current orientation of the culture dish may not be well aligned to the substrate map collected previously. Ideally, we would like to use a similarity measure that can match our map to the template, a region within the substrate image at the current position. This measure must therefore be invariant to scaling, or rotation of the template. The similarity measure will then determine the substrate coordinate of the region that can match the best to the template. Having identified the position that best matches the template, we can program the data collection software to automatically move to that particular location and take the image of the colony. Registration of the image can also be used in real-time using the available registering features. The summary of these processes is illustrated in Figure 4-5.

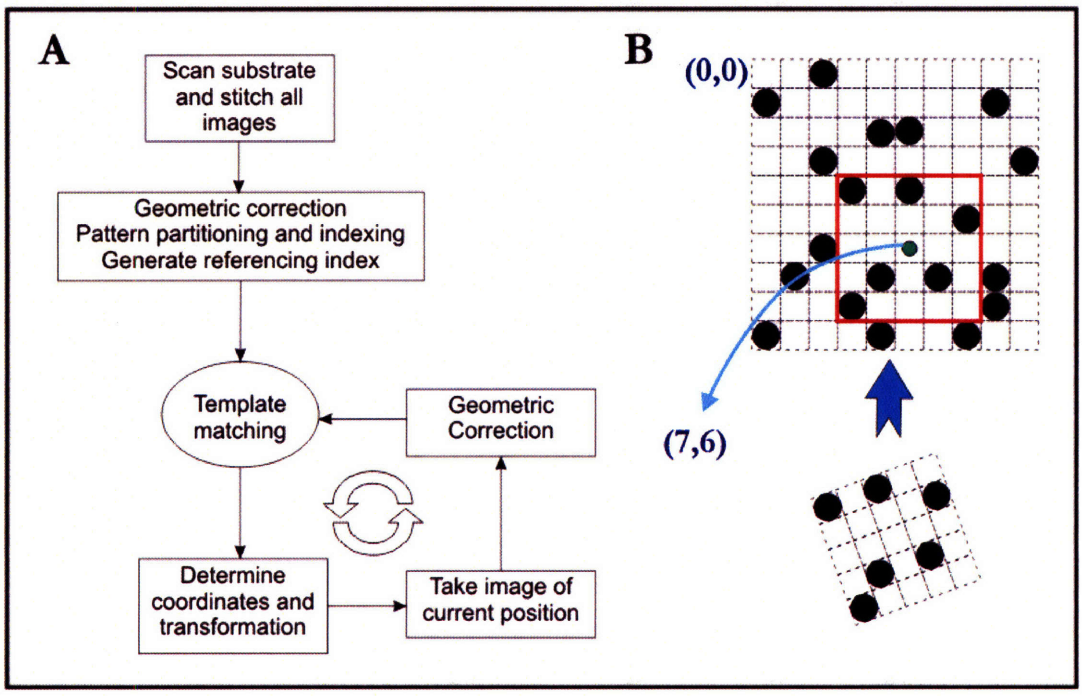

Figure 4-5 Substrate-based coordinates: A) Process flow for procedures to determine coordinate of the image at the current position using template matching. B) Demonstration of template matching. The bottom, smaller image is the image at current position. The top image is overall substrate. While the colony may be moving over time, registration points on substrate plane are fixed and therefore allow accurate alignment of all time-series images.

Table 4-1 Commonly-used similarity measures

Method	Subgroup	Domain	Definition	Operational Costs	Advantages	Drawbacks	References
1. Cross-correlation	Conventional cross-correlation	Spatial	$C(u,v)=\sum_{x,y} m(x,y)t(x-u,y-v)$ $C(u,v)=m(u,v)*t(-u,-v)$	Mul: $N^2(M-N+1)^2$	1. Fast for M>>N	1. bad for large M, N 2. Fail when map energy varies with space 3. varying with map amplitude such as different lighting	113
		Frequency	$C(u,v)=IDFT\left\{DFT(m-\mu_m(u,v))\cdot DFT^*(t-\mu_t)\right\}$	Add: $18M^2\log_2 M$ Mul: $12M^2\log_2 M$ with FFT	1. Fast for large M,N & M ≈ N	1. Require memory that grows with log of map area	113, 114
	Normalized cross-correlation	Spatial	$D(u,v)=\frac{\sum_{x,y}\left[m(x,y)-\mu_m(u,v)\right]\left[t(x-u,y-v)-\mu_t\right]}{\sqrt{\sum_{x,y}\left(m(x-u,y-v)-\mu_m(u,v)\right)^2\sum_{x,y}\left(t(x-u,y-v)-\mu_t\right)^2}}$ (Faster algorithm for normalized cross correlation is suggested in [113])	Add: $3N^2(M-N+1)^2$ Mul: $2N^2(M-N+1)^2$	1. Good for varying map's energy 2. Invariant to intensity scales 3. Range: -1 to 1	1. Not invariant for complicated transformation 2. Slow for large M,N & M ≈ N 3. Inefficient for dissimilar maps	113, 114
2. SSDA: Sequential similarity detection algorithm (also has efficient sequential search strategy)	Conventional absolute differences	Spatial	$E(u,v)=\sum_{x,y}\left\|m(x,y)-t(x-u,y-v)\right\|$	Add: $N^2(M-N+1)^2$	1. Faster than correlation	1. Varying with map amplitude	114, 115
	Normalized absolute differences	Spatial	$F(u,v)=\sum_{x,y}\left\|m(x,y)-\mu_m(u,v)-t(x-u,y-v)+\mu_t\right\|$	Add: $4N^2(M-N+1)^2$	1. Invariant to intensity scales	1. Not invariant for complicated transformation 2. Inefficient for dissimilar maps	114, 115
3. Gradient descent		Spatial	Minimize error function E where: $E=\sum_{\mathbf{x}\in\mathbf{R}}\left[t(\mathbf{x}+\mathbf{h})-m(\mathbf{x})\right]^2$, for $\mathbf{x}=\begin{bmatrix}u\\v\end{bmatrix}$ and $\mathbf{R}$ are all points within the sliding window $t(\mathbf{x}+\mathbf{h})\approx t(\mathbf{x})+\mathbf{h}\cdot\nabla t(\mathbf{x})$	$N^2\log M$	1. Very fast for small translation	1. Bad for textured template 2. Cannot resolve rotation 3. Serial operation	113, 116
4. Fourier methods	Basic phase correlation (translation only)	Frequency	$G(u,v)=IDFT\left(\frac{M(\omega_u,\omega_v)\cdot T^*(\omega_u,\omega_v)}{\left\|M(\omega_u,\omega_v)\cdot T^*(\omega_u,\omega_v)\right\|}\right)$ $G(u,v)=IDFT\left(e^{(\omega_u d_u+\omega_v d_v)}\right)$		1. Scene independent 2. Overcome frequency-dependent noise	1. Good for shifted-template only. Cannot resolve rotated template	114, 117
	Generalized Phase correlation	Frequency	$\log\left(\left\|M(\omega_u,\omega_v)\right\|\right)\rightarrow$ HP Filter $\rightarrow$ log-polar conversion $\rightarrow \Lambda(\log\rho,\Theta)$ $\log\left(\left\|T(\omega_u,\omega_v)\right\|\right)\rightarrow$ HP Filter $\rightarrow$ log-polar conversion $\rightarrow \Pi(\log\rho-\log a_{scale},\Theta-\Theta_{rot})$ phase-correlation of Λ and Π		1. Good for any affine-transforms 2. Scene independent	1. Can only resolve small distortion	117

4.5 Segmentation of ESC images

Image segmentation is an image processing technique used to model an image of interest. In other words, it is the technique to define different regions within an image and assign a specific meaning for each area. Segmented area in the picture should ideally match the boundary of the object in the real world. For our application here, we would like to determine the position where the ESC colonies are located as well as their shapes to help us determine changes in colony motility and proliferation. Self-renewal and differentiation of ESCs are the two important states of ESCs that can be distinguished from one another by the shape of the cells or more directly by biochemical markers. Undifferentiated ESC colonies frequently have round shape with apparent, uniform borders. Differentiating ESC colonies do not preserve the same shape, having fibroblastic shape and heterogeneous morphology. Since any trained eyes can distinguish these two populations of ESCs apart, we also would like to identify each population from an image using segmentation techniques. The ideal segmentation for our application here is to determine accurately the boundaries of each cell population. Most importantly, we also prefer an automatic segmentation technique that will require the least user input to complete the task. Many segmentation techniques have been developed in the past[118-121]; yet, this subject is still an area of current research in image processing. While many fundamental algorithms have been developed, efficiency of image segmentation is still dependent on the applications that we intend to use it for. We will first discuss methods to characterize segmentability of an image and to apply each technique to images of ESC colonies. We will then explain the approach we took to segment ESC colonies in our study.

4.5.1 Evaluating segmentability of ESC images

Before we discuss the technique we used to perform image segmentation of ESCs, it is necessary that we understand the fundamental differences of the image objects that we are trying to classify including: 1) the undifferentiated colonies, 2) the fibroblast-like, differentiating cells and 3) the image background. Once we know all parameters that can distinguish different objects in the image, we can wisely choose the most appropriate segmentation technique(s) for our application. Here, we will demonstrate different methods to evaluate segmentability of the object of our interest within the collected images.

4.5.1.1 Intensity histogram

Intensity histogram is the simplest tool that we can use to show the intensity difference of the object of interest and the image background. Intensity histogram plots the pixel counts for different intensity bins of the image. Figure 4-6 shows an example of histogram of the patterned undifferentiated mESC colonies on substrate, imaged with phase-contrast microscopy. Here, we can see that the image is filled mostly with dark background, shown as a large peak at the intensity of 50. We can also see a small peak centered at approximately 125. This high-intensity peak covers most of the region of the two bright colonies. If we set the threshold at the intensity right between these two peaks, we can then segment the colonies from the dark substrate background easily as shown in Figure 4-6C. However, there are still dark holes in the colonies that require further morphological processes. Overall, undifferentiated colonies with uniform border similar to this example can be segmented more easily from the background based on the strong intensity differences.

We will now look at the segmentability of the undifferentiated and the differentiating ESCs using histograms as an evaluation tool. We can define the expected regions for both

populations by hand-drawing and plot separate histograms for both populations (Figure 4-7). In this example, we found that histograms of both populations are partly overlapping even though the histogram of the undifferentiated ESCs is centered at a much higher intensity. We can see from Figure 4-7E that the histogram of overall image (dotted line) does not have a distinct valley between the peak of the differentiating cells and that of the undifferentiated cells. This problem is caused first by the non-uniformity of background intensity that largely matched the intensity of the differentiating cells. Based on the analysis here, it is very likely that separation of both ESC populations using image thresholding alone will not be an efficient approach.

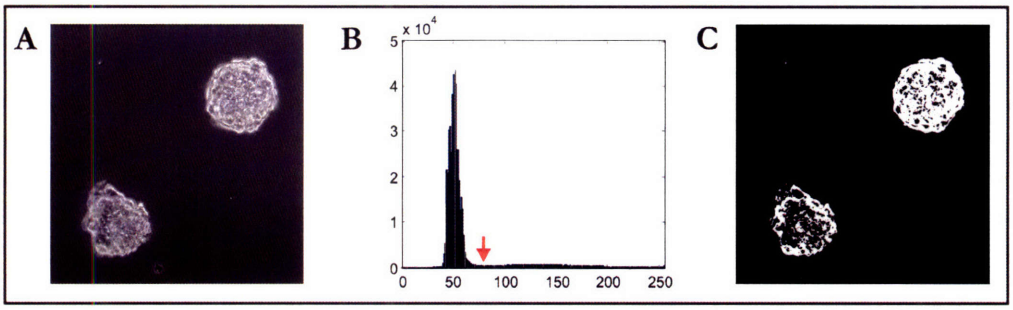

Figure 4-6 Intensity histogram of patterned mESC colonies: A) Original image B) Histogram. Red arrow points to the intensity used for thresholding the image. C) The resulted binarized image.

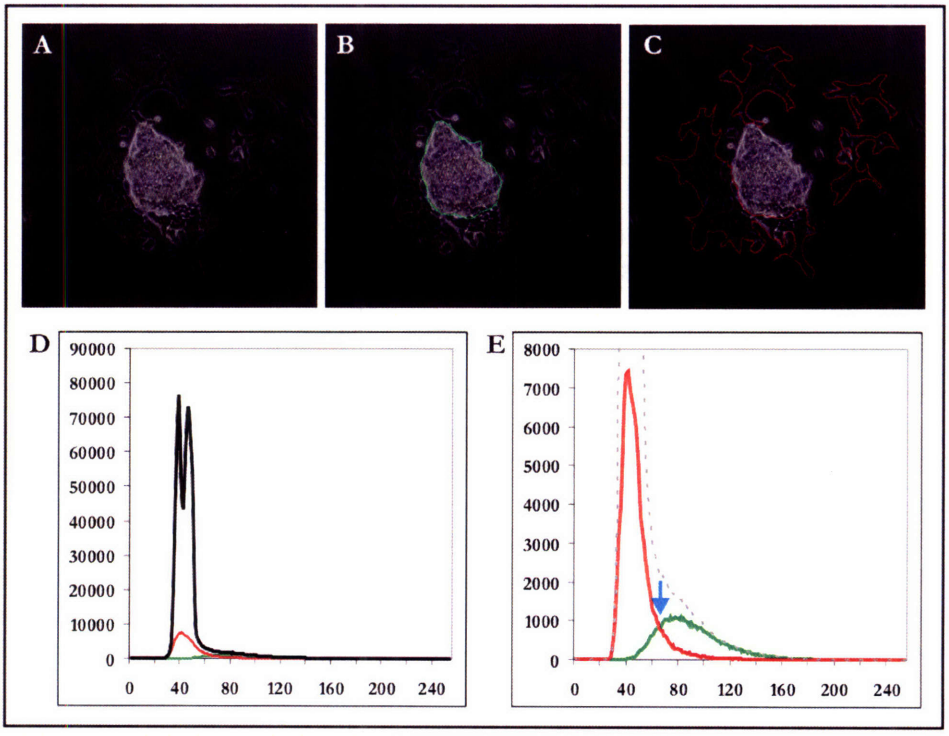

Figure 4-7 Segmentability of mESCs evaluated by histogram: A) Original image of mESCs. B) Boundary of undifferentiating mESCs is traced with green line. C) Differentiating mESCs are traced by red line. D,E) Histogram of overall image (black line in D and black doted line in E), differentiating cells (red line) and undifferentiated cells (green line). Blue arrow is the optimal intensity for thresholding.

4.5.1.2 Scattergram

Scattergram is a plot of intensity gradient magnitude at different image intensity. Scattergram is used often to characterize different regions of an image when there are peaks in the histogram that are significantly higher than the other. For example, when an image contains small region for a bright object and the rest area filled with dark background, there will be one very tall peak in the histogram at a low intensity and another much shorter peak at a higher intensity. This unbalance can distort and obscure algorithms to identify an optimal intensity for thresholding. Figure 4-8 illustrates an example of scattergrams for different regions of colony image. Figure 4-9 shows the scattergram of image regions undifferentiated and differentiating mESCs. The two compartments still have a significant overlay area in the scattergram, comfirming the difficulty in isolating populations of differentiating and undifferentiated ESCs.

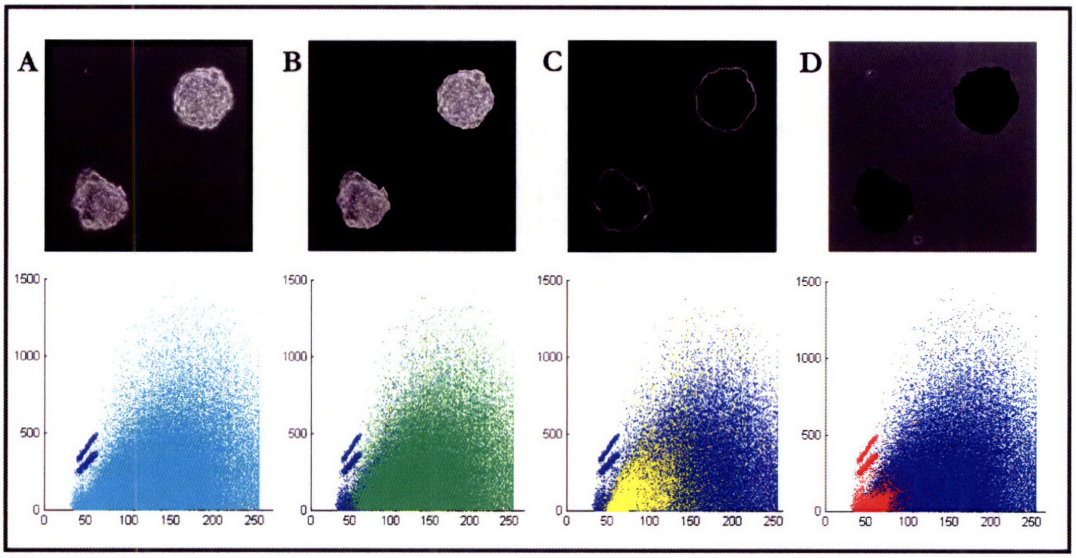

Figure 4-8 Scattergram of different region of mESC image: A) Light blue scatter plots illustrates all data points inside the image except the region at the edge of the image where there is a linearly varying intensity gradient. B) Green scatter plots represent data points of the region inside the colonies. As shown by the plot, the colony region spans across most of the area of scattergram. C) Yellow scatter plots represent data points at the rim of the colony. D) Red scatter plots represent the background of the image. Dark blue plots represent data points of the whole image.

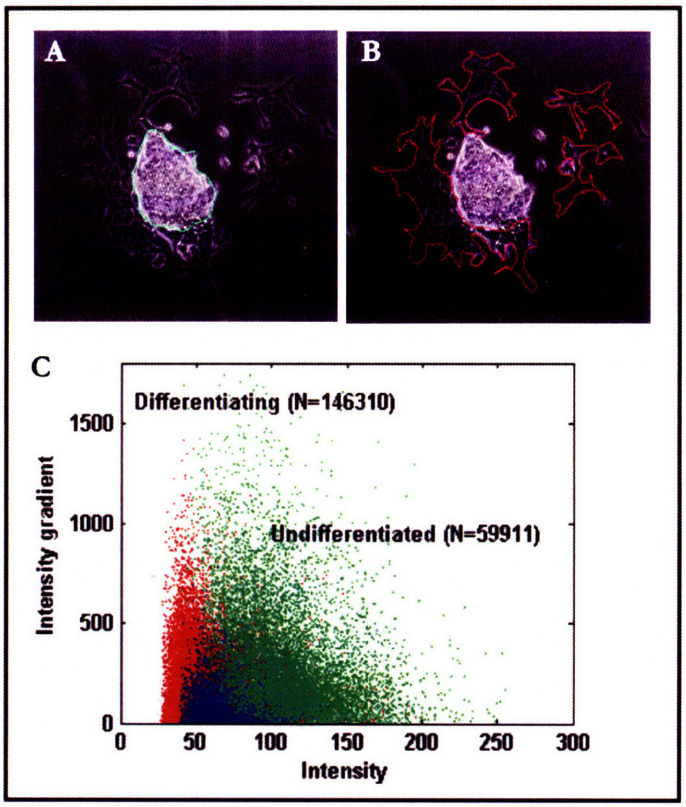

Figure 4-9 Segmentability of mESCs evaluated by scattergram: A) Undifferentiated mESCs segmented manually (green) B) Differentiating mESCs segmented manually (red) C) Scattergram of undifferentiated cells (green), differentiating cell (red) and the overlapped pixels (blue).

4.5.1.3 Sub-band representation

For the images where the regions of our interest hold significantly different spatial frequencies, we may use sub-band representation to evaluate how such frequency differences can be utilized for ESC segmentation. Sub-band representation decomposes an image into smaller images with varying characteristic frequencies, ranging from an image of its DC value to the image with higher frequency change. Figure 4-10 illustrates an example of sub-band representation that was applied to undifferentiated and differentiating mESCs. The bottom right corner of each image represents the high-frequency component of the region. We can see that the undifferentiated region seems to have greater high-frequency component than the differentiating region. An image segmentation method such as edge detection can be used to differentiate regions with different spatial frequency.

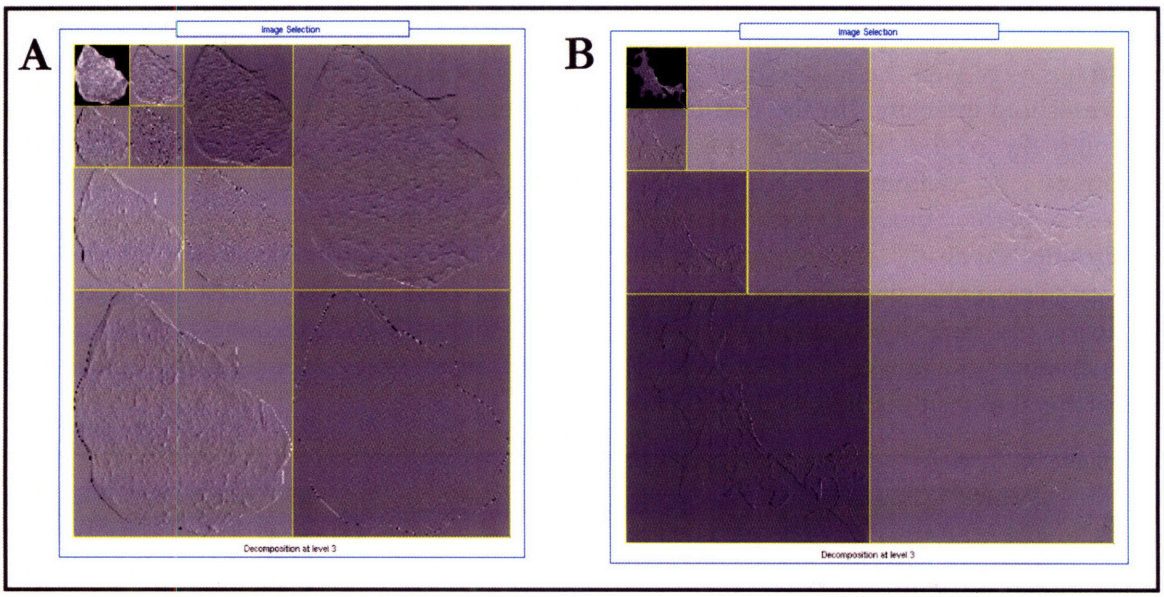

Figure 4-10 Sub-band representation of mESCs: A) Undifferentiated region. B) Differentiating region. The Top-left subimage represents DC-value of the original image. The bottom-right image represent high-frequency component of the image.

4.5.2 Segmentation of ESCs with image thresholding and morphological operators

To perform image segmentation of ESCs, we improve the performance of image thresholding by applying morphological operation to the resulted image. To explain the approach we used to segment colony images, we will split all the operations into three steps: 1) thresholding image, 2) modifying the image with morphological operations and 3) screening the resulted binary image to confirm and select only the object of interest

4.5.2.1 Segmenting ESC colonies preliminarily with thresholding

As we have shown in the previous section, simple image thresholding is not effective enough to segment ESC colonies from the background because of a few reasons. First, there may be regions inside the colonies whose intensity is comparable to the background intensity. This occurs even more so when a phase-contrast microscope is used to record ESC images. The low intensity region inside the colony is possibly generated from the shading at the cell-cell contact points. Second, the image background itself is often distributed non-uniformly across the image. Often, certain regions of the image background will have the intensity as high as colony image. Background intensity correction may be performed if the background change can be modeled by mathematical functions. For the case when background intensity changes unpredictably, a standard technique to get around this problem is to use adaptive thresholding. The idea is to identify and apply different threshold intensities for the different locations in an individual image. In practice, we will break the process of image thresholding further down into two steps: 1) selecting the appropriate threshold and 2) binarizing the image with the threshold chosen. To determine the suitable threshold, we used Otsu's algorithm[122] that was developed to determine global image threshold but only apply to a smaller region of the image that covers colonies we are interested to segment. The advantage of this selection method is to ensure that the output of our threshold selection algorithm will not be distorted by unrelated but uniform

background intensity. Having identified the proper threshold for the region of interest, we can binarize the image either globally or locally with the threshold selected. Figure 4-11 illustrates very well the importance of choosing the appropriate image region to determine the threshold intensity. In the first case where we determine the threshold globally without defining the region of interest (Figure 4-11 A, C and E), the output binary image was incorrect. By defining the appropriate region for threshold identification, we achieved almost a perfect binary image of an ESC colony. The tradeoff is that we now need to determine manually the region of interest, barring an automatic image processing. Nevertheless, it has been shown that automatic thresholding-based segmentation can also be achieved via recursive operation[123] or using neural network to determine the appropriate segmentation parameters[124]. For further study on thresholding methods, the readers are encouraged to visit the following reference[109].

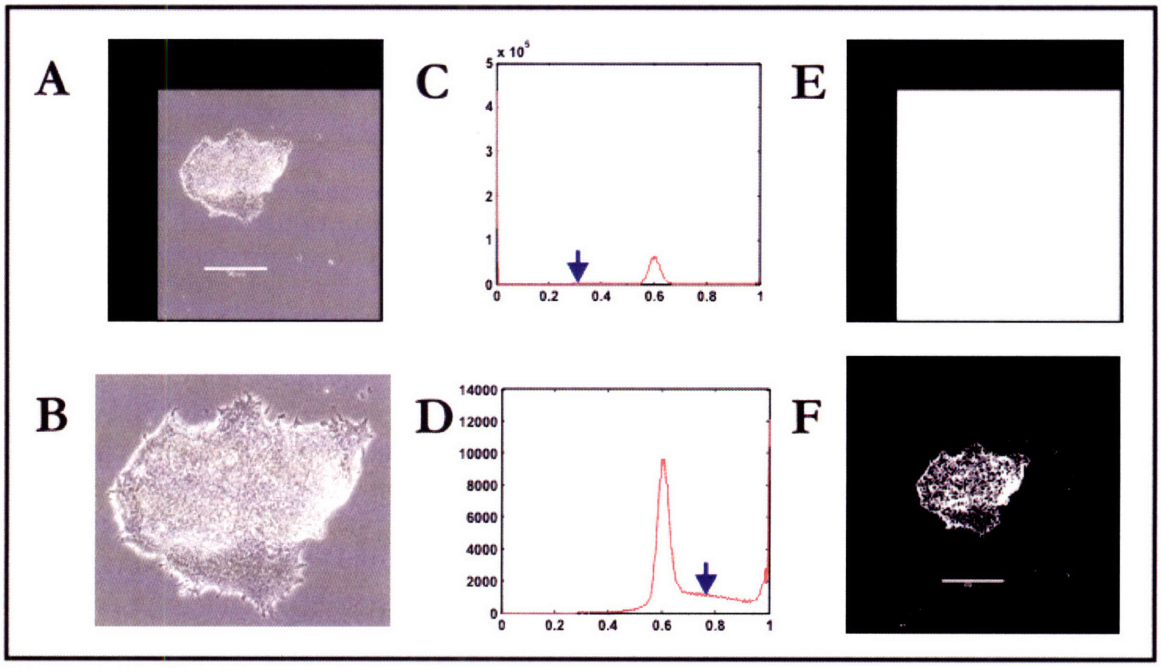

Figure 4-11 Selection of appropriate image threshold: A) The original image of mESC colony with black margin and a white scale bar. B) The cropped image that covers only the object of interest. C) and D) histograms of original image and the cropped image. The arrows represent the normalized thresholds used for each case. E) Output binary image using the threshold determined from the whole image. F) Output binary image using the threshold determined from the cropped image.

4.5.2.2 Completing segmentation of ESC colonies with morphological operations

The binary image of ESC colony derived from the adaptive thresholding method is almost complete except that the colony region is still separated into fragments of white areas. To fix this problem, we can perform morphological operations on the original binary image. Morphological operators are image processing techniques used to analyze and modify the shape and form of objects. Each type of operation applies a function to each pixel of the image, and its effect changes the shape and form of the original object. Before we discuss the morphological operations necessary for our colony analysis, we first also need to define another term, morphological structuring element. Every time that the morphological operations are used, we will need to have a structuring element to define the shape and size of the operating window that is centered at the current pixel. We will next discuss the simplest form of morphological operations which are the operations for binary images. The five important operations that are necessary for colony analysis include: erode, dilate, close, open and fill.

Erode and dilate operations are the morphological operations that are used to shrink or extend an object in the image. For example, if we apply the dilate operation to a single pixel using circular structuring element with the radius of 3 pixel, we will simply have the output object that looks exactly like our circular structuring element. Erode and dilate only operate at the edge of object which is any location in the binary image that have non-uniform pixel values in a region defined by the structuring element. While the effects of both operations are simply opposite of each other, these two operations are not invertible. The next two next morphological operations, open and close, rely solely on the invertible property of erode and dilate operations. Open and close operations simply apply erode and dilate operations right after one another. Open operation first applies erode and then perform dilate. Close operation performs dilate first and then erode. Open operation is normally used to separate two nearby objects that are hanging to each other by a contact point approximately smaller than the structuring element used. Close operation can be used to connect nearby objects that are separated from each other by the distance smaller than the size of the structuring element. Figure 4-12 illustrates an example of close operation that is used to modify a binary image of an mESC colony. We can control its effect using structuring elements of different sizes and/or shapes. From the example, we cannot recover the c colony region using too small structuring element (Figure 4-12C). Too large structuring element will eventually distort the shape of the colony by smoothing out all information at the boundary of the colony region or simply connecting two objects that we do not mean to have (Figure 4-12E). It is therefore necessary that we use these morphological operations carefully in order not to distort the information carried within the colony shape. To help preserve the original shape of the colony, fill operation can be used together with open and close operations to limit the number of operations that can distort the shape of the colony. If we choose the appropriate operations, we can reconstruct a complete colony region from the original binary image (Figure 4-12D). For comprehensive review of morphological operations, the readers are kindly referred to this review[125].

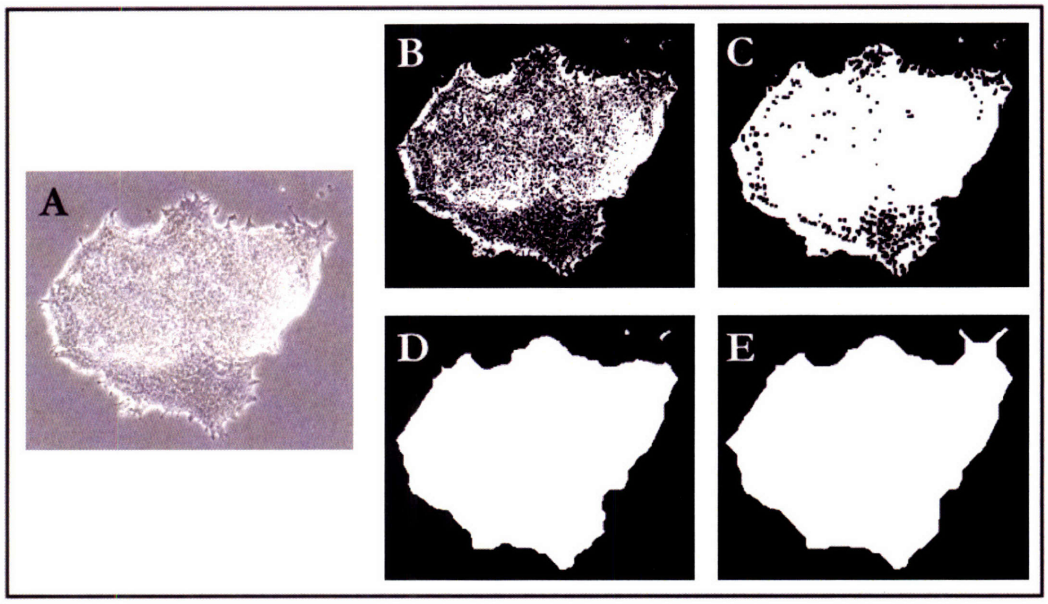

Figure 4-12 Close operation on thresholded colony image: A) Original intensity image. B) Output binary image from adaptive thresholding. C-E) Binary images of mESC colony applied with close operation with varying radius of circular structuring elements: C) 3 pixels D) 15 pixels and E) 30 pixels.

4.5.2.3 Screening for the appropriate colony regions

Now that we have finished the segmentation process, the last task is to screen off other unwanted objects. Figure 4-13 illustrates how colony screening is performed. Usually, the resulted binary image from the segmentation process will contain multiple regions of unwanted objects from the background. These objects can be cell debris or simply some glaring reflection of object on the bottom of the substrate. We can screen off relatively small regions by imposing a criterion on sizes of the segmented regions. Region parameters such as equivalent diameter ($4\times\text{Area}/\pi$) can be used for the comparison. There might still be some objects whose sizes are comparable to the colony of interest, we will then need to define region of interest around the colony and repeat the segmentation process to screen off these large objects. Regardless of the manual screening process, the required time for computation can be done in less than a second. Automatic colony selection will however be more practical, especially when we need to have multiple colony repeats to create a statistically significant observation.

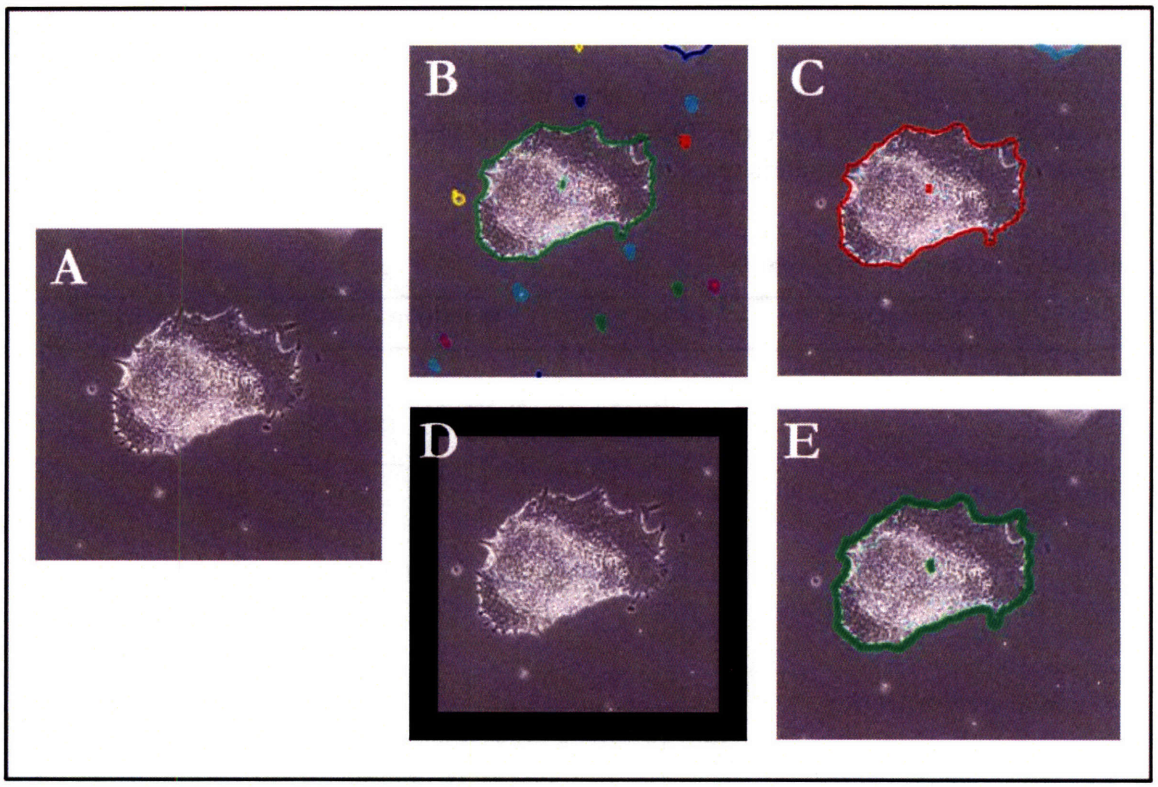

Figure 4-13 Selection of appropriate colony region: A) Original image. B,C&E) Overlay image of original intensity image and the contours of segmented objects. B) Many segmented regions are included when no screening is used. C) The small segmented regions are screened off by imposing a size criterion, leaving only the colony (red) and object of similar size (light blue). D) By defining the appropriate region of interest, we can limit the result of segmentation to only the colony region (E).

4.6 Post-process analysis

4.6.1 Motility and proliferation

We are interested in analyzing the morphological changes of the patterned ESC colonies that might be caused by colony-colony interactions. By analyzing the morphological changes of the colonies with respect to the direction of colony-colony interaction, we can extrapolate whether colony-colony interactions can also influence colony proliferation and/or motility. Since we want to see the effects of colony-colony interactions at the level of single colonies, measuring proliferation of the ESCs in bulk will not be sufficient. We instead used microscopy and image processing techniques to monitor different parameters from its contour. In order to analyze the morphological changes of the colonies, at least two images of colonies are necessary, one taken at the beginning of the experiment and the other at the end. We will assume here that these images have been collected and pre-processed appropriately as described above.

Table 4-2 defines different parameters that can be used quantify colony morphological changes for the study of colony-colony interaction. For our subsequent analysis, we would like to define the following parameters: A is the region in the image that contains all pixels of our interest, C represents the pixels on the contour of the interested region, and t is the monitored timepoint. We will also define $\bar{c}[\ ]$ as a function to create a

colony vector (vector that connects the origin to the centroid of the colony) of the input region, $a[\ ]$ is a function to determine area of the input region, E( ) is the expected value of the input parameter, $p[\ ]$ is a function to determine perimeter of the input region and d are elements of the movement vector. Other parameters are defined in the table. Figure 4-14 shows some of these parameters graphically.

Table 4-2 Colony morphology matrix

Parameters	Definition	Application
1. Single-colony variables		
Centroid (c_A)	(c_{10}, c_{01}) where $c_{lk} \equiv \frac{\int_A x^l y^k dxdy}{\int_A dxdy}$	Motion
Colony vector	$\vec{c}[A] = \begin{bmatrix} c_A(1) \\ c_A(2) \end{bmatrix}$	Motion
Movement vector ($\vec{d}$)	$\vec{c}[A_{t2}] - \vec{c}[A_{t1}] = \begin{bmatrix} d(1) \\ d(2) \end{bmatrix}$	Motion
Movement magnitude	$\left\|\vec{d}\right\| = \sqrt{d(1)^2 + d(2)^2}$	Motion
Movement Direction	$\angle\vec{d} = \arctan\left(\frac{d(2)}{d(1)}\right)$	Motion
Movement speed	$\frac{\left\|\vec{d}\right\|}{\text{t2-t1}}$	Motion
Diffusivity	$\frac{E(\left\|\vec{d}\right\|^2)}{4(t_2 - t_1)}$	Motion
Common region (C)	$A_{t1} \cap A_{t2}$	
Protrusion region (P)	$\overline{A_{t1}} \cap A_{t2}$	
Retraction region (R)	$A_{t1} \cap \overline{A_{t2}}$	
Protrusion vector ($\vec{p}$)	$\vec{c}[P] - \vec{c}[A_{t1}]$	Motion
Retraction vector ($\vec{r}$)	$\vec{c}[A_{t2}] - \vec{c}[R]$	Motion
Area	$a[A] = \int_A dA$	Growth
Perimeter	$p[A] = \int_{C_A} dC$	Growth/Shape
Orientation	Angle between major maxis of the covering ellipse and x axis	Shape

Projected surface area (PSA)	$\frac{4\pi a[A]}{(p[A])^2}$	Shape
2. Double-colony variables		
Inter-colony spacing (D_{in})	Minimum distance between two contours	Interactions
Distance between centroids (D_c)	$\left\|\vec{c}[A_{colony2}]-\vec{c}[A_{colony1}]\right\|$	Interactions
Centroid-path vector ($\overrightarrow{D_c}$)	$\vec{D}_{c,A}=\begin{bmatrix} c_B(1)-c_A(1) \\ c_B(2)-c_A(2) \end{bmatrix}$	Interactions
Angle distorted from centroid path	$\Theta_A = \arccos\left(\frac{\vec{d}_A \cdot \vec{D}_{c,A}}{\left\|\vec{d}_A\right\|\left\|\vec{D}_{c,A}\right\|}\right)$	Interactions
Angle between movement vectors	$\arccos\left(\frac{\vec{d}_1 \cdot \vec{d}_2}{\left\|\vec{d}_1\right\|\left\|\vec{d}_2\right\|}\right)$	Interactions

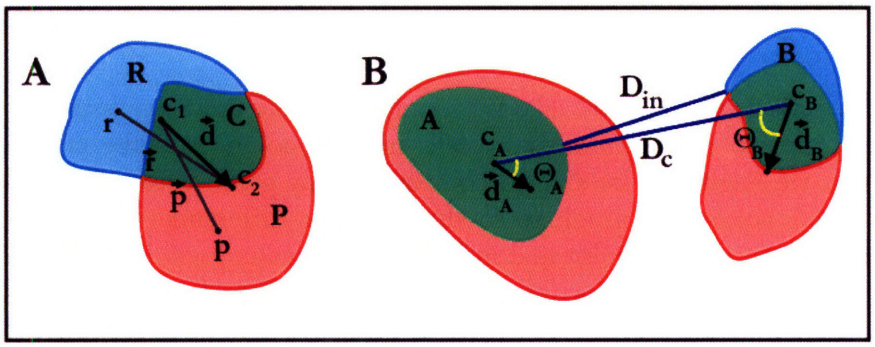

Figure 4-14 Definition of colony regions and vectors: A) Single-colony and B) double-colony movement parameters. Red region represents the protrusion (P) region. Green region represents common region (C). Blue region represents retraction region (R). For the double-colony cases, we call the two colonies A and B accordingly.

The first point that needs to be mentioned here is that the morphological changes of ESC colonies are not exactly the same as regular cell motion. Since cells do not change their areas significantly while migrating, cell motility can be described mainly based on the centroid of cells. ESC colonies change their size quickly with time. The average doubling times of mESCs and hESCs are 15-18 hours and 30-36 hours respectively. If we simply assume that all cells in the colonies are attached to the substrate so that the number of cells is linearly proportional to colony area, colony area will increase by two times for every doubling cycle. If the growth of the colony is also dependent on a diffusive factor that is imposing on the colony, the gradient of such factor can cause the colony to grow biasedly and contribute significantly to the colony movement. We must therefore be aware of the interconnection of growth and movement in ESC colonies while we analyze the effects of colony-colony interactions later on. To compare the standard cell movement matrices and our colony morphology matrix, the readers are referred to previous literatures[126, 127].

Now that we have developed a matrix to explain quantitatively the morphological changes of ESC colonies, we can begin to observe how these parameters are varying for different experimental conditions. In addition to the classification of colony parameters by the number of colonies associated, we will categorize these parameters based on its practical implication into three groups: 1) parameters that represent colony growth, 2) parameters that represent colony motion and 3) parameters that represent colony shape. The growth parameters we have are based mainly on the areas of the colony region derived from segmentation of the colony images (§4.4). We assume for this analysis that colony area grows linearly with the number of cells in each colony. In reality, this assumption is not always valid. Like cancer cells, ESCs are not contact-inhibited and can therefore grow on top of each other, eventually giving multi-layer colonies. It is therefore possible that the colony area may not increase linearly with the number of cells in the colony. Nevertheless, different approaches can be taken to get around this problem. We may force most ESCs within each colony to adhere to substrate by coating the substrate with highly adhesive ECMs such as fibronectin. Even though it has been shown that self-renewal of mESCs was maintained using this approach[72, 73], previous study also showed that changes in cell morphology can plays a critical role on cell fate decision. For example, mesenchymal stem cells that were allowed to attach on the substrate committed to osteogenesis while the cells that were prevented from adhering to the substrate turned into adipocytes[128]. By coating substrate with fibronectin, we might therefore detect the behaviors of colonies that are intrinsically different from the behaviors of colonies cultivated with regular ECMs such as gelatin.

The approach that we will take is to simply use the previous assumption regarding the linear relationship of the number of cells in each colony and the colony area. The expense is that we might not be able to compare colony growth from different cultivating conditions. ESC colonies can adhere to the substrate differently in different cultivating media. For instance, mESCs cultivated in serum-free medium will have flat colonies while the colonies cultivated in serum-containing medium tend to be much rounder. In this particular example, mESC colonies cultivated in serum-containing medium should therefore have greater cell number than the colonies cultivated in serum-free medium for an equal colony area. This assumption is however valid for comparison of colony growth from the same cultivating condition. We can use colony area to compare colony growth between one-colony and two-colony groups in the same experimental conditions. As we will show later in §5.2.1, we used colony area to compare colony growth when the colonies are cultivated in different medium-replenishing intervals and to also observe the effects of varying inter-colony spacing on colony growth. A critical limitation for this method is that local differences in colony growth within each individual colony will not be detected. This problem is universal to all analytical parameters that rely only on colony contour, neglecting mass distribution inside the colony.

The second category of colony morphology parameter includes parameters are used to abstract colony motion. To represent the magnitude and the direction of the colony movement, we define movement vectors that connect the colony centroids at different time points. The magnitude of the movement can thus be represented by the magnitude of colony movement vector. Regarding the direction of motion, we can reference the colony motion to some other reference vectors such as centroid-path vector or simply movement vector of the neighboring colony. The angle between the two vectors can be calculated from their inner product (Table 4-2). Similar to the issue we had earlier with total colony areas,

centroid-based movement vectors reflect only motion of the whole colony and cannot explain local motions of cells within each colony.

The last group of colony morphology parameters explains the colony shape, including perimeter, projected surface area (PSA) and colony orientation. A perfect circle will have PSA of 1. A line will have PSA of 0. Other useful colony-shape parameters that were not mentioned in the matrix include eccentricity, equivalent radius and major and minor axis length (available from MATLAB function "regionprops"). To monitor changes in colony proliferation and motility, we did not rely so much on this type of parameters. However, one appropriate application of these colony-shape parameters is to differentiate undifferentiated colonies with clear round boundary from the differentiating colonies that tend to have inhomogeneous border. Such analysis may be able to predict the percentage of differentiating colonies from the whole experiment in real-time, instead of staining the colonies with self-renewal markers that usually take a few hours to complete.

These three types of colony morphology parameters are adequate to first order for explaining how the morphology of ESC colonies is influenced by the imposing colony-colony interactions. In each analysis, we look for a consistent relationship between the colony morphology parameters and the experimental parameters that we are interested in, such as different types of cultivating medium, initial inter-colony spacing or the number of colonies in each colony group. Before we end this section, it is worthwhile to visit some of the qualitative representations of colony morphological changes. Good qualitative representations of changes in colony morphology can lend us some intuitions about how different parameters in the matrix might be correlated with one another or with the variables being varied in our experiment. The overlay of colony contours (Figure 4-15A) allows us to decide quickly how the colony evolves over time and the direction that the colony moves towards. A movement vector plot (Figure 4-15B) illustrates the distribution of colony movement on the substrate. An angle histogram (Figure 4-15C) can tell us quickly whether there is biased colony growth and movement. We used these representations to postulate how colonies might be changing with the varying experimental parameters and to choose the appropriate parameters from the colony morphology matrix to test our hypotheses. Explanations about how to create these graphic representations are available in appendix section.

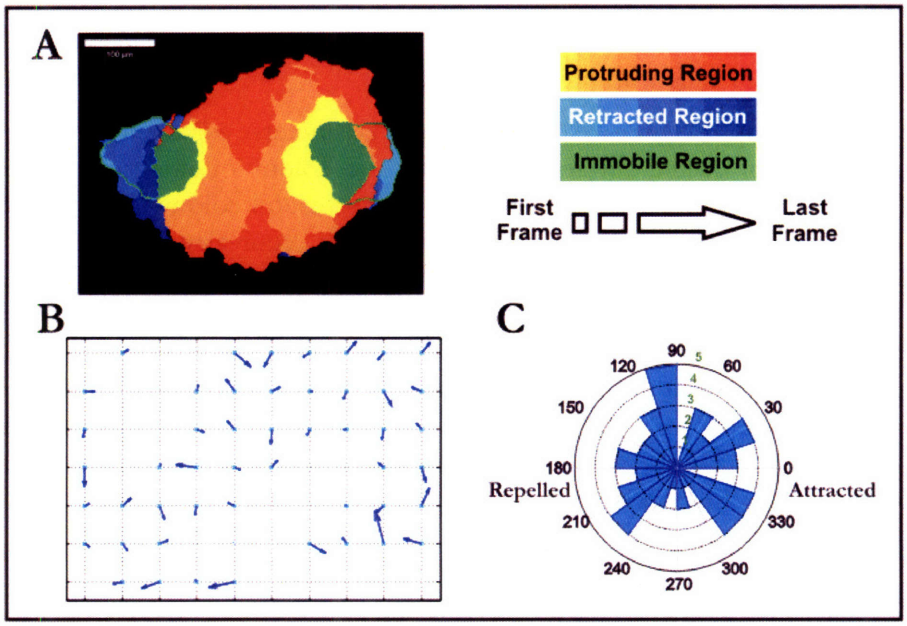

Figure 4-15 Representations of colony morphological changes: A) Colony-contour overlay, B) Movement vector plot and C) Angle distribution of movement direction.

4.6.2 Quantification of self-renewal markers

In addition to colony proliferation and movement, we are also interested in the effects of colony-colony interactions on self-renewal of mESCs. Different self-renewal makers are available and can be categorized into three groups: 1) transcription factors such as Oct-3/4, Sox2, Nanog and Rex-1, 2) cell surface markers such as SSEA-1, CD9, and PECAM-1 and 3) cytoplasmic proteins such as alkaline phosphatase[129, 130]. In our study, we mainly used alkaline phosphatase stain because the assay can be performed easily via an emzymatic-based reaction. To quantify the stain intensity for each colony group, we thresholded the staining images into two regions: 1) the region where the stain intensity is high which will represent locations where self-renewal is maintained and 2) the region where stain intensity is low, representing location where the cells are differentiating. We then calculated for the areas of both regions and normalize them by the total colony area. Figure 4-16 illustrates the operations we described. We will use this method to compare self-renewal of mESC colony groups that are cultivated in serum-free medium with different medium replenishing duration. We will also compare self-renewal and differentiation indexes of ESC colonies from one-colony groups and two-colony groups with varying inter-colony spacing. Consistent differences in self-renewal and differentiation indexes between different colony groups will validate the role of colony-colony interactions on self-renewal of mESCs. Note also that higher intensity inside the colony may also be caused partially by piling up of mESCs. In addition to using fibronectin to promote cell adhesion to substrate, previous studies also tried to normalize the intensity of self-renewal markers across the colony by the intensity of commonly-expressed proteins such as β-actin[72, 73]. Since actin may also localize at certain spots inside the cell, the derivation of normalized self-renewal index must be performed at the single-cell resolution with the assumption that each cell in the colony can be partitioned accurately.

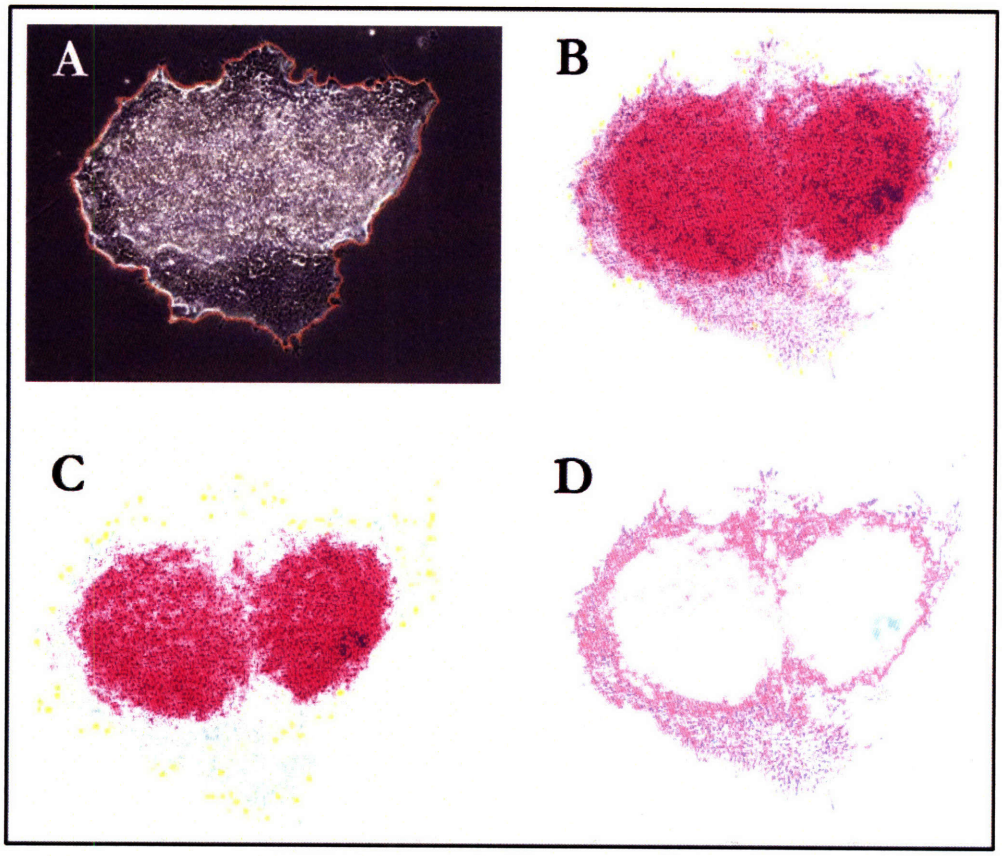

Figure 4-16 Self-renewal marker quantification: A) Original phase-contrast image overlaid with the contour of its binary region (red line) from which colony total area will be calculated. B) The same colony group that was stained with alkaline phosphatase. C) Colony region with high stain intensity, implying maintained self-renewal. D) Colony region with low stain intensity suggesting differentiation. By normalizing the area of colony regions in C) and D), we can quantify self-renewal and differentiation of each colony group approximately.

CHAPTER 5: RESULTS

In this chapter, we will present the results of our investigation whether colony-colony interactions may influence colony growth, motion and self-renewal in mESCs. We first discuss the efficiency of our colony patterning technique and explain some of the difficulty we found in using this technique. In the next section, the analysis of colony behaviors for varying parameters including inter-colony spacing, type of cultivating media, and diffusion time will be reported. We will test whether two nearby mESC colonies that are patterned at varying distane apart can interact with each other. The observed colony behaviors will be compared to the one-colony group. The last section demonstrates our preliminary results of techniques to improve analysis of colony-colony interactions. We will demonstrate how speckle imaging technique may be used to monitor local colony motion and also discuss our developing technique to prevent fluid convection in open-topped platforms using hydrogel formation.

5.1 Patterning mESC colonies with stencils

Using the patterning protocol as discussed previously in §3.2.2, almost 90% of the mESC colonies can be delivered and remained on the substrate after the patterning process (Figure 5-1). The patterned colonies can expand outside the patterning region after the stencil was removed and can grow similarly to mESCs colonies that are cultivated using conventional method. Figure 5-2A shows a mESC colony that was patterned on top of the substrate that was initially coated with fluorescent gelatin just inside the stencil hole. After the stencil was removed, the other substrate area was then coated with regular gelatin. The picture demonstrated that colony could expand beyond the area underneath the stencil hole. Stencil patterning can also be used to pattern different designs of mESC colonies. Figure 5-3 shows different designs of 3-colony patterns and the resulting colonies from the patterning. The efficiency of stencil patterning depends greatly on whether conformal contact between the stencil and the substrate can be achieved. Figure 5-2B shows the result of patterning when there was leakage between stencil and the substrate. In our study, we promote conformal contact between stencil and the substrate surface by adding a few drop of ethanol onto the substrate before attaching the stencil to the substrate. It is also as important to evaporate ethanol off after we already attach stencil to the substrate to prevent any toxicity of ethanol to the cells. Bubbles in the stencil holes must also be removed to ensure that that all colony sites are loaded. Figure 5-2E&F demonstrates the consequence of having bubles in the stencil holes which can block the cells from sinking, and adhering to the substrate surface. Mixing of the cell suspension after loaded into the stencil also helps to spread the cells equally across the substrate.

In our study, we also found that the time that we let mESCs attach to the substrate before we remove the stencil is very critical for the patterning. If we let the cells grow for too long, mESCs can grow on top of the stencil (Figure 5-2C). When we remove stencil from these overgrowth colonies, the colony usually becomes physically damaged and eventually die (Figure 5-2D). In all of our experiment, we let mESCs attached to the substrate between 10-12 hours. Cell loading density is also critical for stencil patterning. We usually load a 2.5-cm-diameter stencil with half a million mESCs that are suspended in 3 ml cultivating medium.

In term of stencil fabrication, the thickness of the stencil we used is in the range of 40-60 μm, resulted from SU-8 posts with the height of 70-90 microns. This stencil thickness helps us to fill in approximately 1 cell layer in each stencil holes. To ensure that no thin PDMS film will be masking the stencil holes, high enough pressurizing force must be applied to the stencil fabrication stack (Figure 3-1B). The use of thick rubber sheet in the stack also helps to distribute uniform pressure across the master wafer.

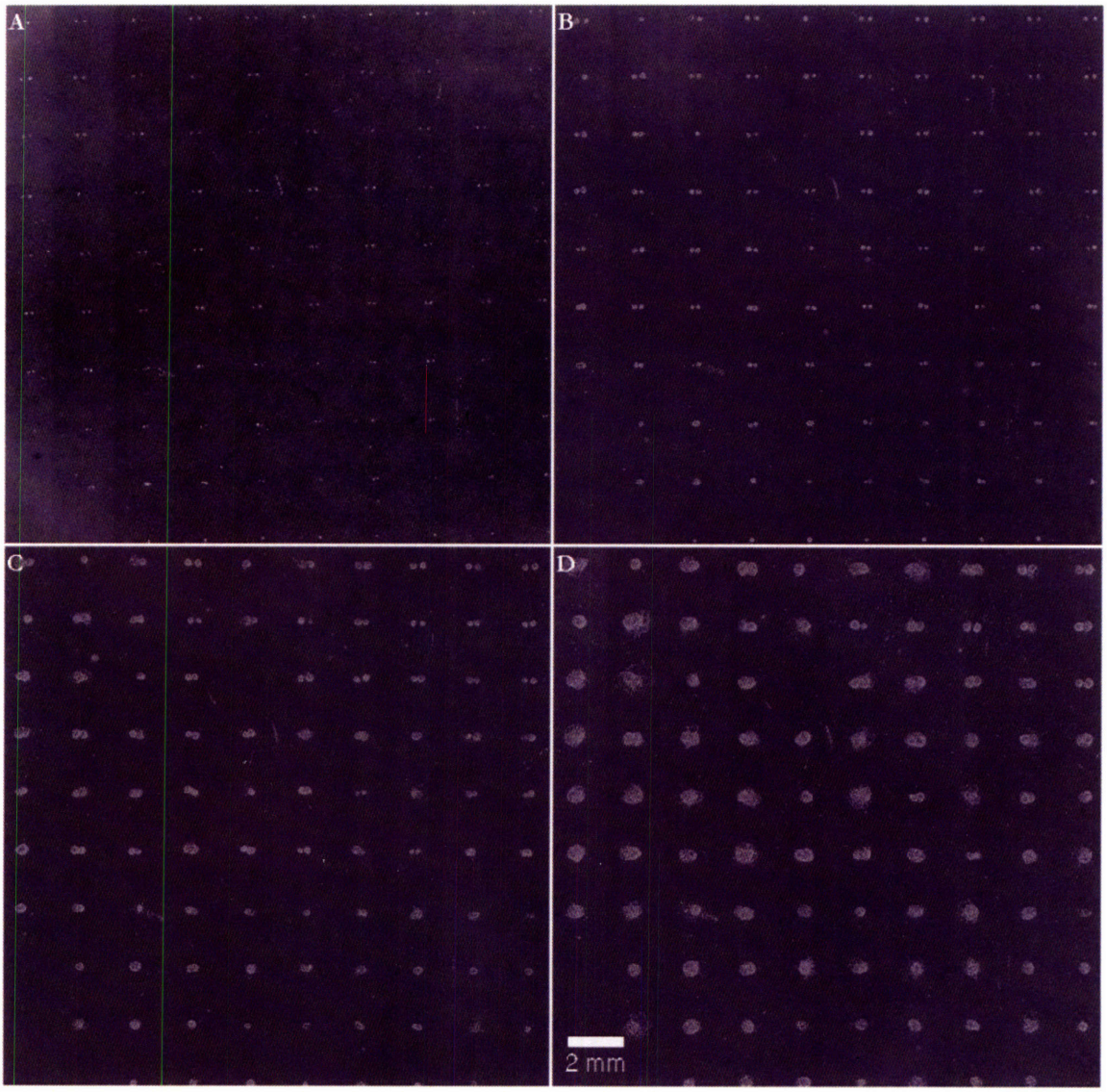

Figure 5-1 Stencil patterning efficiency: Whole-substrate images of patterned mESC colonies cultivated in serum-free medium, replenished every 8 hours at A) 0 hour, B) 24 hours, C) 48 hours and D) 72 hours.

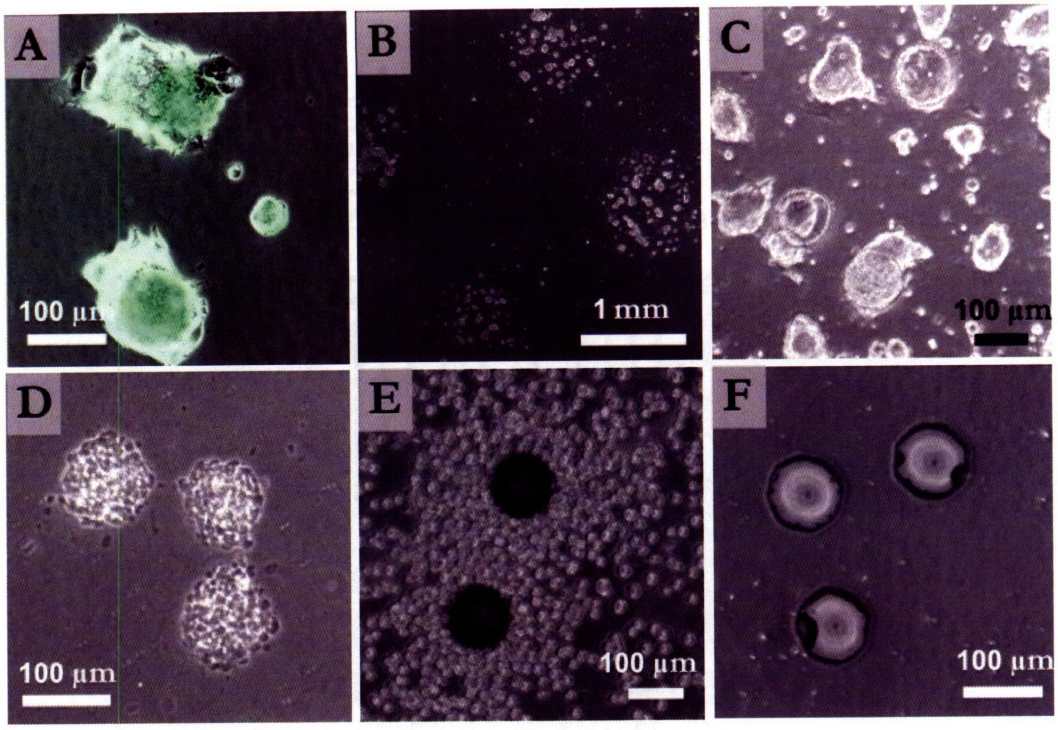

Figure 5-2 stencil patterning with possible difficulties: A) Good patterned colonies patterned on fluorescent gelatin protein (green). B) Poorly resulted pattern caused by improper sealing between stencil and substrate. C) Climbing of colony over the stencil. D) Cell death due to mechanical stress from pealing. E-F) Bubbles sealing stencil holes, preventing cells from filling.

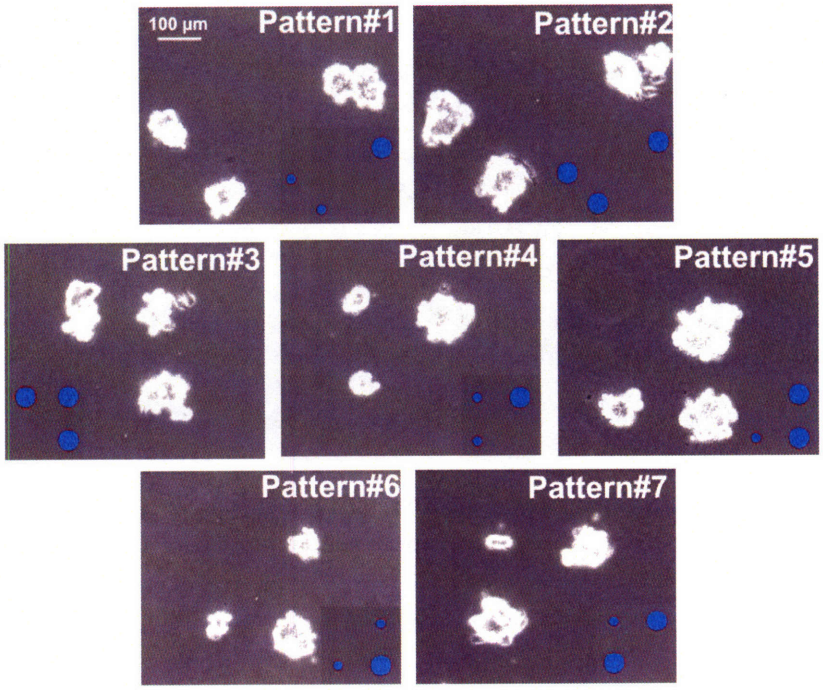

Figure 5-3 Different 3-colony patterns: Using stencil patterning we can achieve different patterning designs of mESC colonies. Shown here are some of the resulted three-colony patterns. Blue circles represent the expected geometry for each colony pattern.

5.2 Assaying colony-colony interactions in different medium conditions

To investigate whether colony-colony interaction can occur between two nearby colonies, we monitored and compared the physical behaviors of the two-colony groups to the one-colony groups. Two main parameters that we are interested are colony proliferation and colony motility. Based on the observed effects of autocrine signaling in mESCs, these are the two parameters that may be controlled by any autocrine gradients established by the colonies. We are also interested to investigate how potential colony-colony interactions might also influence self-renewal of mESCs. The connection of self-renewal and colony-colony interaction may help explain heterogeneity that is sometimes observed while maintaining mESCs *in vitro*. In addition to the comparison of colony behaviors between 1-colony and 2-colony groups, we will also observe how colony morphology may change as we vary these parameters: 1) inter-colony spacing, 2) baseline signal intensity in different cultivating media, 3) medium-replenishing time. There were three cultivating media that we tested: 1) serum-containing medium (with LIF), 2) serum-free medium (with LIF and BMP4) and 3) serum-containing medium without LIF. To collect and analyze the colony images in these studies, we collected images of the whole substrate plane and register the images using the procedure described in §4.3.3. To segment the colony images, we use thresholding-based segmentation as previously described in §4.5.2. Morphological parameters of each colony group were then calculated as described in §4.6. The following sections describe our results.

5.2.1 Colony Proliferation

To determine whether colony-colony interactions can influence colony growth, we asked whether colonies from the two-colony groups would grow slower, faster or equally to the single-colony groups. The total colony areas of each colony group at multiple time points during the experiment were calculated. For that area of two-colony groups, we simply summed the area of both colonies. The effects of colony-colony interactions were also investigated as we vary inter-colony spacing and diffusion time in different cultivating media. The observed results are presented Figure 5-4 and Figure 5-5.

Before we compared colony proliferation among different colony groups, the actual colony areas must first be normalized. The normalization is necessary because all patterned colonies may not have exactly the same colony size at the beginning. For the results of our experiment, colonies in serum-containing medium with 15-hour medium replenishing condition (Figure 5-4B) and colonies in serum containing medium without LIF with 8-hour replenishing condition (Figure 5-4E) had non-uniform colony areas for varying initial inter-colony spacing. To standardize the data, we normalized the areas of each colony group with its total area at the initial time point. Figure 5-5 shows the colony areas after normalization. We will now discuss the observed colony growth in different cultivating conditions.

In serum-containing medium, we replenished the media every 5 (Figure 5-5A) or 15 (Figure 5-5B) hours and monitored the colonies every 15 hours. We compared the normalized area between both medium-replenishing conditions by applying one-way ANOVA to the normalized area across all inter-colony spacing of both groups at the same monitoring time point. The colonies with 15-hr replenishing condition were observed to grow faster that the colonies with 5hr replenishing condition(p=9.9e-7, 3.2e-8, and 4e-4 at 15, 30, and 45 hours respectively). One-colony groups grew slightly slower than two-colony groups in 5-hr replenishing condition but faster or equal to two-colony groups in 15-

hr replenishing condition. After 45 hours, the areas of the colonies in 15-hr replenishing condition were observed to change slightly with varying inter-colony spacing, although this was not statistically significant (p=0.122). We applied 1-way ANOVA to compare only the difference among colony groups with varying inter-colony spacing at 45 hours. Similar trends of colony growth was not observed in 5-hr replenishing condition.

In serum-free medium, the colonies cultivated with 8-hour replenishing condition were observed to grow faster than those in 24-hour replenishing condition (Figure 5-5C&D). The elevated growth rate was observed as early as the first 24 hours of the experiment, across all choices of initial inter-colony spacing. The elevated growth observed here may be due to the limited growth factors in serum-free medium. By changing the medium more often, the colonies could then proliferate without any shortage of the required growth factors. In comparison with colonies in serum-containing medium, such elevated growth was not observed probably because of the excess growth factors in serum. Regarding the effects of colony-colony interactions, we did not observe colony spacing-dependent growth. The colony areas were fairly uniform across all initial inter-colony spacing. Single-colony groups also grew approximately as fast as the two-colony groups.

In serum-containing medium without LIF, similar colony growth was observed for both 8-hour and 24-hour replenishing conditions (Figure 5-5E&F). Single-colony groups also grew similarly as the two-colony groups. It is therefore suggestive from the results that removal of LIF from the medium did not strengthen the effect of colony-colony interactions on mESC growth because inter-colony spacing-dependent growth was not observed nor any difference in growth between one-colony and two-colony groups. Note also that the colony areas for varying initial inter-colony spacing here are more distributed than the ones in serum-containing medium. The standard deviations of normalized areas across all colony groups at 45 hours in serum-containing medium, replenished every 5 and 15 hours were 1.06 and 1.57 respectively. On the other hand, the standard deviations of normalized areas across all colony groups at 48 hours in serum-containing medium without LIF, replenished every 8 and 24 hours were 2.83 and 3.52 respectively. This result is probably caused by colony differentiation when LIF was removed from the medium and must also be the result of limited sample size in this experiment. Differentiation causes mESCs to become more fibroblast-like and therefore have greater colony areas. Since mESC colonies may not differentiate all at once, the colony areas may therefore become more distributed than the ones in serum-containing medium where self-renewal is well preserved.

To summarize our observation, no distinct effect of colony-colony interactions on colony growth was observed in any cultivating conditions we tested.

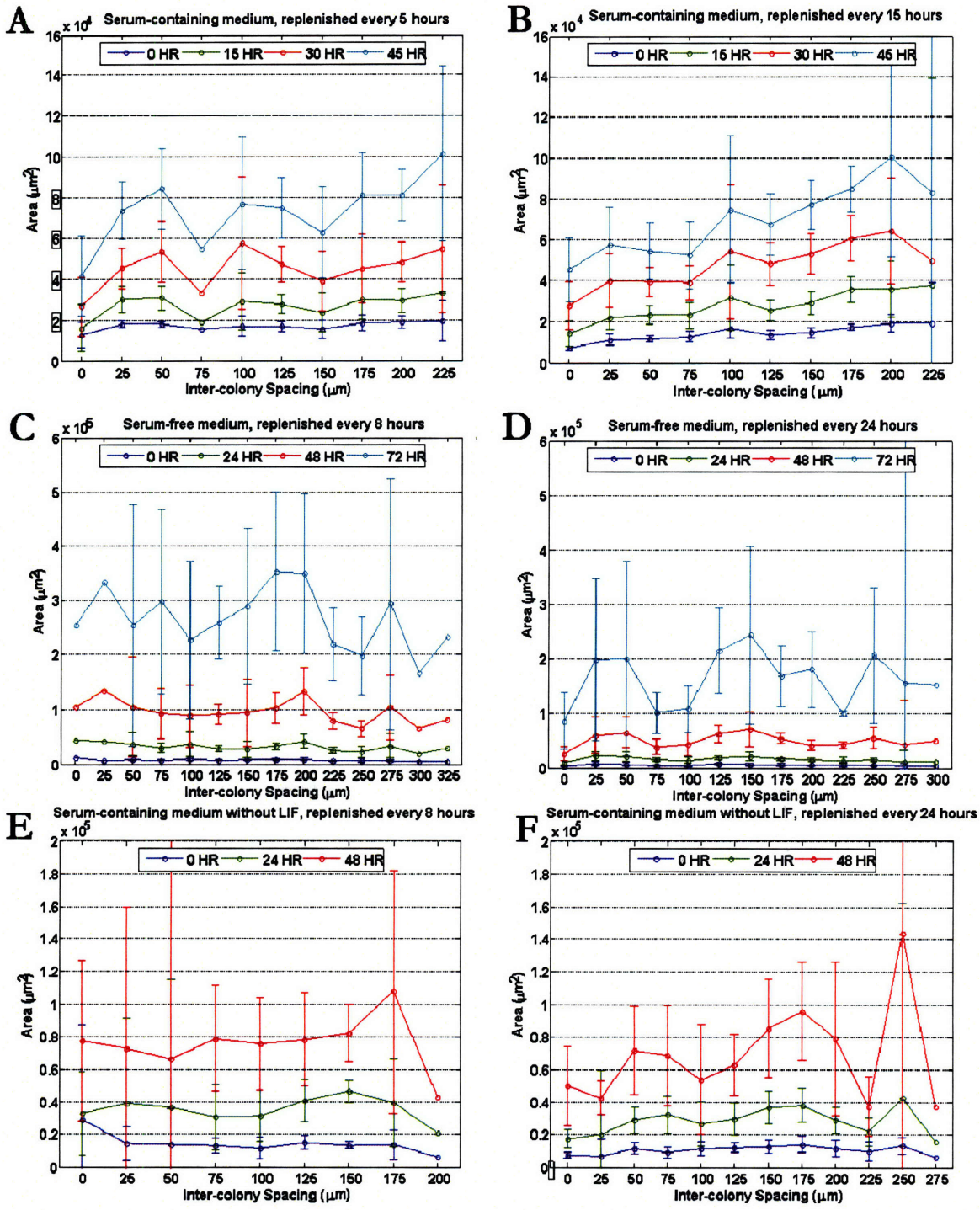

Figure 5-4 Averaged actual area: Each data point show averaged actual area of each colony group with the corresponding initial inter-colony spacing at the initial time point and over the monitored time. All data points are presented with 95% confidence intervals. Data points with inter-colony spacing of zero micron represent colony growth of one-colony groups.

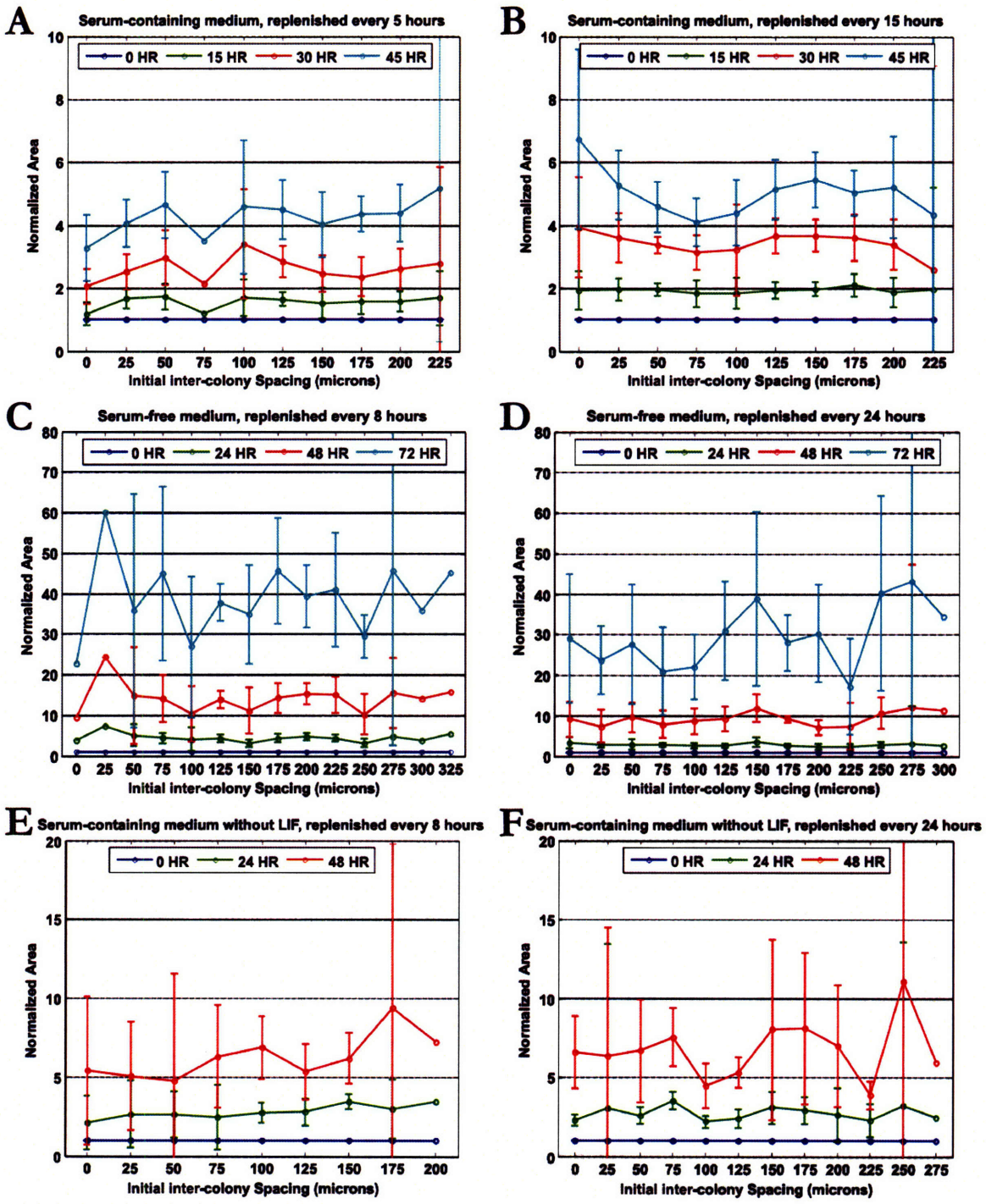

Figure 5-5 Averaged normalized area: Each data point show averaged normalized area of each colony group with the corresponding initial inter-colony spacing at initial time point and the monitored time. All data points are presented with 95% confidence intervals. Area of each colony group was normalized by its initial area taken right after we removed the stencil. Data points with inter-colony spacing of zero micron represent colony growth of one-colony groups.

5.2.2 Colony motion

To investigate whether we can observe any potential colony-colony interactions by their affect on colony motility, we compare the displacements of the one-colony groups with those of the two-colony groups that were still not fused throughout the experiment. The reason why we only use the unfused two-colony groups is that we cannot determine the displacement of the two colonies accurately after colonies already fused. We still however used data from the fused colonies and interpreted them as single-colony groups at the next time point. The displacement used for the analysis here was measured from the mean displacement for each colony group within two consecutive monitoring time points. For experiment in serum-containing medium, the displacement represents colony motion within each 15 hour period. For the experiment in serum-free medium and serum-containing medium without LIF, the displace represent colony movement within 24 hours. We assumed here that movement of colonies during different time period of the experiment is similar. In other words, displacements of an individual colony during the first incubation period will be equally valued and comparable to the ones in the later incubation period. This assumption is reasonable because any colony-colony interactions would be reset after every time the medium is changed. Therefore, as long as we keep the incubation period constant throughout the experiment, colonies will be experiencing approximately identical signal intensity for the same inter-colony spacing. One argument may be that the colony displacement might also be dependent on colony area which is increasing during the experiment. Our analysis however showed that colony displacement did not depend on colony area.

Among all cultivating conditions we tested, the only cultivating condition that shows an interesting outcome was the colony displacement in serum-free medium with 8-hour replenishing condition (Figure 5-6C). In this group, one-colony groups were observed to have the largest displacement in comparison with the displacement of all two-colony groups except the group with 325-μm spacing. A trend of increasing displacement magnitude seemed to be observed with increasing inter-colony spacing, although this observations was not statistically significant (p=0.81). For the results observed in other cultivating medium, there seemed to be no relationship between colony-colony interactions and the colony motility. The motility of one-colony groups was similar to that of the two-colony groups. There was no significant change in colony displacement for varying inter-colony spacing. Since it is still possible that the colonies may move towards the nearby colonies without any changes in displacement, we next verified whether colony-colony interactions might simply influence the direction of colony motion.

First, we compared direction of colony motion between one-colony groups and two-colony groups. Since the orientation of the colonies in any two-colony groups may be dissimilar at different locations on the substrate, we compensated for this inexactness by representing movement direction of the colonies in reference with the path connecting their centroids for two-colony groups ($\overline{D_c}$, Figure 4-14). We also assumed here that movement of each colony in the two-colony groups is independent. The results of this analysis are shown in Figure 5-7. For all cultivating conditions, movement direction of the one-colony groups distributes randomly in all directions. Significant biased movements of the two-colony groups were not observed in any cultivating conditions. We then asked further whether biased movement direction could be observed for different inter-colony spacing. Figure 5-8 demonstrated the angle that each colony movement vector distorted from the centroid path

(Θ,Figure 4-14) for different groups of inter-colony spacing (represented in different colors). The results suggested no biased movement directions for any group of varying inter-colony spacing. Data points within each group scattered randomly, with no crowding at any specific angles.

We have shown previously that ESC colonies do not prefer to move towards or away from each other in any cultivation media with the design criteria we used here. Based on our analysis, both colonies of the two-colony groups were observed to move randomly in all cultivating media we tested. However, these results were obtained with the assumption that both of the colonies in each colony pair move independently of each other. Our final analysis is therefore to investigate whether each colony in the two-colony groups can in fact move dependently of each other. To test this hypothesis, we first calculated for angle between the movement vectors of the two colonies and looked for inter-colony spacing that might give rise to consistent relative motion of the two colonies. Zero degree means that the colonies move in the same direction, which can mean that colonies are chasing each other or simply moving in parallel to each other. One-hundred and eighty degrees suggest that colonies are moving in the opposite direction. The result of this analysis is presented in Figure 5-9 with the box plot presenting medians and quartiles. The smaller the box plots, the more consistent motions of the two colonies. Even with our small sample sizes, we already observed randomly distributed angles between the two movement colonies for different inter-colony spacing of all cultivating conditions. The whisker bars, representing the range that cover 1.5 times of inter-quartile, of most box plots already span to cover all possible angles. Based on the data we observed so far, it is very likely that the colonies in the two-colony group moved independently of each other, and also independently of the inter-colony spacing in all tested cultivating conditions.

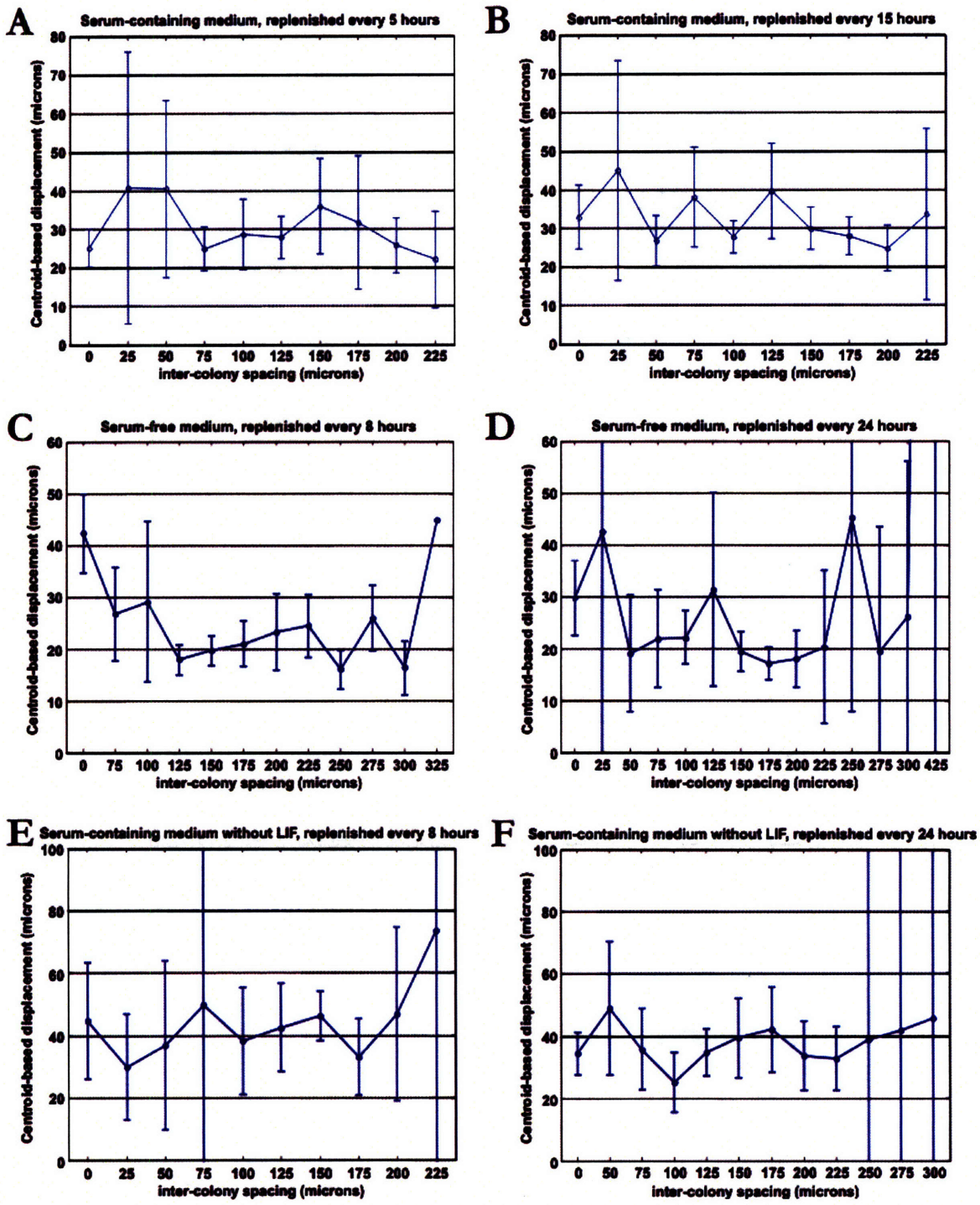

Figure 5-6 Centroid-based displacement: The displacements of colonies in serum-containing medium (A and B) were calculated for every 15-hour incubation period. The displacements of the colonies in serum-free medium (C and D) as well as in serum-containing medium with LIF (E and F) were calculated for every 24-hour incubation period.

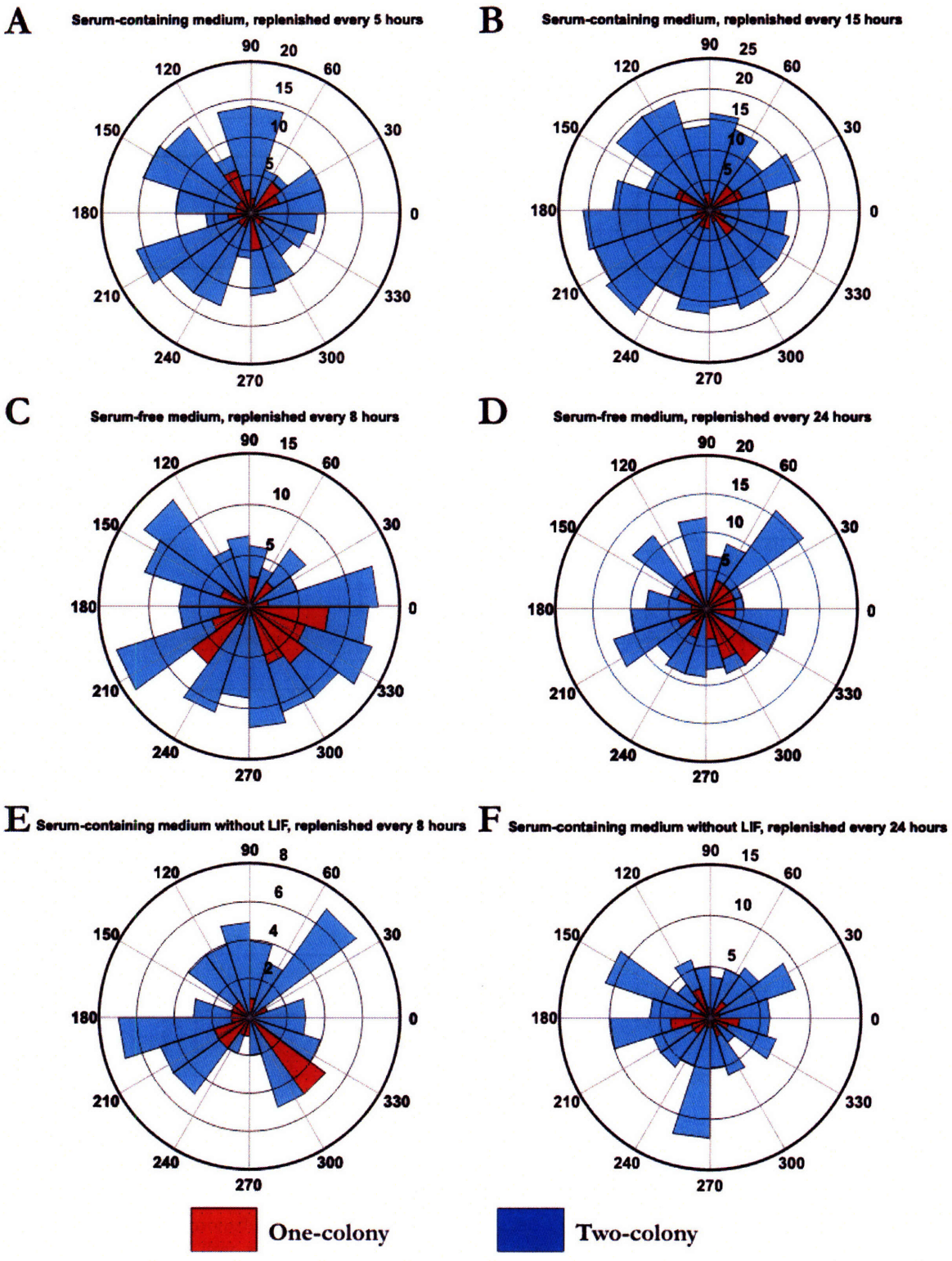

Figure 5-7 Colony movement directions: Each plot represents the angle histogram of the colony movement. For two-colony groups, zero degree represents the direction approaching the neighboring colony. One hundred and eighty degrees represents the direction away from its neighbor. For one-colony groups, the angles are arbitrary but consistent for each experiment.

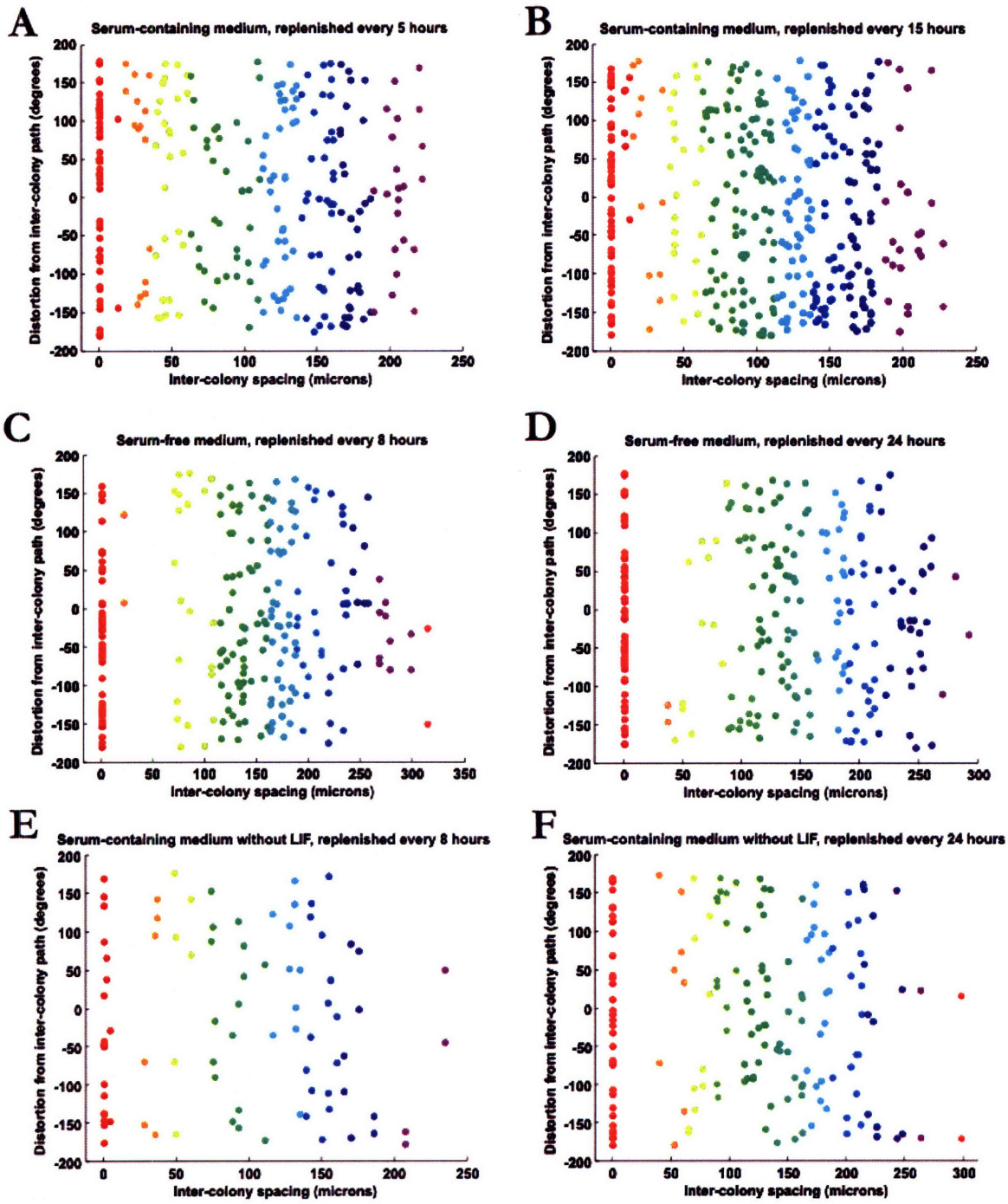

Figure 5-8 Colony movement directions for varying inter-colony spacing: Each colored dot represents an actual data point within their assigned groups of inter-colony spacing. Zero inter-colony spacing represents data points for the one-colony groups. The distortion angle was calculated in reference with the line connecting centroids of the colony pairs at the beginning of each incubation period.

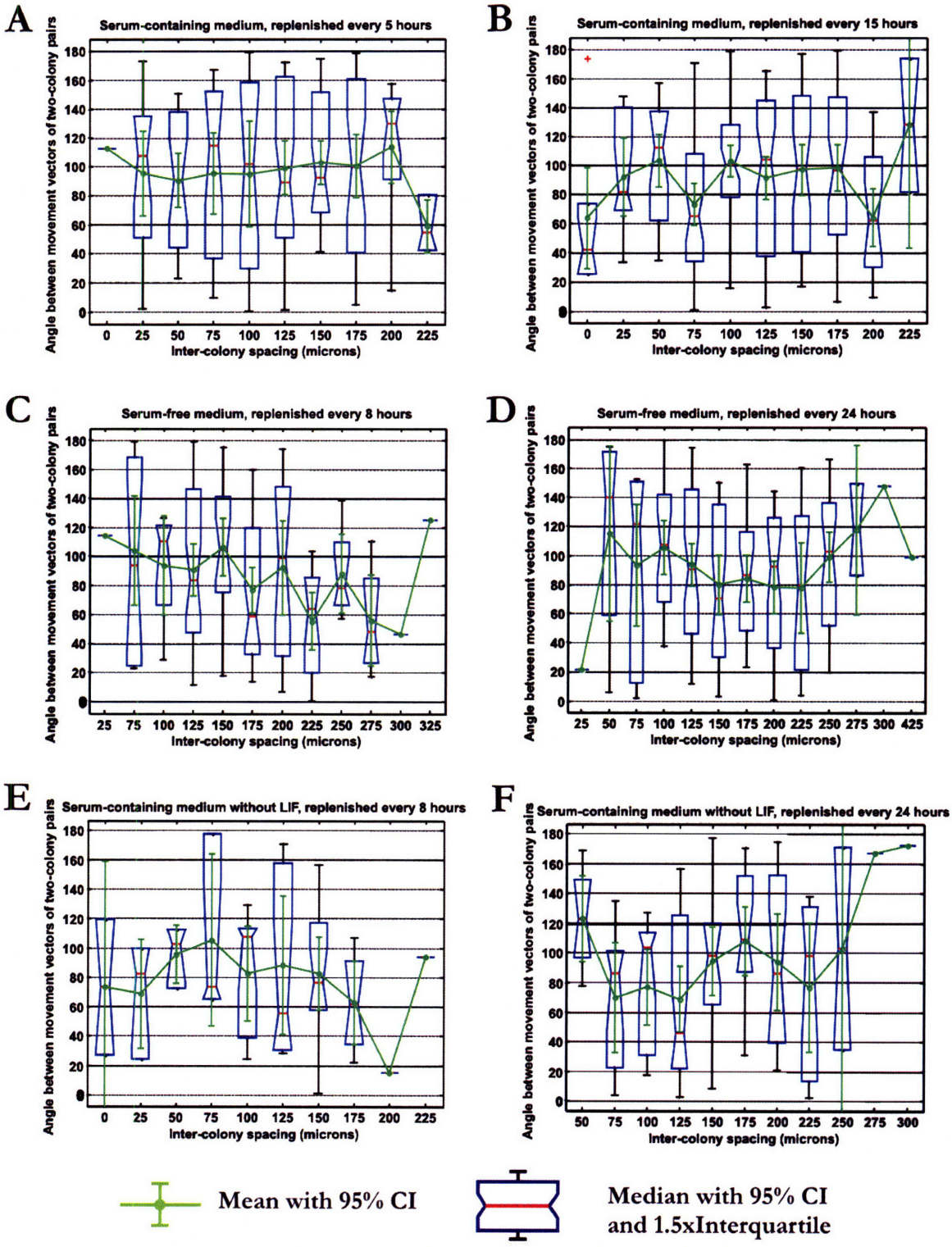

Figure 5-9 Angles between movement vectors for varying inter-colony spacing: Green plots represent means of the angle with 95% confidence interval. The box plot shows median (red bar) and upper and lower quartiles of the data within each group. The whisker bars represent the range of the data within 1.5 times of the interquartile. The notch between the box represent 95% confidence interval of the median.

5.2.3 Colony fusion

Colony fusion is the ultimate product of colony proliferation and colony movement. The increased rate of colony growth can accelerate the time it takes before two nearby colonies will collide to each other. Similarly, biased colony motion either towards or away from each other can also influence the onset of colony fusion. Elevated proliferation at a local region of the colony can also give rise to larger colony motion. Colonies that are more mobile also provide the colony with greater chances to be exposed to growth inducing signals. In this situation, monitoring the time required for colony fusion may serve to represent the ultimate, composite consequence of colony-colony interactions on colony morphology. Figure 5-10 shows the results from the analysis of colony fusion time in our experiment. Note that comparison of colony fusion time of colonies from two different media must be interpreted with care because colony areas from the two experiments might not be comparable to each other.

For mESC colonies that were cultivated in serum-free medium, the colony groups that were cultivated with 8-hr replenishing condition fused together slightly sooner than the groups cultivated with 24-hr replenishing condition. This result agrees with our previous analysis of colony areas in serum-free medium where we found that the colony groups with 8-hr replenishing condition had greater colony areas than the groups with 24-hr replenishing condition. Our previous analysis of colony movement in serum-free medium also showed that there was no significant difference in colony movement between the two medium-replenishing conditions. It is therefore possible that colony growth is the main cause of the accelerated colony fusion in the 8-hr replenishing condition. mESC colonies that were cultivated in serum-containing medium showed less significant difference in colony fusion time for the two medium-replenishing conditions. This result also agrees with our previous observations where we found comparable absolute colony areas and colony motility in the two tested medium-replenishing conditions. The analysis of colony fusion time in serum-containing medium without LIF also agrees with our previous results even though confidence intervals might be a litter wider than other groups due to its small sample size. These results suggest that analysis of colony fusion may in fact reflect the overall effects of colony-colony interactions on colony morphology. To validate this postulation, further investigation needs to be done to demonstrate how colony fusion time may change with different sizes of patterned colonies.

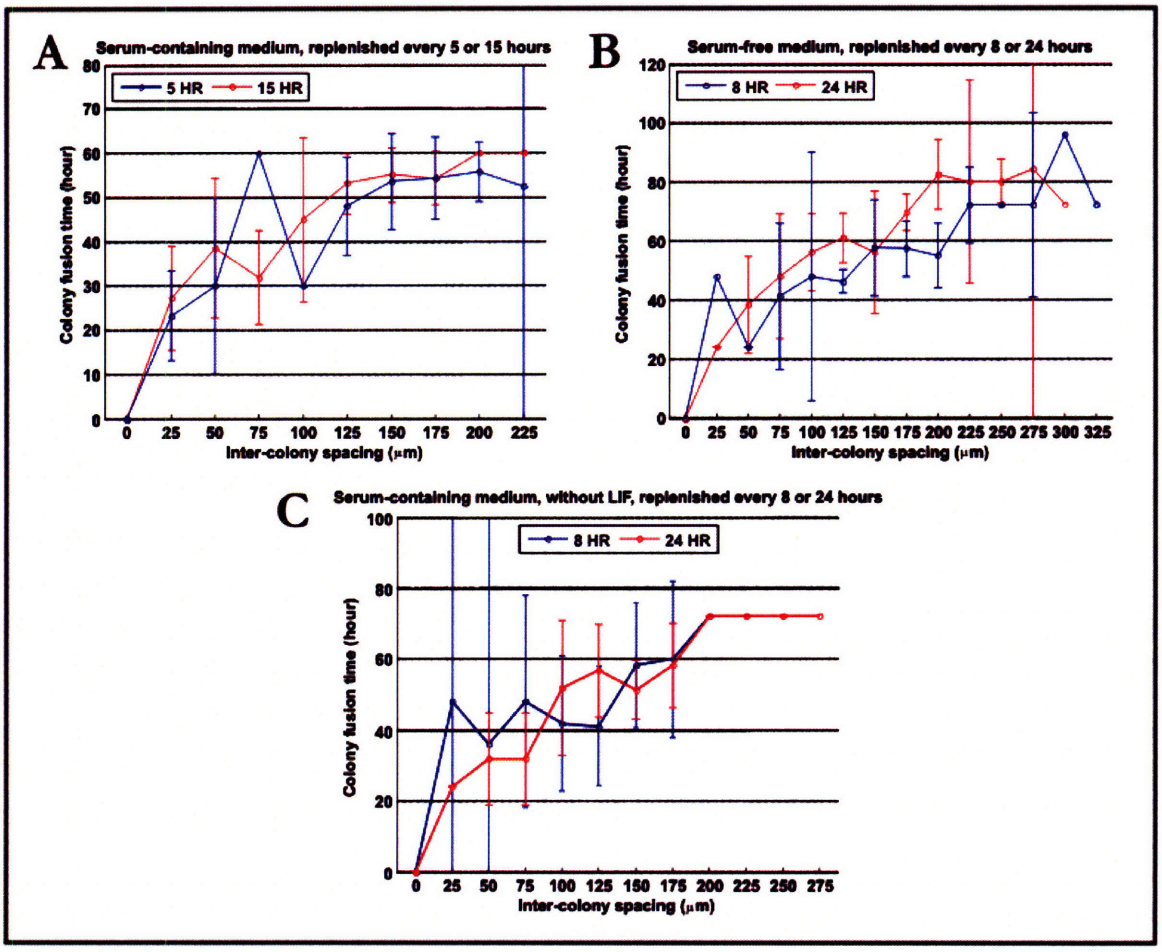

Figure 5-10 Colony fusion time: The presented results were averaged from discrete colony monitoring. The fusion time of colonies in serum-containing medium (A) was monitored every 15 hours. The fusion time of colonies cultivated in both the serum-free medium (B) and the serum-containing medium without LIF was monitored every 24 hours. Note that plots of colony fusion in serum-containing medium, serum-free medium and serum-containing medium without LIF are only valid for the data points with the fusion time below 60 hours, 96 hours and 72 hours, respectively. The data points with larger fusion time simply mean inadequate time for colony fusion. All plots are presented with 95% confidence intervals.

5.2.4 Self-renewal marker

We previously investigated the roles of colony-colony interactions on the morphological changes of mESCs at the single-colony level. Here, we looked into how colony-colony interactions might affect cell fate decision of mESCs. Self-renewal is the resulted cell fate occurring when ESCs are prohibited from differentiation and apoptosis and promoted to proliferate. We therefore chose to monitor self-renewal to preliminarily examine changes in cell fate decision due to colony-colony interactions. Different self-renewal markers are available as we discussed previously (§3.7). Here we chose to quantify self-renewal of the colonies using alkaline phosphatase staining. Due to our time limit, we managed to obtain complete analysis of self-renewal changes only for mESC colonies cultivated in serum-free medium. Figure 5-11 and Figure 5-12 illustrate results of alkaline phosphatase staining for either 8 hours or 24 hours medium-replenishing conditions, performed three days after the stencil was removed. Figure 5-13 shows the result of semi-quantitative analysis of the stain for both groups using the analytical method discussed previously (§3.7). No significant difference was observed for either 8-hour or 24-hour medium-replenishing conditions or for varying initial inter-colony spacing. Nevertheless, there appeared to be a potential increasing trend of alkaline phosphatase expression as initial inter-colony spacing varied from 150 to 225 microns in the 8-hour replenishing condition. Further investigation is yet required to confirm this trend. Note also that the localizations of alkaline phosphatase in mESC colonies cultivated in serum-containing medium and serum-free medium were dissimilar. Colonies in serum-free medium had high expression of alkaline phosphatase inside the colonies (Figure 5-14) while the colonies in serum-containing medium had high staining at the colony edge (Figure 5-15). Similar results were observed for two repeats in the same cultivating condition. These results may partly be due to the difference in colony morphology of the two medium types. Patterned colonies in serum-containing medium were observed to have hemispheric shapes. mESCs that were cultivated in serum-free medium could adhere better to the substrate, resulted in flat pancake-like colonies. We postulate that lower expression of self-renewal marker inside the hemispheric colonies was caused by apoptosis of cells inside the colonies. Similar cell death was observed during embryoid body formation usually obtained for mESC differentiation[131, 132]. This hypothesis can be tested quickly using apoptosis staining assay such as the TUNEL assay. Three-dimensional colony shape was also found to induce differentiation of mESCs even in serum-containing medium supplemented with LIF [133]. The three-dimensional shape of the colony may also be the reason why we earlier observed limited colony motility in serum-containing medium.

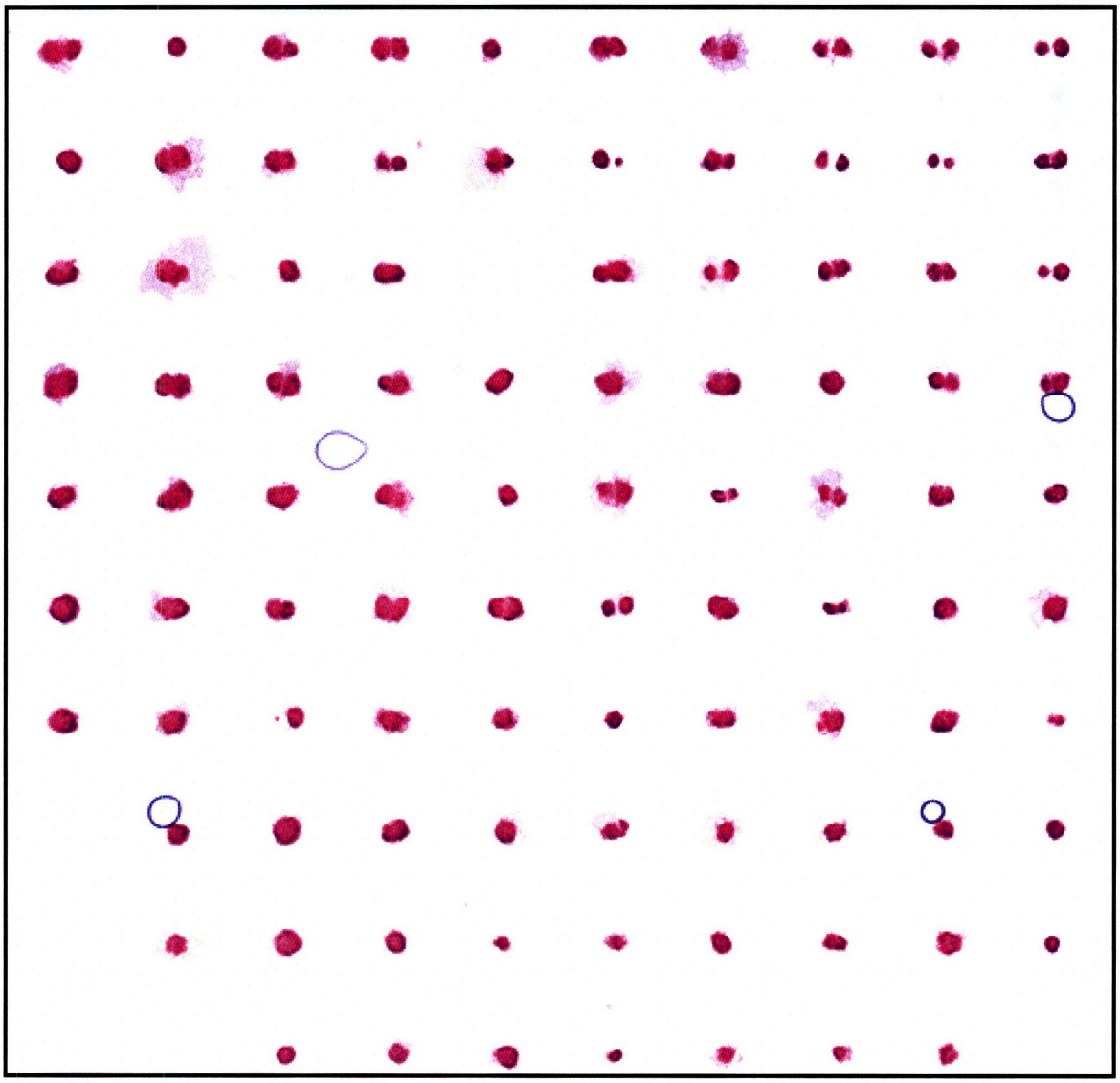

Figure 5-11. Alkaline phosphatase staining of patterned mESCs cultivated in serum-free medium, replenished every 8 hours

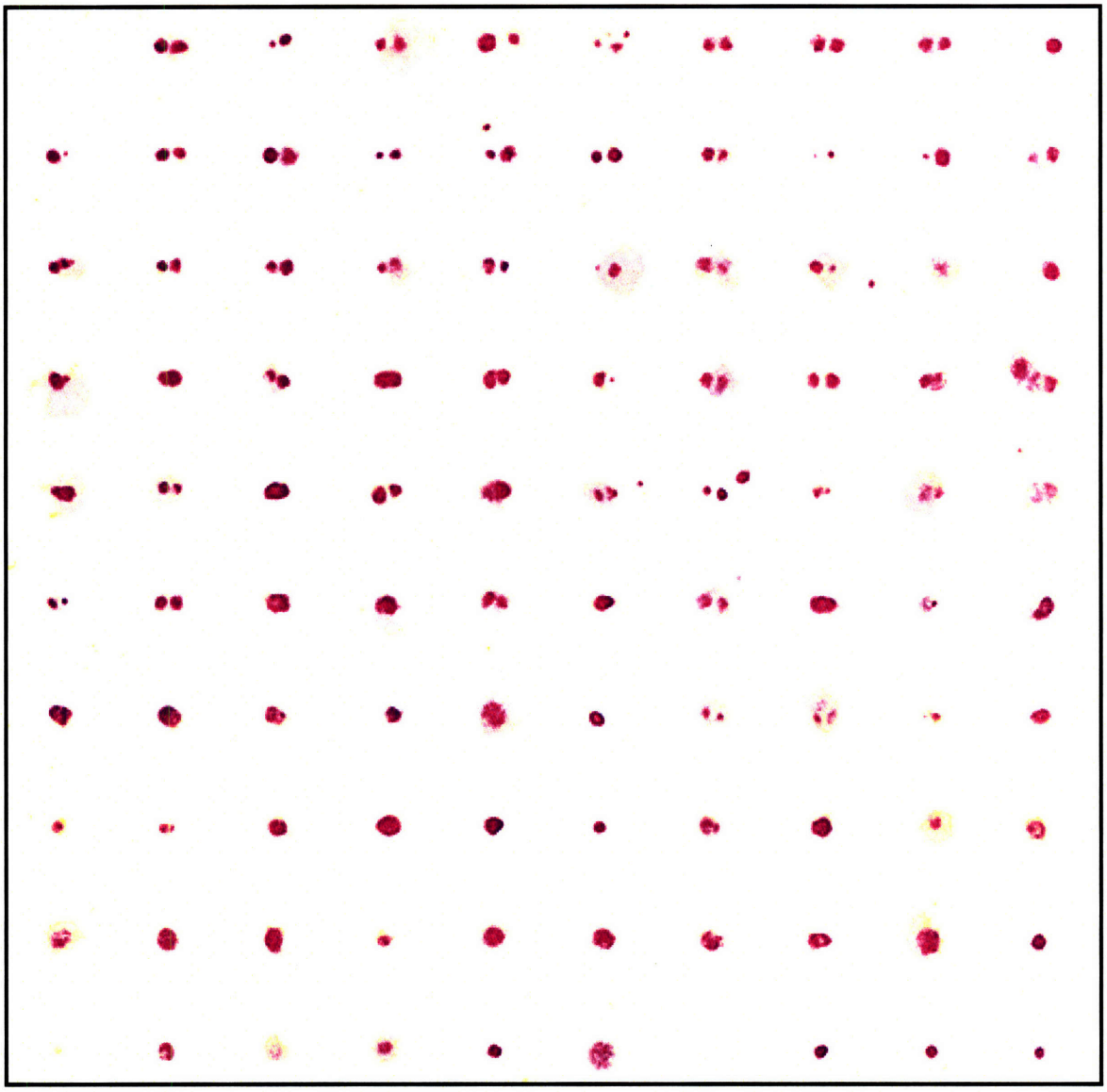

Figure 5-12. Alkaline phosphatase staining of patterned mESCs cultivated in serum-free medium, replenished every 24 hours

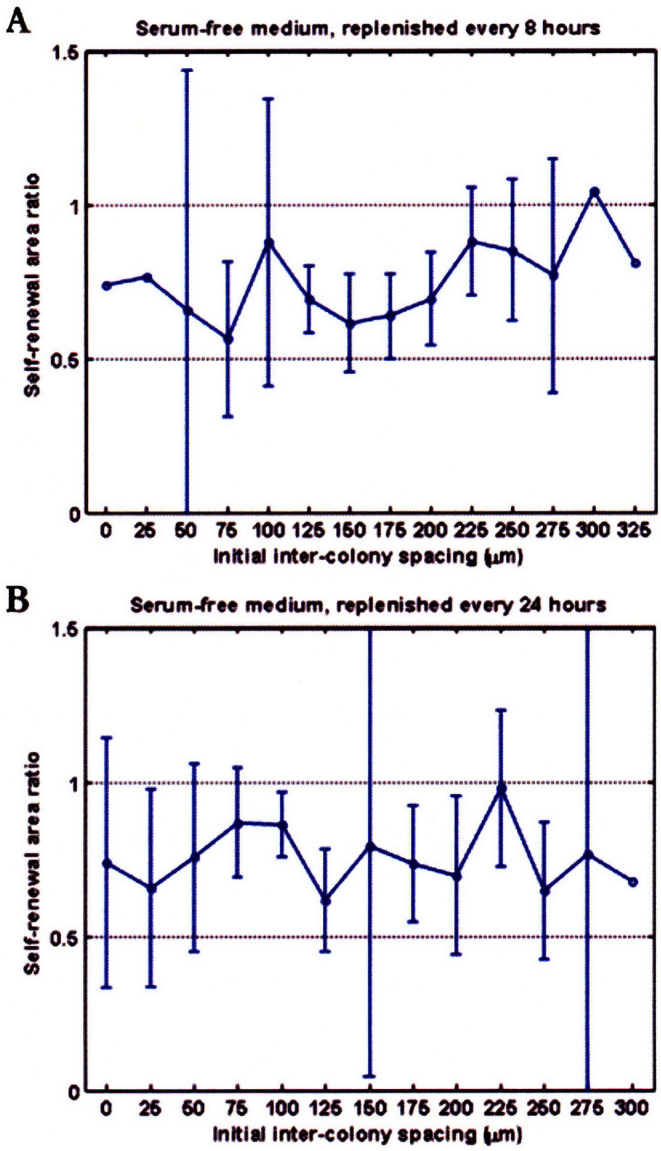

Figure 5-13 Semi-quantification of alkaline phosphatase in mESC colonies cultivated in serum-free media that: Both plots are presented with 95% confidence intervals. Zero inter-colony spacing represents single colony groups.

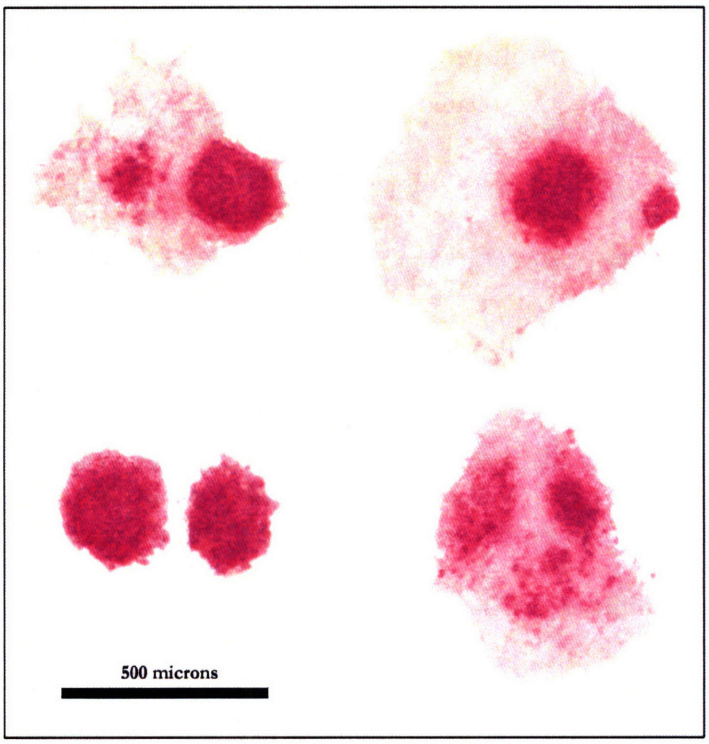

Figure 5-14 Different colony morphology and common self-renewal areas of mESC colonies in serum-free medium: pink region represents area with positive alkaline phosphatase staining. The colonies were flat and attached well to the substrate.

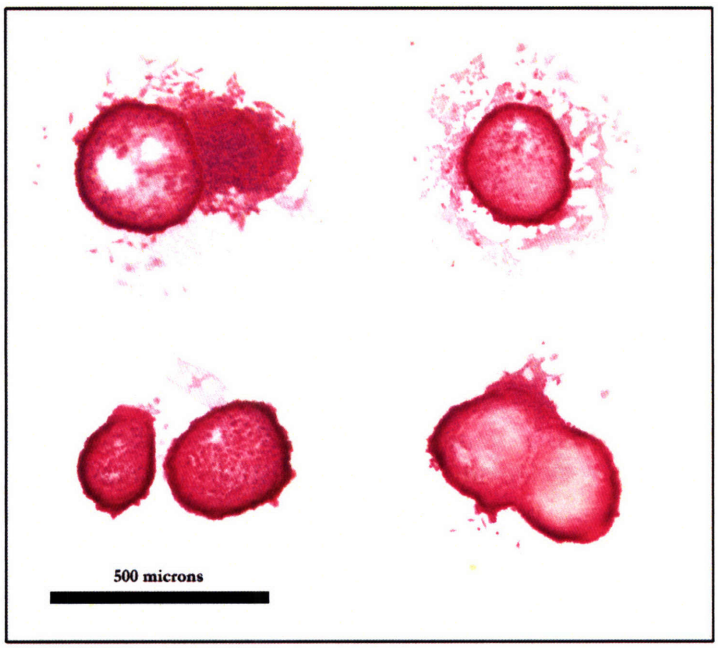

Figure 5-15 Different colony morphology and common self-renewal areas of mESC colonies in serum-containing medium: pink region represents area with positive alkaline phosphatase staining. The colonies were round and many detached from the substrate after the staining.

5.3 Techniques to improve analysis of colony-colony interactions

5.3.1 Tracking local morphological changes with speckle imaging

We have previously investigated colony proliferation and colony movement using contour-based analysis. One of the disadvantages of this method is that we cannot observe the local morphological changes within the individual colony. Such local changes may prove to be important for our analysis later on because most chemical gradients developed by cell-secreted signaling molecules are often effective only within a few cell diameters away from the secreted cell. It is therefore required that we have tools that can detect local effects of colony-colony interactions in addition to the assays to observe overall colony behaviors.

We have developed a speckle imaging technique to monitor local changes in colony morphology (§2.1 and §3.5). To test the practicality and efficiency of this method, we first checked biocompatibility of the dye (DiI) and also tested whether the dye might also affect cell fate of mESCs. Figure 5-16A illustrates proliferation of mESCs with varying incubation period for dye incorporation. The result showed that DiI affect cell survival very slightly. There was a small decrease of cell proliferation at the first day of the experiment for mESCs that were incubated with DiI for 20 minutes. Similar drop in mESC growth was however not observed at the third day of the experiment. Our preliminary result of self-renewal marker showed positive Oct-4 expression in mESCs that were incorporated with DiI after three days (Figure 5-16E). Having determined compatibility of the dye, we determined the speckle mixing ratio between the unlabeled and labeled cells that could best resolve local colony morphological changes. Colonies with 15% labeled mESCs were observed to give the most efficient distribution of speckles on the colony for the speckle analysis later on (Figure 5-16B-D).

We next applied speckle imaging technique to monitor local morphological changes of the patterned mESC colonies. Our goal is to characterize how cells inside the colony migrate over time in addition to overall colony changes obtained from contour-based analysis. Figure 5-17 illustrates the morphological changes of speckled colonies that were cultivated in serum-containing medium with 15-hour replenishing condition. The pictures of colonies and speckles were monitored right before the medium was changed. At the first two time points, the colony contours were still uniform. Speckles were observed to distribute equally across both colonies. At 30 hours and 45 hours of the experiment, we began to observe non-uniform colony growth and motion in the left colony, at the top and bottom of the colony. Figure 5-18 shows the results of colony motion analysis using both the colony contours and the speckle imaging technique. The contour-based analysis can only tell the overall colony motion and growth based on the calculation of colony centroids and area changes. With speckle imaging, actual colony motion and growth within the individual colony can possibly be extrapolated from the movement vectors of each speckle spot. Figure 5-18D shows the movement vectors that were obtained from speckle analysis of the speckle. Corresponding speckles from the two time points were mapped manually using fiducial information at each speckle spot. Based on the result of speckle analysis that shows greater local colony motion at the right edge of the left colony, it can be postulated that cells at the centers of the left colony remained almost stationary on the substrate while cells at the colony edge expanded towards the other colony. It should also be noted that the example of speckle imaging presented here was by far the best case we obtained among all other colony groups that were also speckle-stained. Some speckled-stained colonies were observed to have uniform distribution of speckle throughout the experiment. The speckles

in other colonies became too faded over time, inhibiting appropriate matching of speckles between different time points. For these groups of colonies, it may work most efficiently to instead reference the whole groups of speckle spots rather than trying to map each individual speckle. In addition, we may stain the colonies in a more predictable shape in order to simplify mapping of the labeled cells as the colony grows over time. Time-lapsed analysis of speckle-stained colonies may also help simplify referencing of speckles over time. This preliminary result showed that it may be possible to monitor local morphological changes in mESC colonies using a labeling method that can distinguish cells in the colony apart in the motion analysis.

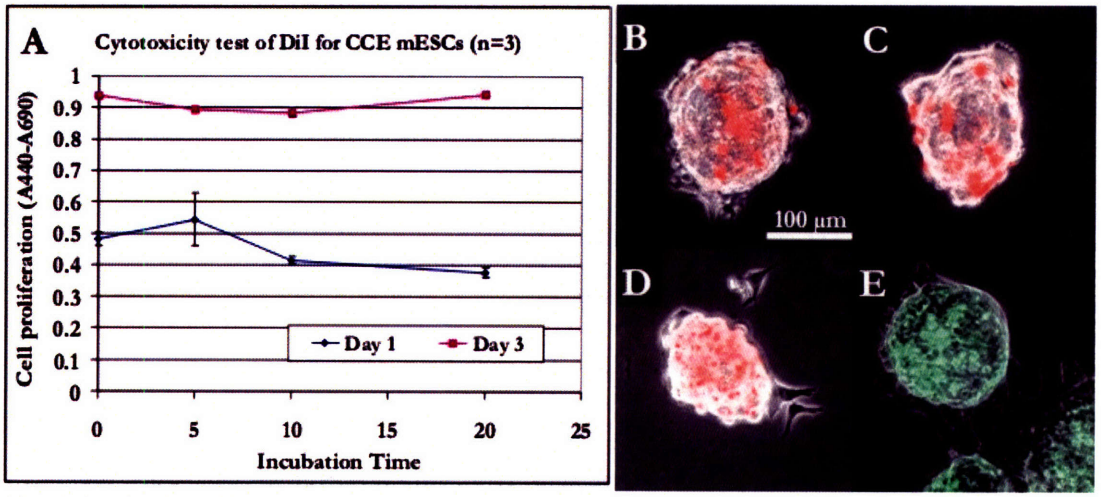

Figure 5-16 Efficiency of speckle imaging: A) Proliferation of mESCs that were stained with DiI measured by WST-1 assay for varying dye incubation period at day 1 and day 3. B-C) Different mixing ratios of labeled and unlabeled mESCs were tested: B) 5%, C) 15% and D) 45%. E) Oct-4 staining of speckle-stained colonies.

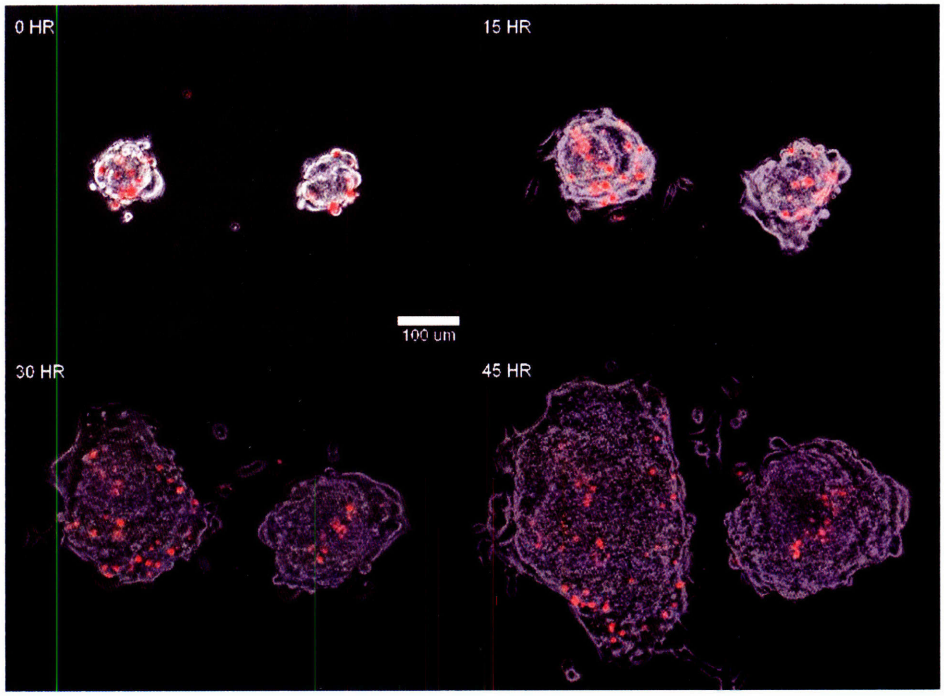

Figure 5-17 Speckle imaging technique for analysis of local colony motions: These mESC colonies were patterned and cultivated in serum-containing medium. Images of colonies and speckles were obtained every 15 hours of the experiment.

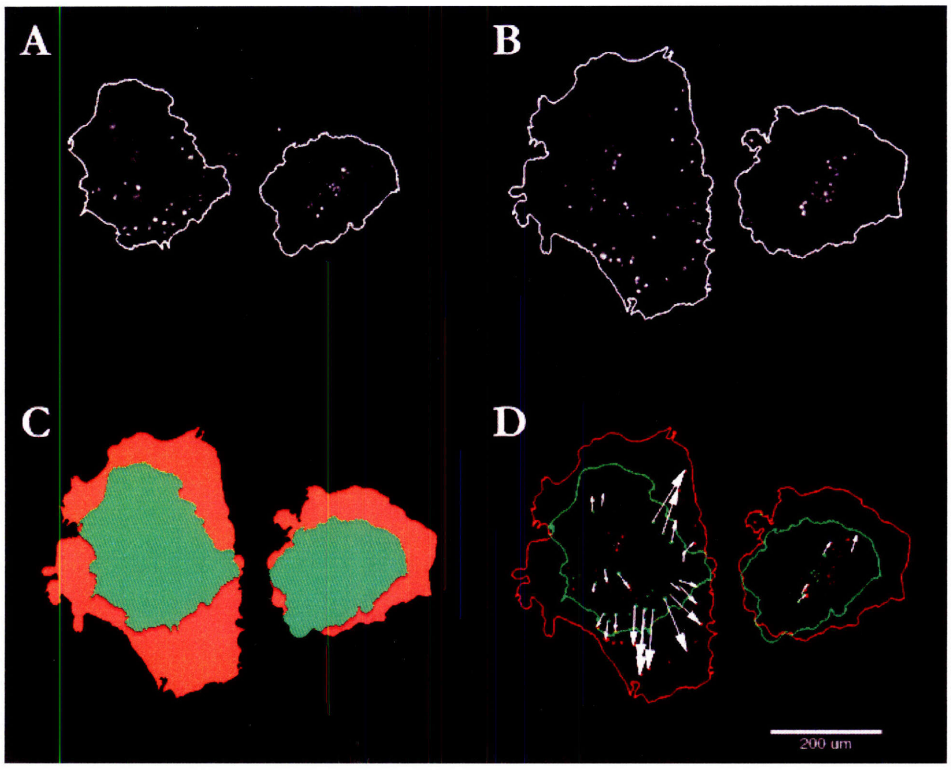

Figure 5-18 Analysis of local colony motion: A-B) Overlay image of colony contour and speckles of the patterned mESC colonies in serum-containing medium at 30 hours and 45 hours of the experiment. C) Contour-based analysis of the colony morphological changes. D) Speckle-based analysis of local colony motion.

5.3.2 Limiting fluid convection with hydrogel formation

One of the issues commonly discussed and debated for the *in vitro* experimental analysis of cell responses to cell-secreted signaling factors is the generation of fluid convection in the open-topped culturing platforms. This type of fluid convection, or Marangoni flow, can be developed spontaneously due to variations in fluid temperature or solute concentration that ultimately cause surface tension differences at the fluid interface[134, 135]. Such phenomenon has been proven to be critical at least in chemical systems where homogeneous reactions in the fluid can generate spiral flow wave on the liquid surface[136]. For biological systems, the nature of the system is somewhat different from the chemical system. The production source of the signaling molecules is inhomogenous, usually only at the bottom of the liquid volume. In addition to secreting diffusive signaling factors, cells can also secreted ECMs and a group of enzymes called matrix metalloproteinases that are aimed to remodel ECMs on the substrate. Some of these ECMs such as fibronectin and proteoglycans can bind to cell-secreted diffusive factors, therefore acting like storage for the diffusive molecules. As the cells secret more ECMs surrounding its vicinity, these ECMs also become more viscous. Such environments may be sufficient to shield cells from their fluidic environment and may prove to be the reasons why some *in vitro* biological systems do not suffer from Marangoni flow even in the open-topped condition[137].

Regardless of the above arguments for biological systems, we developed a method to achieve a convection-free platform for open-topped cell culturing. In brief, we form hydrogel on top of the cells and the substrate surface. Hydrogels are water-insoluble materials, either synthetic or natural, that can absorb large volume of aqueous solutions. Hydrogels are usually created from long polymer molecules that are cross-linked via multiple types of crosslinkers, creating porous scaffolds that allows efficient diffusion of nutrient and waste exchange[138]. We have tested preliminarily the use of alginate hydrogel to limit convection in the open-topped culturing platform. We formed alginate hydrogel on top of the substrate or surrounding the cell-plated cover slips as discussed previously (§3.4). Figure 5-19 illustrated diffusion of fluorescein that was injected underneath the alginate gel formed on top of the tissue culture dish. Figure 5-19B showed normalized intensity of fluorescein cross-sectioning the center of the injected spot. The plot shows no drifting of the peak center, suggesting negligible convection in the system. By fitting the dye intensity at varying time points to the general diffusion equation:

$$C = \frac{M}{2(\pi Dt)^{\frac{1}{2}}} e^{-x^2/4Dt}, \tag{4.19}$$

we obtained diffusivity of fluorescein in alginate hydrogel equal to $3.3\times10^{-6}\,\mathrm{cm}^2/\mathrm{s}$, a value only slightly lower than the reported diffusivity of fluorescein in water ($\approx 6\times10^{-6}\,\mathrm{cm}^2/\mathrm{s}$). Our analysis therefore confirmed that fluorescein can diffuse freely in alginate and was not interfered by spontaneous fluid convection when the tissue culture substrate was coated with alginate hydrogel. We also tried once to form alginate hydrogel on top of the patterned colonies in serum-containing medium but the hydrogel seemed to degrade and loosen from the substrate surface over time. Such issue might however be resolved easily by adding calcium ions to the medium, allowing cross-linking of alginate molecules to be better maintained over time.

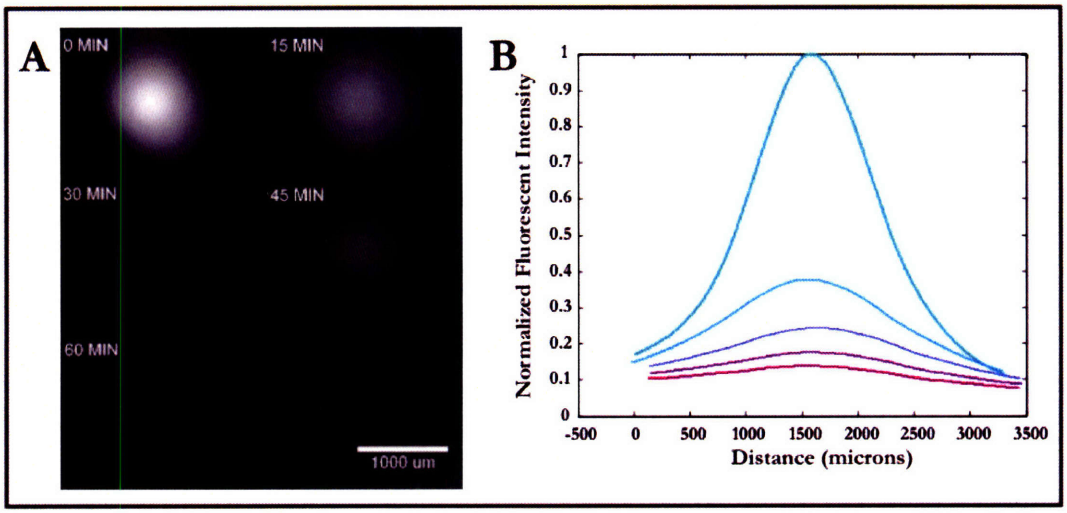

Figure 5-19 Diffusion in alginate scaffold: A) Images of fluorescein diffusion in alginate hydrogel that was formed to cover the surface of tissue culture dish. B) Normalized intensity of fluorescein across the location where the dye was injected over time.

CHAPTER 6: SUMMARY & FUTURE DIRECTIONS

In this thesis, we have described a system that can be used to investigate the roles of colony-colony interactions in ESCs. We demonstrated how to use stencil patterning techniques to fabricate mESC colonies on a culturing substrate and attempted to mimic simple interactions between ESC colonies that can be readily interpreted. We showed how colony proliferation and motion can be estimated using the colony contours. An investigation of the roles of colony-colony interactions on growth, motion, and self-renewal of the patterned mESC colonies were performed in three different cultivating media. We however observed no strong relationship between colony-colony spacing and changes in colony morphology in any medium conditions we tested. We will discuss in this chapter some of the issues which may contribute to the results we observed and propose some techniques that may help improve the analysis of colony-colony interactions in ESCs.

6.1 Automatic data collection and analysis

The rate-determining step of our experiment was the images registration and segmentation processes, where we had to register and segment images of mESC colonies manually, with a slight aid from the customized software that we developed to guess the initial segmentation parameters (Appendix: Colony analysis software). The requirement of human inspection for each image limits our ability to scale the experiment up to larger sample sizes. Post-collection image processes also prevent correction of the images that may contain erroneous information such as improper focusing and brightness. We have discussed previously how substrate coordinates can be obtained from the locations of fluorescent beads that we attached to the bottom of the substrate. The substrate coordinates may also be used to help register images on the fly. Together with an image analytical module, these pre-collection data processes will ensure that our collected images are pristine for analysis later on. Automatic image segmentation may also be performed using machine learning techniques such as neural networks to help determine suitable segmentation parameters for different categories of input images[124]. These techniques will allow us to save time for image analysis and will be generally useful for the analysis of cell behaviors of patterned cells that are evenly distributed on the substrate.

6.2 Redefining appropriate conditions to exhibit effects of interactions

We have observed in our analysis that colony-colony interactions did not play significant roles on the physical changes of mESCs colonies. We found that colony growth, motility and fusion of mESC colonies in the two-colony groups were not statistically different from the behaviors of the one-colony groups in any cultivating conditions that were tested. Different reasons may explain the results we observed here. First, the background concentration of the signaling molecules may be too small for the cells to sense and respond to. One important observation that we neglected from our previous study was that fusion of mESC colonies occurred evidently when we cultured the cells at high cell density (15 million cells/10 ml or 1.5 million cells/ml). In comparison to the high-cell density condition, the experiments that we conducted have much lower cell concentration (maximum of 200 colonies/4 ml or approximately 15,000 cells/ml). It is therefore possible that the effects of colony-colony interactions will only be evident in the microenvironment with high cell density. Second, it has been showed in at least two autocrine systems (IL-2

and EGF) that the concentration of autocrine factors that the cells can exhibit graded response to is very narrow, confining within only two orders of magnitude of the ligand concentration[139, 140]. Outside this range, gradient of autocrine factors will simply give uniform effects in cells. The switch-like cell response to autocrine factors was also observed for the autocrine signaling of GP130 ligand in mESCs[73]. Figure 6-1 illustrates both of the hypotheses we discussed here.

In order to determine the range of interaction intensity that may affect physical behaviors of mESC colonies, we must compare the responds from colonies that are cultivated in different conditioned media. We may vary the conditioned media by changing the incubation period. If we find that colonies respond differentially in a particular concentration of conditioned medium, we may use this medium to reinvestigate the roles of colony-colony interactions in mESCs.

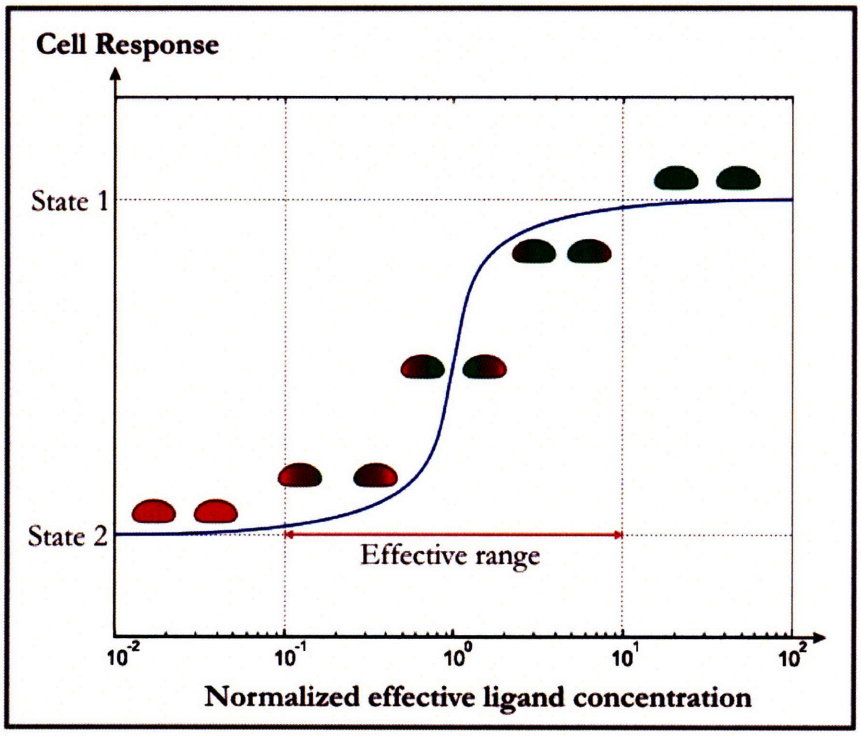

Figure 6-1 Hypothesis of the effective range of ligand concentration: The concentration of signaling ligands outside the effective range will result in uniform cell response, either cell state 1 or state 2. The concentration of the signaling ligands is governed by the background concentration as well as the local concentration gradient surrounding each colony. The background gradient will determine the range of concentration the local gradients are situated. Local concentration gradient determines the magnitude of the difference in cell response across an individual colony.

One may argue also that gradients of signaling factors might be interfered and disrupted by spontaneous fluid flow in the open-top platform. To verify this argument, a few approaches can be taken. First, we could use another cell line for which autocrine signaling has been confirmed and well characterized. Since we know the appropriate concentration range of the diffusive signals that the cells will respond to, such a positive control group will help us determine whether signaling gradients can in fact be generated and maintained in our developed platform. Examples of these cell lines include 1) interleukin-2

secreting T cells (NOI-90[26], TCC[141]), 2) TGFα secreting cell lines (MCF-7[142], A431[143], MDA468[144], autocrine clone#1[145]). For the biological systems of which the underlying signaling factors are known, we may also be able to create a rigorous positive control of cell responses under the signaling gradients using microfluidic technology. Previous studies have shown that such approach is capable to investigate the effect of signal stimulation for as small as a single cell[98]. Using such technique, we can achieve a fixed signaling gradient that does not vary with the output cell responses.

6.3 Improving techniques to reference colonies

We have presented in this thesis the use of patterned ESC colonies for the study of colony-colony interactions. We have also shown the preliminary usage of speckle imaging technique to monitor local morphological changes within an individual colony. The patterning technique can be performed easily and can achieve over ninety percent patterning efficiency (§5.1). The method we used to create speckle-stained colonies however can only create colony with randomly distributed speckles spots. While a few of these labeled colonies contained referable speckles, most colonies included ineffective speckles which could not be referred to their original positions at previous time points. The staining in some colonies also faded away over time as cells in the colony have divided for multiple times. It is the random position of the speckles that prevent us from achieving an effective referencing technique to monitor local colony motion.

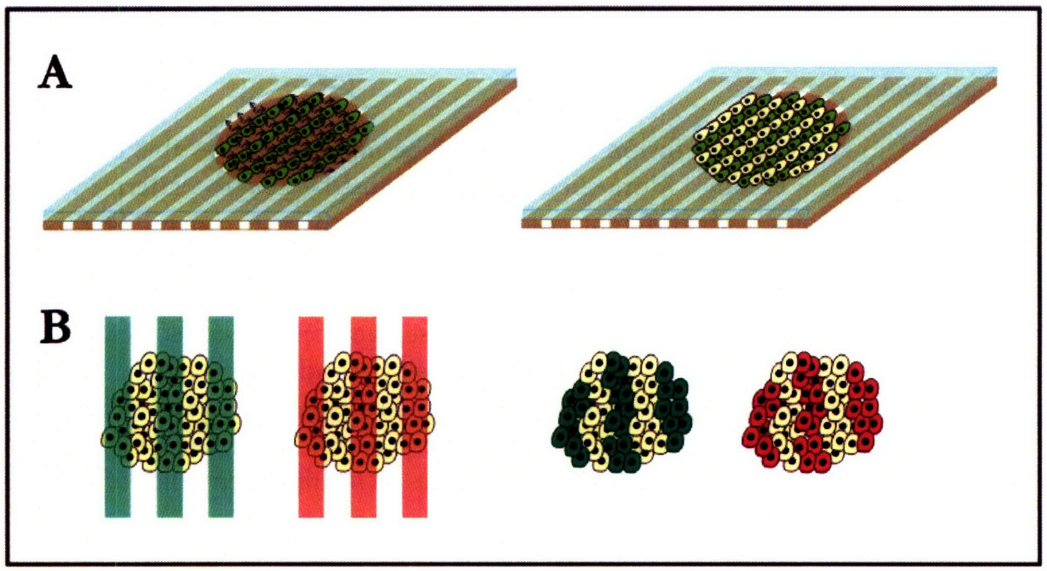

Figure 6-2 Patterning color-striped colonies: A) Using DEP approach, the labeled cells are deflected from the electrode. Once the voltage is turned off, we can pattern the second cell type between the labeled cells. We may also need to stamp adhesive ECM on top of the substrate to promote cell adhesion. B) We can also create striped colonies using microfluidic techniquq to generate alternate color streams of dye which we can then expose to the already patterned colony. The resulted colonies should have labeled cells only for the region where the fluid was mixed with the dye.

Using additional microtechnological techniques, it is possible that we can form speckle-stained colonies that will be more effective for colony referencing. Figure 6-2 illustrates the two methods that can be used to colorize colonies in a more meticulous mean. We may use negative dielectrophoretic (n-DEP) forces to deflect the labeled cells from the

electrode stripes, creating regions for the unlabeled cells that are added later to land in between. Microfluidic stream focusing may be used to stain colonies in stripes as shown in the figure while the technique may not be as scalable as the DEP approach. While the dye intensity may also degrade using these techniques, these striped colonies are probably less affected by cell division because the striped regions can still be extrapolated from the rigorous and uniform distribution of the labeled cells within each stripe. Deformation of the colored stripes also allows quick analysis of changes in the local colony motion. One may also resolve the degradation problem of the dye intensity by transfecting the cells with foreign genes of fluorescent proteins such as GFP. Since these proteins can also be produced by the cells themselves, the intensity of labeled cells should not degrade as the cells divide.

6.4 Patterning multiple cell types with stencils

In addition to the better referencing of locations of each colony, we may also want to generate two different populations of ESC colonies right next to each other to study the biology of colony fusion. While colony fusion also serves to be a marking endpoint of colony-colony interactions in our previous study, the effect of colony fusion may also prove to be significant on cell fate decision of ESCs. We know from our observation that fibroblast-like cells at the border of each colony are beginning to lose its ability to self-renew. However, as two ESC collide, it is these cells which finally turn into the inside of the newly generated colony. The fact that most of the fused cells still have high self-renewal marker expression inside its colony has surprise us and also make us wonder whether there is a specific properties inside each colony that can almost refresh the ability of ESCs to maintain their self-renewal.

In order to study colony fusion effects, it will be necessary to be able to differentiate cell mass from the each colony. More specifically, we must be able to pattern two types of colonies such as colonies with different colors right next to each other. This is a long-standing challenge for cell patterning. Most cell patterning techniques can give rise to complete manipulation of one cell type on the substrate while the second cell type may be plated to cover the rest substrate surface. In our case, we hope to still achieve two nearby colonies that still have similar shapes. This imposing condition requires that we have complete control of positions for both cell types on the substrate. Figure 6-3 illustrates our proposed technique to pattern two different cell types accurately on the substrate. We use microfluidic channels to help deliver different cell types to nearby open holes of the stencil.

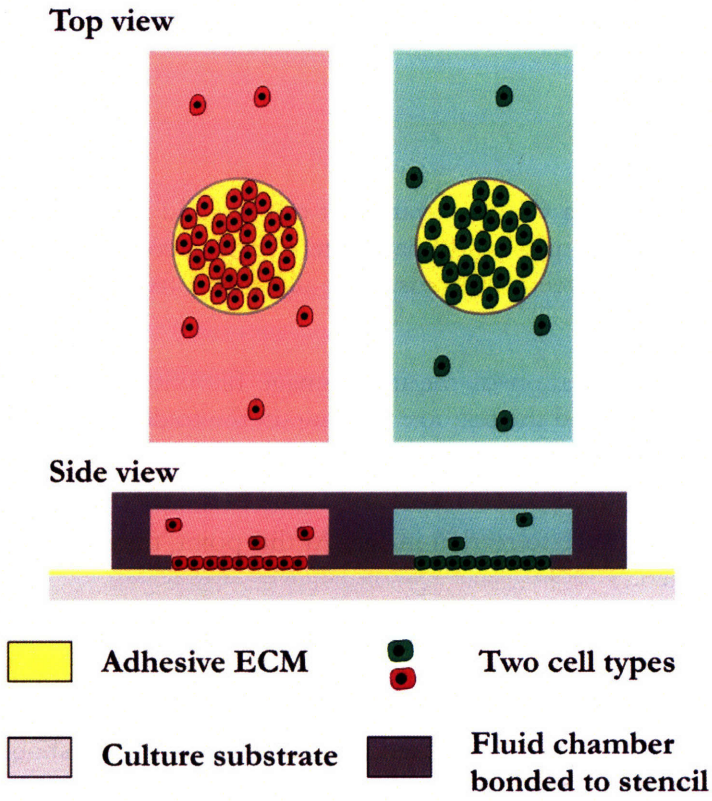

Figure 6-3 New stencil cell patterning technique for two cell types: A microfluidic chamber is bonded on top of the stencil. The fluidic chamber is used to deliver multiple cell types at the nearby location. Clamping of the device to the substrate will be sufficient to seal the fluidic channels. We may also stamp or coat an adhesive ECM on top of the substrate surface to promote cell adhesion. After all cells in the open region already adhere to the substrate, we may remove the fluidic chamber from the substrate, leaving patterned colonies of different cell types on the substrate.

6.5 Contributions

We have demonstrated in this thesis a method that can pattern accurately and simultaneously multiple ESC colonies on a substrate. This patterning method allows natural colony growth, unlike previously reported ESC patterning techniques that use ECM patterning and thus limit the growth of ESCs in a confined boundary. We showed how this patterning technique can be used to vary colony-colony spacing of mESC colonies as a way to potentially vary colony-colony interactions. Under the culture conditions tested, we did not observe any evident effects of colony-colony interactions in the cultivating conditions tested. We have developed approaches to analyze images of ESC colonies to approximate colony growth, migration and self-renewal. We finally examined the efficiency of speckle imaging technique for monitoring of local colony motions.

Regarding its biological impact, our work contributes to improvement of the current techniques to maintain self-renewal of ESCs in vitro. Comprehensive understanding of how mESC colonies interact with one another may help us decipher the heterogeneous phenotypes observed across the whole population of ESCs during *in vitro* cultivation. Identification of the underlying signals of colony-colony interactions in ESCs will help us determine the appropriate niche that can sustain self-renewal of ESCs faultlessly in long term.

APPENDIX: COLONY ANALYSIS SOFTWARE

ColonyAnalysis

ColonyAnalysis is a GUI software that can be used to perform image segmentation, and calculate for basic morphological parameters such as colony area, centroid, inter-colony spacing, and distance between centroids. The use this software, the user can simply follow the following instructions.

1. Determine the location of the input image file under **Source Filename** or simply click the box behind the textbox to bring up the folder search menu.

2. Determine the filename of the input image under **Filename**

3. Click **Load Picture** to read in image. At this point, the input image should be shown on the screen.

4. To perform image segmentation, three segmentation methods are available, including: 1) Edge-based, 2) Thresholding-based and 3) Combine. It is suggested that the user choose **thresholding** method to for segmentation of ESC colonies. Once the radio button is clicked, the thresholding level should be updated. The initially assigned thresholding level is calculated using Otsu's algorithm from the *whole* image.

5. To redefine the thresholding for specific region within the image, click **Define Threshold Area** which will bring up a rectangular region for the user to determine the object of interest.

6. The user can also limit the image region for segmentation by pushing the button **ROI selection**. A polygon can then be drawn around the area which is intended to be segmented. The user can double click or hit enter to finish the drawing. The user can also determine the upper and lower limit of the object of interest by determining the range of minimum and maximum diameter in the box **Minimum/Maximum colony size**

7. At this point, the program is ready to perform segmentation. Simply push the button **Process picture** to perform the operation. After a few second the segmented images will be drawn on the screen.

8. If the program gives an error, it means that there is no object of the specified size and thresholding value. The user may hit load picture, observe the histogram of the image in the bottom right corner diagram and redefine thresholding level. The **Strel Radius** may need to also be modified. The larger the strel radius, the higher chance that two nearby objects will be combined together. The use of strel radium is intended to correct any dark hole within the object of interest. By increasing the strel radius in this case, we may be able to get a close-line object.

9. To get a single-frame colony analysis, the user can simply click the buttom **Show Details**. Another window will pop up, showing the morphological parameters of

the image. There is also a **Save** button that the user can use to export the data. The outout excel file will be saved at the location specified by **Target Folder**. To use the save function, the user must first click the button **Start XLS** in the main window.

10. To perform multi-frame analysis, the user need to first segment each image as discussed previously. Once the segmented image is shown, the user can click the button **Add to Stack** that will store in image at each time frame. The user now needs to repeat segmentation process and add all frames to stack. Once satisfy, the user can click the button **Analyze Stack** that will pop up the result of the multi-frame analysis.

11. Other toolboxs include:

    a. **Zoom** – zoom in/out

    b. **Contrast Adjust** – Pop up image tool to adjust image brightness and contrast

    c. **Add white** – is used to draw write region, to add area for segmentation process

    d. **Add black** – is used to draw black region, to remove area from segmentation process

    e. **Imadjust** – is used to automatically stretch the mage to represent all intensity in the output image

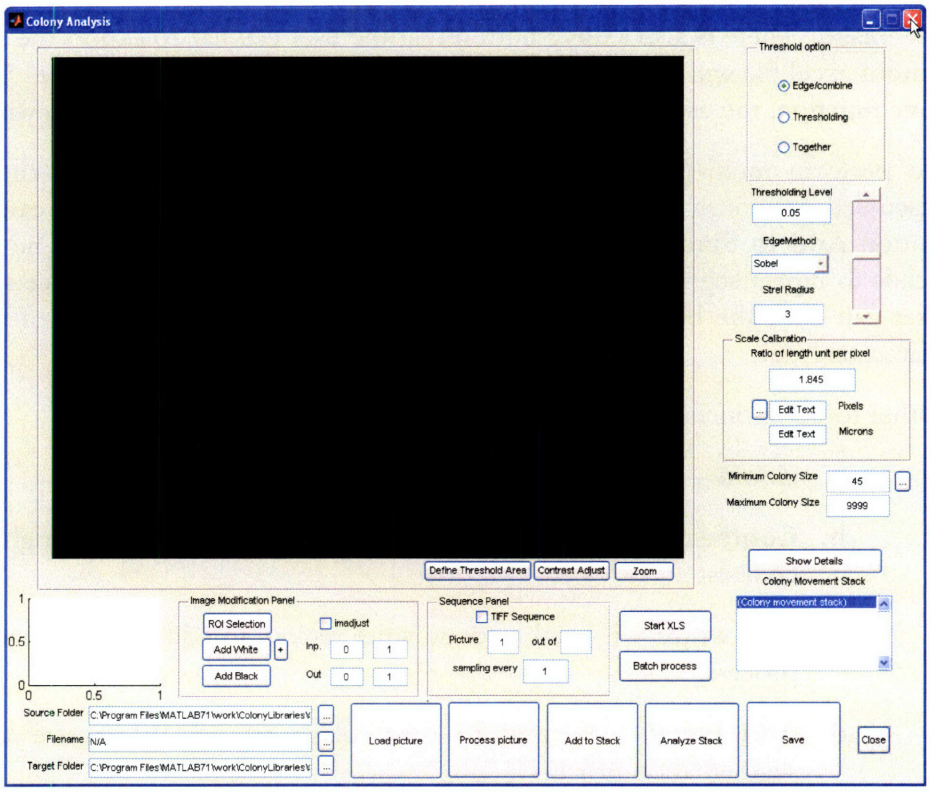
Colony Analysis
Threshold option
Edge/combine
Thresholding
Together
Thresholding Level
0.05
EdgeMethod
Sobel
Strel Radius
3
Scale Calibration
Ratio of length unit per pixel
1.845
Edit Text
Pixels
Edit Text
Microns
Minimum Colony Size
45
Maximum Colony Size
9999
Define Threshold Area
Contrast Adjust
Zoom
Show Details
Colony Movement Stack
(Colony movement stack)
Image Modification Panel
ROI Selection
imadjust
Add White
Inp.
Add Black
Out
Sequence Panel
TIFF Sequence
Picture
out of
sampling every
Start XLS
Batch process
Source Folder
C:\Program Files\MATLAB71\work\ColonyLibraries\
Filename
N/A
Target Folder
C:\Program Files\MATLAB71\work\ColonyLibraries\
Load picture
Process picture
Add to Stack
Analyze Stack
Save
Close

REFERENCES

1. Odorico, J.S., Kaufman, D.S. & Thomson, J.A. Multilineage differentiation from human embryonic stem cell lines. *Stem Cells* **19**, 193-204 (2001).
2. Thomson, J.A. et al. Embryonic stem cell lines derived from human blastocysts. *Science* **282**, 1145-1147 (1998).
3. Keller, G. Embryonic stem cell differentiation: emergence of a new era in biology and medicine. *Genes Dev* **19**, 1129-1155 (2005).
4. Naveiras, O. & Daley, G.Q. Stem cells and their niche: a matter of fate. *Cell Mol Life Sci* **63**, 760-766 (2006).
5. Liu, N., Lu, M., Tian, X. & Han, Z. Molecular mechanisms involved in self-renewal and pluripotency of embryonic stem cells. *J Cell Physiol* **211**, 279-286 (2007).
6. Sun, Y., Li, H., Yang, H., Rao, M.S. & Zhan, M. Mechanisms controlling embryonic stem cell self-renewal and differentiation. *Crit Rev Eukaryot Gene Expr* **16**, 211-231 (2006).
7. Pessina, A. & Gribaldo, L. The key role of adult stem cells: therapeutic perspectives. *Current Medical Research and Opinion* **22**, 2287-2300 (2006).
8. Denker, H.W. Potentiality of embryonic stem cells: an ethical problem even with alternative stem cell sources. *J Med Ethics* **32**, 665-671 (2006).
9. Moore, K.E., Mills, J.F. & Thornton, M.M. Alternative sources of adult stem cells: a possible solution to the embryonic stem cell debate. *Gend Med* **3**, 161-168 (2006).
10. Riess, P. et al. Embryonic stem cell transplantation after experimental traumatic brain injury dramatically improves neurological outcome, but may cause tumors. *J Neurotrauma* **24**, 216-225 (2007).
11. Przyborski, S.A. Differentiation of human embryonic stem cells after transplantation in immune-deficient mice. *Stem Cells* **23**, 1242-1250 (2005).
12. Andrews, P.W. The selfish stem cell. *Nat Biotechnol* **24**, 325-326 (2006).
13. Draper, J.S. et al. Recurrent gain of chromosomes 17q and 12 in cultured human embryonic stem cells. *Nat Biotechnol* **22**, 53-54 (2004).
14. Maitra, A. et al. Genomic alterations in cultured human embryonic stem cells. *Nat Genet* **37**, 1099-1103 (2005).
15. Lauss, M. et al. Single inner cell masses yield embryonic stem cell lines differing in lifr expression and their developmental potential. *Biochem Biophys Res Commun* **331**, 1577-1586 (2005).
16. Stewart, M.H. et al. Clonal isolation of hESCs reveals heterogeneity within the pluripotent stem cell compartment. *Nat Methods* **3**, 807-815 (2006).
17. Mikkola, M. et al. Distinct differentiation characteristics of individual human embryonic stem cell lines. *BMC Dev Biol* **6**, 40 (2006).
18. Rao, B.M. & Zandstra, P.W. Culture development for human embryonic stem cell propagation: molecular aspects and challenges. *Curr Opin Biotechnol* **16**, 568-576 (2005).
19. Niwa, H. How is pluripotency determined and maintained? *Development* **134**, 635-646 (2007).
20. Qin, H. et al. Regulation of apoptosis and differentiation by p53 in human embryonic stem cells. *J Biol Chem* **282**, 5842-5852 (2007).
21. Pyle, A.D., Lock, L.F. & Donovan, P.J. Neurotrophins mediate human embryonic stem cell survival. *Nat Biotechnol* **24**, 344-350 (2006).

22. Lin, T. et al. p53 induces differentiation of mouse embryonic stem cells by suppressing Nanog expression. *Nat Cell Biol* **7**, 165-171 (2005).
23. Li, L. & Xie, T. Stem cell niche: structure and function. *Annu Rev Cell Dev Biol* **21**, 605-631 (2005).
24. Morrison, S.J., Shah, N.M. & Anderson, D.J. Regulatory mechanisms in stem cell biology. *Cell* **88**, 287-298 (1997).
25. Quesenberry, P.J. & Becker, P.S. Stem cell homing: Rolling, crawling, and nesting. *P Natl Acad Sci USA* **95**, 15155-15157 (1998).
26. Sahraoui, Y. et al. Autocrine IL-2-dependent growth of a newly established CD3+, CD16-, CD56+, CD57+, J(H)-, TCRbeta-, TCRgamma- leukemia cell line (NOI-90). *Leukemia* **11**, 245-252 (1997).
27. Lin, H.F. The self-renewing mechanism of stem cells in the germline. *Current Opinion in Cell Biology* **10**, 687-693 (1998).
28. in Molecular cell biology, Edn. 5th. (eds. H.F. Lodish, P.T. Matsudaira, C. Kaiser & M. Krieger) 199-231 (W.H. Freeman and Company, New York; 2004).
29. Hoffman, L.M. & Carpenter, M.K. Characterization and culture of human embryonic stem cells. *Nature Biotechnology* **23**, 699-708 (2005).
30. Hwang, N.S. et al. Effects of three-dimensional culture and growth factors on the chondrogenic differentiation of murine embryonic stem cells. *Stem Cells* **24**, 284-291 (2006).
31. Liu, H., Lin, J. & Roy, K. Effect of 3D scaffold and dynamic culture condition on the global gene expression profile of mouse embryonic stem cells. *Biomaterials* **27**, 5978-5989 (2006).
32. Watt, F.M. & Hogan, B.L. Out of Eden: stem cells and their niches. *Science* **287**, 1427-1430 (2000).
33. Smith, A.G. et al. Inhibition of pluripotential embryonic stem cell differentiation by purified polypeptides. *Nature* **336**, 688-690 (1988).
34. Williams, R.L. et al. Myeloid leukaemia inhibitory factor maintains the developmental potential of embryonic stem cells. *Nature* **336**, 684-687 (1988).
35. Niwa, H., Burdon, T., Chambers, I. & Smith, A. Self-renewal of pluripotent embryonic stem cells is mediated via activation of STAT3. *Genes Dev* **12**, 2048-2060 (1998).
36. Cartwright, P. et al. LIF/STAT3 controls ES cell self-renewal and pluripotency by a Myc-dependent mechanism. *Development* **132**, 885-896 (2005).
37. Ying, Q.L., Nichols, J., Chambers, I. & Smith, A. BMP induction of Id proteins suppresses differentiation and sustains embryonic stem cell self-renewal in collaboration with STAT3. *Cell* **115**, 281-292 (2003).
38. Ying, Q.L., Stavridis, M., Griffiths, D., Li, M. & Smith, A. Conversion of embryonic stem cells into neuroectodermal precursors in adherent monoculture. *Nat Biotechnol* **21**, 183-186 (2003).
39. Qi, X. et al. BMP4 supports self-renewal of embryonic stem cells by inhibiting mitogen-activated protein kinase pathways. *Proc Natl Acad Sci U S A* **101**, 6027-6032 (2004).
40. Burdon, T., Stracey, C., Chambers, I., Nichols, J. & Smith, A. Suppression of SHP-2 and ERK signalling promotes self-renewal of mouse embryonic stem cells. *Dev Biol* **210**, 30-43 (1999).
41. Avery, S., Inniss, K. & Moore, H. The regulation of self-renewal in human embryonic stem cells. *Stem Cells Dev* **15**, 729-740 (2006).

42. Kristensen, D.M., Kalisz, M. & Nielsen, J.H. Cytokine signalling in embryonic stem cells. *Apmis* **113**, 756-772 (2005).
43. Xu, R.H. et al. BMP4 initiates human embryonic stem cell differentiation to trophoblast. *Nat Biotechnol* **20**, 1261-1264 (2002).
44. Humphrey, R.K. et al. Maintenance of pluripotency in human embryonic stem cells is STAT3 independent. *Stem Cells* **22**, 522-530 (2004).
45. Daheron, L. et al. LIF/STAT3 signaling fails to maintain self-renewal of human embryonic stem cells. *Stem Cells* **22**, 770-778 (2004).
46. Xu, C. et al. Feeder-free growth of undifferentiated human embryonic stem cells. *Nat Biotechnol* **19**, 971-974 (2001).
47. Amit, M. et al. Clonally derived human embryonic stem cell lines maintain pluripotency and proliferative potential for prolonged periods of culture. *Dev Biol* **227**, 271-278 (2000).
48. Xu, C. et al. Basic fibroblast growth factor supports undifferentiated human embryonic stem cell growth without conditioned medium. *Stem Cells* **23**, 315-323 (2005).
49. Beattie, G.M. et al. Activin A maintains pluripotency of human embryonic stem cells in the absence of feeder layers. *Stem Cells* **23**, 489-495 (2005).
50. James, D., Levine, A.J., Besser, D. & Hemmati-Brivanlou, A. TGFbeta/activin/nodal signaling is necessary for the maintenance of pluripotency in human embryonic stem cells. *Development* **132**, 1273-1282 (2005).
51. Sato, N., Meijer, L., Skaltsounis, L., Greengard, P. & Brivanlou, A.H. Maintenance of pluripotency in human and mouse embryonic stem cells through activation of Wnt signaling by a pharmacological GSK-3-specific inhibitor. *Nat Med* **10**, 55-63 (2004).
52. Moon, R.T., Bowerman, B., Boutros, M. & Perrimon, N. The promise and perils of Wnt signaling through beta-catenin. *Science* **296**, 1644-1646 (2002).
53. van Es, J.H., Barker, N. & Clevers, H. You Wnt some, you lose some: oncogenes in the Wnt signaling pathway. *Curr Opin Genet Dev* **13**, 28-33 (2003).
54. Olourni, A., McPhee, T. & Dedhar, S. Regulation of E-cadherin expression and beta-catenin/Tcf transcriptional activity by the integrin-linked kinase. *Biochim Biophys Acta* **1691**, 1-15 (2004).
55. Orsulic, S., Huber, O., Aberle, H., Arnold, S. & Kemler, R. E-cadherin binding prevents beta-catenin nuclear localization and beta-catenin/LEF-1-mediated transactivation. *J Cell Sci* **112 (Pt 8)**, 1237-1245 (1999).
56. Nagano, K. et al. Large-scale identification of proteins expressed in mouse embryonic stem cells. *Proteomics* **5**, 1346-1361 (2005).
57. Guo, Y., Graham-Evans, B. & Broxmeyer, H.E. Murine embryonic stem cells secrete cytokines/growth modulators that enhance cell survival/anti-apoptosis and stimulate colony formation of murine hematopoietic progenitor cells. *Stem Cells* **24**, 850-856 (2006).
58. Yang, F.C. et al. Hyperactivation of p21ras and PI3K cooperate to alter murine and human neurofibromatosis type 1-haploinsufficient osteoclast functions. *J Clin Invest* **116**, 2880-2891 (2006).
59. Uzan, G., Prandini, M.H., Rosa, J.P. & Berthier, R. Hematopoietic differentiation of embryonic stem cells: an in vitro model to study gene regulation during megakaryocytopoiesis. *Stem Cells* **14 Suppl 1**, 194-199 (1996).
60. Hamaguchi-Tsuru, E. et al. Development and functional analysis of eosinophils from murine embryonic stem cells. *British Journal of Haematology* **124**, 819-827 (2004).

61. Guo, Y., Hangoc, G., Bian, H., Pelus, L.M. & Broxmeyer, H.E. SDF-1/CXCL12 enhances survival and chemotaxis of murine embryonic stem cells and production of primitive and definitive hematopoietic progenitor cells. *Stem Cells* **23**, 1324-1332 (2005).
62. Nunomura, K. et al. Cell surface labeling and mass spectrometry reveal diversity of cell surface markers and signaling molecules expressed in undifferentiated mouse embryonic stem cells. *Mol Cell Proteomics* **4**, 1968-1976 (2005).
63. Eppig, J.T. et al. The Mouse Genome Database (MGD): from genes to mice--a community resource for mouse biology. *Nucleic Acids Res* **33**, D471-475 (2005).
64. De Miguel, M.P., Cheng, L., Holland, E.C., Federspiel, M.J. & Donovan, P.J. Dissection of the c-Kit signaling pathway in mouse primordial germ cells by retroviral-mediated gene transfer. *Proc Natl Acad Sci U S A* **99**, 10458-10463 (2002).
65. Heinrich, P.C., Behrmann, I., Muller-Newen, G., Schaper, F. & Graeve, L. Interleukin-6-type cytokine signalling through the gp130/Jak/STAT pathway. *Biochem J* **334 (Pt 2)**, 297-314 (1998).
66. Ichihara, M., Hara, T., Kim, H., Murate, T. & Miyajima, A. Oncostatin M and leukemia inhibitory factor do not use the same functional receptor in mice. *Blood* **90**, 165-173 (1997).
67. Takahashi, H. & Shibuya, M. The vascular endothelial growth factor (VEGF)/VEGF receptor system and its role under physiological and pathological conditions. *Clin Sci (Lond)* **109**, 227-241 (2005).
68. Gale, N.W. & Yancopoulos, G.D. Growth factors acting via endothelial cell-specific receptor tyrosine kinases: VEGFs, angiopoietins, and ephrins in vascular development. *Genes Dev* **13**, 1055-1066 (1999).
69. Ball, S.G., Shuttleworth, C.A. & Kielty, C.M. Vascular endothelial growth factor can signal through platelet-derived growth factor receptors. *J Cell Biol* (2007).
70. Ogawa, K., Matsui, H., Ohtsuka, S. & Niwa, H. A novel mechanism for regulating clonal propagation of mouse ES cells. *Genes Cells* **9**, 471-477 (2004).
71. Yamane, T., Dylla, S.J., Muijtjens, M. & Weissman, I.L. Enforced Bcl-2 expression overrides serum and feeder cell requirements for mouse embryonic stem cell self-renewal. *Proc Natl Acad Sci U S A* **102**, 3312-3317 (2005).
72. Davey, R.E. & Zandstra, P.W. Spatial organization of embryonic stem cell responsiveness to autocrine gp130 ligands reveals an autoregulatory stem cell niche. *Stem Cells* **24**, 2538-2548 (2006).
73. Davey, R.E., Onishi, K., Mahdavi, A. & Zandstra, P.W. LIF-mediated control of embryonic stem cell self-renewal emerges due to an autoregulatory loop. *Faseb J* (2007).
74. Tan, J.L., Liu, W., Nelson, C.M., Raghavan, S. & Chen, C.S. Simple approach to micropattern cells on common culture substrates by tuning substrate wettability. *Tissue Engineering* **10**, 865-872 (2004).
75. Nelson, C.M., Raghavan, S., Tan, J.L. & Chen, C.S. Degradation of micropatterned surfaces by cell-dependent and -independent processes. *Langmuir* **19**, 1493-1499 (2003).
76. Tan, J.L., Tien, J. & Chen, C.S. Microcontact printing of proteins on mixed self-assembled monolayers. *Langmuir* **18**, 519-523 (2002).
77. Mrksich, M., Dike, L.E., Tien, J., Ingber, D.E. & Whitesides, G.M. Using microcontact printing to pattern the attachment of mammalian cells to self-

assembled monolayers of alkanethiolates on transparent films of gold and silver. *Experimental Cell Research* **235**, 305-313 (1997).
78. Ostuni, E., Kane, R., Chen, C.S., Ingber, D.E. & Whitesides, G.M. Patterning mammalian cells using elastomeric membranes. *Langmuir* **16**, 7811-7819 (2000).
79. McDonald, J.C. & Whitesides, G.M. Poly(dimethylsiloxane) as a material for fabricating microfluidic devices. *Accounts of Chemical Research* **35**, 491-499 (2002).
80. Bhatia, S.N., Yarmush, M.L. & Toner, M. Controlling cell interactions by micropatterning in co-cultures: Hepatocytes and 3T3 fibroblasts. *Journal of Biomedical Materials Research* **34**, 189-199 (1997).
81. Nelson, C.M. & Chen, C.S. Cell-cell signaling by direct contact increases cell proliferation via a PI3K-dependent signal. *Febs Letters* **514**, 238-242 (2002).
82. Luk, Y.Y., Kato, M. & Mrksich, M. Self-assembled monolayers of alkanethiolates presenting mannitol groups are inert to protein adsorption and cell attachment. *Langmuir* **16**, 9604-9608 (2000).
83. Morra, M. & Cassineli, C. Non-fouling properties of polysaccharide-coated surfaces. *Journal of Biomaterials Science-Polymer Edition* **10**, 1107-1124 (1999).
84. Liu, V.A., Jastromb, W.E. & Bhatia, S.N. Engineering protein and cell adhesivity using PEO-terminated triblock polymers. *Journal of Biomedical Materials Research* **60**, 126-134 (2002).
85. Chen, C.S., Mrksich, M., Huang, S., Whitesides, G.M. & Ingber, D.E. Geometric control of cell life and death. *Science* **276**, 1425-1428 (1997).
86. Thomas, C.H., Lhoest, J.B., Castner, D.G., McFarland, C.D. & Healy, K.E. Surfaces designed to control the projected area and shape of individual cells. *Journal of Biomechanical Engineering-Transactions of the Asme* **121**, 40-48 (1999).
87. Roberts, C. et al. Using mixed self-assembled monolayers presenting RGD and (EG)(3)OH groups to characterize long-term attachment of bovine capillary endothelial cells to surfaces. *Journal of the American Chemical Society* **120**, 6548-6555 (1998).
88. Folch, A., Jo, B.H., Hurtado, O., Beebe, D.J. & Toner, M. Microfabricated elastomeric stencils for micropatterning cell cultures. *J Biomed Mater Res* **52**, 346-353 (2000).
89. Rettig, J.R. & Folch, A. Large-scale single-cell trapping and imaging using microwell arrays. *Anal Chem* **77**, 5628-5634 (2005).
90. Grier, D.G. A revolution in optical manipulation. *Nature* **424**, 810-816 (2003).
91. Ashkin, A., Dziedzic, J.M., Bjorkholm, J.E. & Chu, S. Observation of a Single-Beam Gradient Force Optical Trap for Dielectric Particles. *Optics Letters* **11**, 288-290 (1986).
92. Voldman, J., Braff, R.A., Toner, M., Gray, M.L. & Schmidt, M.A. Holding forces of single-particle dielectrophoretic traps. *Biophysical Journal* **80**, 531-541 (2001).
93. Rosenthal, A. & Voldman, J. Dielectrophoretic traps for single-particle patterning. *Biophysical Journal* **88**, 2193-2205 (2005).
94. Irimia, D., Geba, D.A. & Toner, M. Universal microfluidic gradient generator. *Anal Chem* **78**, 3472-3477 (2006).
95. Dertinger, S.K.W., Chiu, D.T., Jeon, N.L. & Whitesides, G.M. Generation of gradients having complex shapes using microfluidic networks. *Anal Chem* **73**, 1240-1246 (2001).
96. Jeon, N.L. et al. Neutrophil chemotaxis in linear and complex gradients of interleukin-8 formed in a microfabricated device. *Nature Biotechnology* **20**, 826-830 (2002).

97. in Molecular cell biology, Edn. 5th. (eds. H.F. Lodish, P.T. Matsudaira, C. Kaiser & M. Krieger) 621-637 (W.H. Freeman and Company, New York; 2004).
98. Sawano, A., Takayama, S., Matsuda, M. & Miyawaki, A. Lateral propagation of EGF signaling after local stimulation is dependent on receptor density. *Developmental Cell* **3**, 245-257 (2002).
99. Beebe, D.J., Mensing, G.A. & Walker, G.M. Physics and applications of microfluidics in biology. *Annu Rev Biomed Eng* **4**, 261-286 (2002).
100. Deen, W.M. Analysis of transport phenomena. (Oxford University Press, New York; 1998).
101. Rathjen, P.D., Toth, S., Willis, A., Heath, J.K. & Smith, A.G. Differentiation inhibiting activity is produced in matrix-associated and diffusible forms that are generated by alternate promoter usage. *Cell* **62**, 1105-1114 (1990).
102. Zandstra, P.W., Le, H.V., Daley, G.Q., Griffith, L.G. & Lauffenburger, D.A. Leukemia inhibitory factor (LIF) concentration modulates embryonic stem cell self-renewal and differentiation independently of proliferation. *Biotechnology and Bioengineering* **69**, 607-617 (2000).
103. Bitard, J. et al. Mutations in the immunoglobulin-like domain of gp190, the leukemia inhibitory factor (LIF) receptor, increase or decrease its affinity for LIF. *Journal of Biological Chemistry* **278**, 16253-16261 (2003).
104. Forsten, K.E. & Lauffenburger, D.A. The Role of Low-Affinity Interleukin-2 Receptors in Autocrine Ligand-Binding - Alternative Mechanisms for Enhanced Binding Effect. *Molecular Immunology* **31**, 739-751 (1994).
105. Folch, A. & Toner, M. Microengineering of cellular interactions. *Annu Rev Biomed Eng* **2**, 227-256 (2000).
106. Budge, S.E. & Mayampurath, A.M. in 38th Asilomar Conference on Signals, Systems and Computers, Vol. 2. (ed. M.B. Matthews) 1535-1539 (IEEE, Pacific Grove, California; 2004).
107. Schalkoff, R.J. Digital image processing and computer vision. (John Wiley & Sons, Inc., New York; 1989).
108. Jahne, B. in Handbook of computer vision and applications, Vol. 2 194-206 (Academic press, San Diego; 1999).
109. Davies, E.R. Machine vision : theory, algorithms, practicalities, Edn. 2nd. (Academic Press, San Diego; 1997).
110. Sonka, M., Hlavac, V. & Boyle, R. Image processing, analysis and machine vision, Edn. 1. (Chapman & Hall, London; 1993).
111. Wolberg, G. Digital image warping. (IEEE Computer Society Press, Los Alamitos, Calif.; 1992).
112. Pettersson, P.M. & Edso, T., Edn. G06K 1/12, 19/06. (ed. W.I.P. Organization)2001).
113. Lewis, J.P. in Vision Interface 120-1231995).
114. Lisa Gottesfeld, B. A survey of image registration techniques. *ACM Comput. Surv.* **24**, 325-376 (1992).
115. Barnea, D. & Silverman, H. A class of algorithms for fast digital image registration. *IEEE Transactions on Computers* **21**, 179-186 (1972).
116. Lucas, B.D. & Kanade, T. in DARPA Imaging Understanding Workshop 121-1301981).

117. Reddy, B.S. & Chatterji, B.N. An FFT-based technique for translation, rotation, and scale-invariant image registration. *IEEE Transactions on Image Processing* **5**, 1266-1271 (1996).
118. Tarachandani, A. & Boltz, D. Review of the basic image processing and segmentation techniques for biological images. *Journal of Imaging Science and Technology* **50**, 233-242 (2006).
119. Cufi, X., Munoz, X., Freixenet, J. & Marti, J. A review of image segmentation techniques integrating region and boundary information. *Advances in Imaging and Electron Physics, Vol 120* **120**, 1-39 (2002).
120. Pal, N.R. & Pal, S.K. A Review on Image Segmentation Techniques. *Pattern Recognition* **26**, 1277-1294 (1993).
121. Bezdek, J.C., Hall, L.O. & Clarke, L.P. Review of Mr Image Segmentation Techniques Using Pattern-Recognition. *Medical Physics* **20**, 1033-1048 (1993).
122. Otsu, N. Threshold Selection Method from Gray-Level Histograms. *Ieee T Syst Man Cyb* **9**, 62-66 (1979).
123. Jian, G., Liyuan, L. & Weinan, C. in ICSP'96 1155-11581996).
124. Kuntimad, G. & Ranganath, H.S. Perfect image segmentation using pulse coupled neural networks. *Ieee Transactions on Neural Networks* **10**, 591-598 (1999).
125. Soille, P. in Handbook of computer vision and applications, Vol. 2. (eds. B. Jahne, H. Haubecker & P. Geibler) 627-681 (Academic Press, San Deigo; 1999).
126. Soll, D.R. & Voss, E. in Motion Analysis of Living Cells. (eds. D.R. Soll & D. Wessels) 25-52 (Wiley-Liss, Inc., New York; 1998).
127. Alt, W., Deutsch, A. & Dunn, G. Dynamics of cell and tissue motion. (Birkhauser, Basel ; Boston; 1997).
128. McBeath, R., Pirone, D.M., Nelson, C.M., Bhadriraju, K. & Chen, C.S. Cell shape, cytoskeletal tension, and RhoA regulate stem cell lineage commitment. *Developmental Cell* **6**, 483-495 (2004).
129. Koestenbauer, S. et al. Embryonic stem cells: Similarities and differences between human and murine embryonic stem cells. *American Journal of Reproductive Immunology* **55**, 169-180 (2006).
130. Ginis, I. et al. Differences between human and mouse embryonic stem cells. *Developmental Biology* **269**, 360-380 (2004).
131. Coucouvanis, E. & Martin, G.R. Signals for death and survival: a two-step mechanism for cavitation in the vertebrate embryo. *Cell* **83**, 279-287 (1995).
132. Coucouvanis, E. & Martin, G.R. BMP signaling plays a role in visceral endoderm differentiation and cavitation in the early mouse embryo. *Development* **126**, 535-546 (1999).
133. Hamazaki, T., Oka, M., Yamanaka, S. & Terada, N. Aggregation of embryonic stem cells induces Nanog repression and primitive endoderm differentiation. *J Cell Sci* **117**, 5681-5686 (2004).
134. Atencia, J. & Beebe, D.J. Controlled microfluidic interfaces. *Nature* **437**, 648-655 (2005).
135. Yu, H.M., Meyvantsson, I., Shkel, I.A. & Beebe, D.J. Diffusion dependent cell behavior in microenvironments. *Lab on a Chip* **5**, 1089-1095 (2005).
136. Wu, Y.Q., Vasquez, D.A., Edwards, B.F. & Wilder, J.W. Convective Chemical-Wave Propagation in the Belousov-Zhabotinsky Reaction. *Physical Review E* **51**, 1119-1127 (1995).

137. Hui, E.E. & Bhatia, S.N. Micromechanical control of cell-cell interactions. *Proc Natl Acad Sci U S A* **104**, 5722-5726 (2007).
138. Jen, A.C., Wake, M.C. & Mikos, A.G. Review: Hydrogels for cell immobilization. *Biotechnology and Bioengineering* **50**, 357-364 (1996).
139. Lauffenburger, D. & Cozens, C. Regulation of Mammalian-Cell Growth by Autocrine Growth-Factors - Analysis of Consequences for Inoculum Cell-Density Effects. *Biotechnology and Bioengineering* **33**, 1365-1378 (1989).
140. Shvartsman, S.Y., Wiley, H.S., Deen, W.M. & Lauffenburger, D.A. Spatial range of autocrine signaling: modeling and computational analysis. *Biophys J* **81**, 1854-1867 (2001).
141. Claret, E., Renversez, J.C., Zheng, X.Q., Bonnefoix, T. & Sotto, J.J. Valid Estimation of Il2-Secretion by Pha-Stimulated T-Cell Clones Absolutely Requires the Use of Anti-Cd25 Monoclonal-Antibody to Prevent Il2-Consumption. *Immunology Letters* **33**, 179-186 (1992).
142. Fontana, J.A., Nervi, C., Shao, Z.M. & Jetten, A.M. Retinoid antagonism of estrogen-responsive transforming growth factor alpha and pS2 gene expression in breast carcinoma cells. *Cancer Res* **52**, 3938-3945 (1992).
143. Reiss, M., Stash, E.B., Vellucci, V.F. & Zhou, Z.L. Activation of the autocrine transforming growth factor alpha pathway in human squamous carcinoma cells. *Cancer Res* **51**, 6254-6262 (1991).
144. Hamburger, A.W. & Pinnamaneni, G. Interferon-induced enhancement of transforming growth factor-alpha expression in a human breast cancer cell line. *Proc Soc Exp Biol Med* **202**, 64-68 (1993).
145. Oehrtman, G.T., Wiley, H.S. & Lauffenburger, D.A. Escape of autocrine ligands into extracellular medium: Experimental test of theoretical model predictions. *Biotechnology and Bioengineering* **57**, 571-582 (1998).